

# Circumnuclear Dust in Nearby Active and Inactive Galaxies. I. Data<sup>1</sup>

Paul Martini <sup>2</sup>, Michael W. Regan <sup>3</sup> John S. Mulchaey <sup>2</sup>, Richard W. Pogge<sup>4</sup>,

## ABSTRACT

The detailed morphology of the interstellar medium (ISM) in the central kiloparsec of galaxies is controlled by pressure and gravitation. The combination of these forces shapes both circumnuclear star formation and the growth of the central, supermassive black hole. We present visible and near-infrared *Hubble Space Telescope* images and color maps of 123 nearby galaxies that show the distribution of the cold ISM, as traced by dust, with excellent spatial resolution. These observations reveal that nuclear dust spirals are found in the majority of active and inactive galaxies and they possess a wide range in coherence, symmetry, and pitch angle. We have used this large sample to develop a classification system for circumnuclear dust structures. In spite of the heterogeneous nature of the complete sample, we only find symmetric, two-arm nuclear dust spirals in galaxies with large scale bars and these dust lanes clearly connect to dust lanes along the leading edges of the large scale bars. Not all dust lanes along large scale bars form two arm spirals, however, and several instead end in nuclear rings. We find that tightly wound, or low pitch angle, nuclear dust spirals are more common in unbarred galaxies than barred galaxies. Finally, the extended narrow line region in several of the active galaxies is well-resolved. The connection between the

---

<sup>1</sup>Based on observations with the NASA/ESA *Hubble Space Telescope* obtained at the the Space Telescope Science Institute, which is operated by the Association of Universities for Research in Astronomy, Incorporated, under NASA contract NAS5-26555.

<sup>2</sup>Carnegie Observatories, 813 Santa Barbara St., Pasadena, CA 91101-1292, martini@ociw.edu, mulchaey@ociw.edu

<sup>3</sup>Space Telescope Science Institute, 3700 San Martin Drive, Baltimore, MD 21218, mregan@stsci.edu

<sup>4</sup>Department of Astronomy, Ohio State University, 140 W. 18th Ave., Columbus, OH 43210, pogge@astronomy.ohio-state.edu

ionized gas and circumnuclear dust lanes in four of these galaxies provides additional evidence that a significant fraction of their extended narrow line region is ambient gas photoionized *in situ* by the active nucleus. In a future paper, we will use our classification system for circumnuclear dust to identify differences between active and inactive galaxies, as well as barred and unbarred galaxies, in well-matched subsamples of these data.

*Subject headings:* galaxies: active – galaxies: Seyfert – galaxies: nuclei – galaxies: ISM – ISM: structure – dust, extinction

## 1. Introduction

The kinematics of the cold interstellar medium (ISM) largely determines the future star formation and black hole growth in galaxies. In the circumnuclear region of most galaxies, corresponding to approximately the central kiloparsec, both pressure and gravitational forces can dominate these kinematics. In the absence of velocity information, observations of dust lanes in absorption from visible and near-infrared (NIR) images can provide a snapshot of the cold ISM.

Before the advent of *HST*, high spatial resolution observations of dust in the circumnuclear region were only possible for relatively nearby galaxies, including our own (Morris & Serabyn 1996), Andromeda (McElroy 1983; Ciardullo et al. 1988), and several other relatively nearby galaxies where circumnuclear dust is apparent on photographic plates in, for example, the Carnegie Atlas of Galaxies (Sandage & Bedke 1994). Large single-band *HST* programs have vastly expanded the number of galaxies with high spatial resolution observations (resolutions less than 50 parsecs; Malkan, Gorjian, & Tam 1998; Carollo, Stiavelli, & Mack 1998; Ferruit, Wilson, & Mulchaey 2000). These observations have revealed a wealth of detail in the circumnuclear structure of spiral galaxies and show that this nuclear structure is frequently quite different from the large scale morphology in any given galaxy. Multiband observations of smaller samples of active galaxies clearly show that much of this circumnuclear structure is due to nuclear dust (Elmegreen et al. 1998; Quillen et al. 1999), although mostly material that is only a factor of a few higher density than the ambient ISM (Regan & Mulchaey 1999; Martini & Pogge 1999).

One of the most common dust features found in the circumnuclear region are nuclear dust spirals, which exhibit a wide range of intrinsic shapes. These include symmetric, two-arm spirals, one-arm spirals, and chaotic, multiarm spirals (Elmegreen et al. 1998; Laine et al. 1998; Regan & Mulchaey 1999; Martini & Pogge 1999). A number of theoretical models

exist that can give rise to coherent dust structures in the circumnuclear region, although in all cases some differential rotation is required to form the spiral structure. Galaxies with strong, large scale bars form shock fronts along the leading edges of their bar (Prendergast 1983; Athanassoula 1992) and hydrodynamic simulations show that this inflowing material can form symmetric and two-arm or “grand design” spiral structure in the circumnuclear region (Englmaier & Shlosman 2000; Patsis & Athanassoula 2000). Maciejewski et al. (2002) recently modeled the circumnuclear region of barred galaxies and found grand design nuclear spirals similar to those found by (Englmaier & Shlosman 2000). While the nuclear spirals in Englmaier & Shlosman (2000) only corresponded to weak perturbations, the gas velocity field of the spirals in Maciejewski et al. (2002) had a large negative divergence, characteristic of strong shocks and similar to the shocks in the large-scale bar. Significant inflow is likely to be associated with these spirals shocks, as shown by Fukuda et al. (1998).

More chaotic, or “flocculent” spirals can form in the circumnuclear region from pressure forces, or acoustic turbulence, in the ISM (Elmegreen et al. 1998; Montenegro, Yuan, & Elmegreen 1999). Detailed studies of the LINERs NGC 4450 and NGC 4736 by Elmegreen, Elmegreen, & Eberwein (2002) show that the azimuthal Fourier transform spectra have a power law slope of  $-5/3$ , characteristic of turbulence. These structures therefore appear to be formed by the same turbulent processes that create structure in the ISM of galaxies at larger radii, but have been sheared by the presence of some differential rotation in the circumnuclear region and given a spiral appearance. Recent hydrodynamic simulations of the central ISM also naturally produce a filamentary, spiral structure in surface density with pressure and gravitational forces Wada & Norman (1999, 2001). Both these analytic and numerical studies suggest some inflow can occur due to turbulence alone.

The nuclear dust spirals on these small scales (they are generally a kiloparsec or less in length) are distinct from their host galaxy spiral arms both spatially and in composition. Nuclear spirals rarely extend out of the region dominated by the central bulge. Observations of Seyfert galaxies over many kiloparsecs show that while the grand design nuclear spirals appear to connect to the dust lanes along the large scale bar, most types of nuclear spirals do not connect to the large-scale spiral arms (Pogge & Martini 2002). These nuclear spirals also appear to only be enhancements in the dust surface density and not sufficiently overdense to be self-gravitating. Only a small number of nuclear dust spirals have associated star formation (e.g. NGC 4321, Coma D15: Knapen et al. 1995; Caldwell, Rose, & Dendy 1999) and NIR observations do not show enhancements in the stellar surface density associated with the spirals (Martini et al. 2001). In addition, density waves tend to get stronger with increasing radius, whereas the nuclear spirals get weaker with increasing radius (Montenegro, Yuan, & Elmegreen 1999; Elmegreen, Elmegreen, & Eberwein 2002).

One of the primary motivations for most of these multiband observations was to study the circumnuclear environment of active galaxies in order to determine the processes that removed angular momentum from host galaxy material and fueled the central, supermassive black hole. Recent *HST* programs have provided strong evidence that all galaxies with a spheroid component have a supermassive black hole (Richstone et al. 1998; Ferrarese & Merritt 2000; Gebhardt et al. 2000; Ferrarese et al. 2001; Gebhardt et al. 2001). This result has added new urgency to the question of how nuclear activity is fueled and why it is not currently fueled in all galaxies. Nuclear spiral structure was proposed as a mechanism for fueling nuclear activity because it was both discovered in nearly all of the observations of active galaxies and that these structures could be formed by shocks (Regan & Mulchaey 1999; Martini & Pogge 1999).

Both bar-driven inflow and acoustic turbulence are theoretically viable mechanisms for the removal of angular momentum. In the case of inflow from large-scale bars, the gas and dust loses essentially all of its angular momentum in the shock front at the leading edge of the bar. For acoustic turbulence, the shocks in the ISM caused by the turbulence could dissipate sufficient energy and angular momentum to lead to significant inflow (Elmegreen, Elmegreen, & Eberwein 2002). However, aside from the absence of kinematic data to demonstrate that inflow does occur, the selective investigation of active galaxies resulted in relatively few comparable observations of inactive galaxies. Such observations are needed to determine if there is an excess of nuclear spiral structure, or other morphological features, in active galaxies over inactive galaxies of similar Hubble types and luminosities. We have obtained *HST* observations of a significantly larger sample of both active and inactive galaxies to perform this analysis and present the data and a morphological study of each of the galaxies in our sample. In a future paper (Martini et al. 2002) we compare the circumnuclear environment of active and inactive galaxies for a well-matched subsample of these data, as well as discuss some interesting results on differences in the circumnuclear environments of barred and unbarred galaxies.

## 2. Sample Selection and Data Processing

### 2.1. Sample Selection

This galaxy sample was initially formed from the 91 Seyfert galaxies that meet the Revised Shapely-Ames (RSA) catalog magnitude requirement ( $B_T < 13.4$  mag) discussed by Maiolino & Reike (1995), minus those with  $v > 5000$  km s<sup>-1</sup> and axial ratios  $R_{25} > 0.35$ , to insure the circumnuclear region could be studied at high spatial resolution with minimal inclination effects. The resulting sample comprises 67 Seyfert galaxies, of which eight were

GTO targets. Inactive galaxies with approximately the same velocity, inclination, Hubble type, and luminosity were selected for each of 67 these Seyferts. Additional Seyfert and non-Seyfert galaxies of particular interest were then added to increase the sample of nearby galaxies. From this input catalog, 104 galaxies were observed as part of a NICMOS snapshot program (SN 7330; PI Mulchaey). The galaxies observed with NICMOS, minus those that already had unsaturated, WFPC2 F606W images from *HST*, then formed the input catalog of 88 galaxies for our WFPC2 snapshot program (SN 8597; PI Regan) and 76 of these galaxies have been observed to date. To these galaxies we have added the NICMOS observations of Seyfert 2s (GO 7867; PI Pogge) from the CfA Survey (Huchra & Burg 1992), in order to place them on a common classification scheme, and the RSA Seyferts observed by NICMOS GTO programs, to create the final sample of 123 galaxies. Table 1 lists the most common name(s) for each galaxy and provides the *HST* program that obtained the visible and NIR images. The WFPC2 filter used for the visible-wavelength image is also listed; the F160W filter (hereafter *H*) was used for all of the NICMOS observations.

Comparison of the circumnuclear dust properties of active and inactive galaxies requires reliable classifications. While the active galaxies are clearly active, the question of just what constitutes a inactive galaxy is much more dependent on the quality of previous observations. The inactive galaxies in this sample are generally bright and nearby, and therefore have been observed with sufficient sensitivity to detect at least a bright active nucleus, but genuine nuclear activity at very low levels usually can not be ruled out. For example, three of the 35 inactive RSA galaxies observed for the original NICMOS snapshot program were later reclassified as Seyfert 2 galaxies by the Palomar Survey (Ho et al. 1997) and a comparable number were classified as LINERs. In Table 2 we list the type of nuclear activity present in each galaxy from Table 1, as well as references to the original work and most recent classification. For the inactive galaxies, we list references to any surveys that could have detected some level of nuclear activity if it were present.

The question of whether or not a galaxy possesses a large-scale bar presents a problem comparable to the presence of nuclear activity. While all of the galaxies have been observed as part of the RC3 (de Vaucouleurs et al. 1991) and have visible-wavelength observations, many galaxies that do not appear to have bars based on visible-wavelength data do have them when studied in the NIR (McLeod & Rieke 1995; Mulchaey, Regan, & Kundu 1997). A large fraction of the galaxies in this sample were observed in the NIR, although there are nevertheless many apparently unbarred galaxies that do not have NIR observations. The classification of these unbarred galaxies are not as reliable as the unbarred galaxies that do have NIR observations. Nevertheless, aside from a few striking exceptions such as NGC 1068 (Scoville et al. 1988; Thronson et al. 1989), very few galaxies that show no evidence for a bar at visible wavelengths are strongly barred in the NIR (Mulchaey, Regan, & Kundu 1997).

Table 2 lists the bar classification for each galaxy, along with a flag to represent the quality of the bar classification.

Table 2 also lists the distance to each of these galaxies used to compute the projected spatial scale of the images shown in Figure 1. As the Catalog of Nearby Galaxies (Tully 1988) was the single largest source for these distances, we have adopted a Hubble constant of  $H_0 = 75 \text{ km s}^{-1} \text{ Mpc}^{-1}$ . For galaxies that did not have a previously published distance, we have used the relationship derived by Yahil, Tammann, & Sandage (1977) to estimate the distance.

## 2.2. Initial Processing

The majority of the visible-wavelength images were obtained as part of the snapshot program SN 8597. These consist of two exposures of length 140s and 400s obtained through the F606W filter and with the galaxy centered on the PC chip. The image pairs were processed through the standard calibration pipeline and then combined with an XVista script as described in Pogge & Martini (2002). The remaining visible wavelength images were obtained from the *HST* archive and constitute either image pairs similar to those obtained for SN 8597, or single exposures. These later observations required additional steps to remove the cosmic ray contamination and to process these images we have developed a new algorithm, which is described in the next section.

The NIR images were all processed by the standard NICMOS pipeline developed at STScI. Many of the earliest images were obtained while this pipeline was still under development and were later recalibrated with new procedures and reference files as they became available. The basic details of the NICMOS reduction steps are described in Regan & Mulchaey (1999) for SN 7330 and Martini & Pogge (1999) for GO 7867. The galaxies not observed by either of these programs were obtained from the STScI archive and processed by the best reference and calibration files. None of the images were processed with CALNIB, instead the final shift and add step and any cosmic ray cleaning was performed in IRAF<sup>5</sup>.

---

<sup>5</sup>IRAF is distributed by the National Optical Astronomy Observatories, which are operated by the Association of Universities for Research in Astronomy, Inc., under cooperative agreement with the National Science Foundation.

### 2.3. Cosmic Ray Removal

Techniques for the removal of cosmic rays fall into two general families. The first relies on multiple images of the same field, such as those obtained as part of our snapshot program. Here cosmic rays are identified as an anomalously large intensity increase in a given pixel and can be rejected when the images are combined. The second method is for the case where only a single image is available. In this latter case cosmic rays are detected by the deviation of a given pixel by a certain threshold over the variation in the neighboring pixels and the value of this pixel is then replaced with some value calculated from the neighboring pixels.

For the galaxies from the *HST* archive with only single observations, the majority of which were from snapshot program SN 5479 (Malkan, Gorjian, & Tam 1998), we developed a new method of cosmic ray detection and removal based on detailed knowledge of the *HST* point spread function (PSF) and the fact that cosmic rays produce image artifacts which are usually sharper than the PSF. To identify cosmic rays, the original image is convolved with a PSF model generated with the TINYTIM software (Krist & Hook 1999) and then this convolved image is divided back into the original image to form  $I/(I \otimes P)$ , where  $I$  is the original image,  $P$  is the PSF, and  $\otimes$  is the convolution operator. Pixel values greater than two in this divided image were empirically determined to nearly always correspond to bad pixels and these pixels were flagged and replaced by the average pixel value in the immediate vicinity in the original image. Cosmic rays were typically found to contaminate neighboring pixels within approximately one pixel of those identified by this technique. We therefore smoothed an initial mask of the flagged pixels with a 3x3 boxcar kernel to generate a final mask of all contaminated pixels. Each of these masked pixels was then replaced by the mean value of a 5x5 pixel box centered on the pixel, minus any other masked pixels within this region.

This technique is based on the “structure map” concept detailed in Pogge & Martini (2002), where a structure map is defined as:

$$S = \left[ \frac{I}{I \otimes P} \right] \otimes P^t \quad (1)$$

where  $S$  is the structure map and  $P^t$  is the transpose of the model PSF,  $P^t(x, y) = P(-x, -y)$ . The cosmic ray detection image differs from the structure map as the original image is simply divided by a convolved version of itself, and not then convolved again by the transpose of the PSF. The image used for cosmic ray detection is similar to the second “correction image” formed in typical implementations of Richardson-Lucy (R-L) image restoration (Richardson 1972; Lucy 1974), although formally this latter image is  $(I \otimes P^t) \otimes P$ . In practice, image anomalies such as cosmic rays or saturated stars needed to be removed

from the galaxies we studied in Pogge & Martini (2002) as the structure maps overemphasized these features to the point of obliterating neighboring physical structures of interest. In several instances we also cleaned images by hand or used the method of Laplacian edge detection described by van Dokkum (2001).

## 2.4. Color maps

The visible-wavelength images were calibrated with the standard calibration header keywords to approximately correspond to either ground-based  $V$  or  $I$  band, depending on the filter. All of the NIR observations were obtained through the NICMOS F160W filter, which is close to, but slightly broader than, a ground-based  $H$  filter. The majority of these observations were obtained with NICMOS Camera 2, although 22 observations were obtained with NICMOS Camera 1. These NIR observations were converted to  $H$  magnitudes per square arcsecond using the standard NICMOS photometric calibration. The visible and NIR images, hereafter referred to as the  $V$  and  $H$  images, respectively, were then rebinned onto a common plate scale of  $0.02''$  per pixel and differenced to form  $V - H$  color maps. Figure 1 shows these  $V$ ,  $H$ , and  $V - H$  images for all 123 galaxies.

The angular resolution difference of  $\sim 2.6$  between the diffraction limit of *HST* at the effective wavelengths of the F606W and F160W filters results in very different spatial resolutions in the two filters. This effect is particularly striking for the active galaxies with bright nuclei, such as NGC 1068 or NGC 4151. The nuclei of these galaxies have striking red rings due to the prominence and larger radius of the airy diffraction rings in the NIR data. One way to mitigate the effects of these artifacts is to convolve the respective images by the PSF of the other in order to achieve a common angular resolution. However, the large mismatch in angular resolution between these frames effectively means that the excellent angular resolution of the  $V$  observations is significantly degraded. In fact, while the angular resolution mismatch is quite striking in the active nuclei, in general it does not effect the interpretation of dust morphology in the circumnuclear environment. This is because the  $V$  data are approximately a factor of five more sensitive to dust extinction (for a standard Milky Way reddening law) than the  $H$  data and thus nearly all of the information on the dust morphology is contained in the  $V$  frames and the  $H$  data mostly provides a measure of the true stellar light distribution in the absence of dust. To prove this point, and confirm that the angular resolution mismatch between  $V$  and  $H$  does not introduce spurious dust features which could impact on our analysis, we have created a series of color maps with the  $V$  and  $H$  data convolved to the same angular resolution and compared these convolved color maps with the unconvolved frames. A subset of these comparison frames are shown in Fig-

ure 32 for galaxies with particularly striking circumnuclear dust morphology. While these panels clearly show that the PSF-matching process smooths out dust features, it neither erases them completely nor leads to spurious features.

### 3. Classification

The wide variety of different circumnuclear dust structures in Figure 1 illustrates striking similarities and differences to the larger scale morphology of galaxies. Most of these color maps show spiral lanes of dust and many of these nuclear spirals bear close resemblance to the grand design and multiarm spirals of varying pitch angle common to large scale spiral structure many kiloparsecs in extent. However, while such dust spirals appear to be quite common, many galaxies with well-ordered large scale structure have very chaotic circumnuclear environments, e.g. NGC 3351. In addition, while circumnuclear spiral structure of some form is present in most these galaxies, it is much less frequently as ordered and symmetric as large scale spiral structure. Perhaps most importantly, the dust structures in the circumnuclear region only rarely appears to have any associated star formation, whereas only a small fraction of all large scale spirals (e.g. NGC 7377 and IC 5063) are purely defined by dust, rather than star formation. The NIR images also do not show evidence for any enhancement in the stellar surface density associated with the spirals, whereas large-scale, grand design (Elmegreen & Elmegreen 1984) and flocculent (Thornley 1996) spirals show some enhancements in the NIR. Because of these physical and morphological differences, particularly in the spiral structure, we have decided to develop a separate classification system for circumnuclear dust, rather than attempt to continue Malkan, Gorjian, & Tam (1998)’s extension of the Hubble classification scheme to smaller scales.

While the morphological differences between circumnuclear dust spirals and large scale, predominantly stellar spirals merit a different classification system, their similarities lead naturally to a parallel approach. Sandage & Bedke (1994), in their introduction to the Carnegie Atlas of Galaxies, describe how the philosophy behind the Hubble system is an amalgam of the extreme empiricist and rationalist approaches to classification in its synthesis of observational data with physical insight and intuition. We endeavored to use a similar approach in the development of criteria for classification of nuclear dust structures. This is largely because the circumnuclear dust classification is based on the Hubble system, as well as the fact that some physical intuition (or prejudice) is unavoidable. Nevertheless, we have developed this classification system with reference to the various morphological phenomena in the circumnuclear dust and have avoided reference to nuclear activity and any host galaxy properties (with the exception of inclination). This approach was adopted to avoid bias

imposed by the large scale structure that could obscure genuinely new characteristics of the circumnuclear region. In the following section, and in greater detail in a future paper, we discuss the relation between these different classes and nuclear and host galaxy properties. The presence of several connections between the circumnuclear classifications and both host and nuclear properties does suggest that real and distinct physical phenomena are connected to these different classes and we are not simply imposing order on chaos.

### 3.1. Morphological Classes

In our previous studies of circumnuclear structure in active galaxies, we noted that all of them are rich in dust structures and in most cases this dust takes the form of spiral features with greater or lesser degrees of coherence. The samples studied by Regan & Mulchaey (1999) and Martini & Pogge (1999) showed that circumnuclear dust structures have varying degrees of symmetry, number of spiral arms, and coherence, but were too small to search for the morphological trends necessary to establish a classification scheme for circumnuclear dust structures. In their recent morphological study of active and HII galaxies, Malkan, Gorjian, & Tam (1998) did provide new classifications for many galaxies based on much smaller-scale structure than those used for the original RSA or RC3 classification, however in most cases these classifications were still largely based on the large-scale structure, rather than the dust morphology in the circumnuclear environment at spatial scales less than a kiloparsec. The color maps presented here more clearly show the dust morphology at radii as small as several resolution elements from the nucleus in all but the brightest active galaxies. These observations clearly show trends in the circumnuclear morphology that are similar, but not identical, to the larger-scale morphology and the most obvious similarity is in the nuclear spiral dust structure. This structure ranges from symmetric, two-arm spirals that appear similar to the beautiful grand-design spirals NGC 1566 and NGC 5194, to multiarm spirals similar to NGC 2336, to spirals with only a few scattered arcs of dust. A significant fraction of the galaxies have no circumnuclear dust spirals and instead simply have more amorphous dust structures or have no dust structure in their circumnuclear region at all. We have divided the galaxies with clear evidence for spiral structure into four different classes, created a fifth class for those galaxies with chaotic circumnuclear dust, and a sixth class for galaxies that have no evidence of nonuniform dust. Each of these classes are described below and an example of each class is shown in Figure 33.

### 3.1.1. *Grand Design Nuclear Spirals (GD)*

This class is defined by the presence of a symmetric, two arm dust spiral such as shown in NGC 5643 (shown in Figure 33) and NGC 1300. These spirals appear similar to the grand design spirals found in the disks of many galaxies, yet these nuclear spirals are on scales less than a kiloparsec, rather than the many kiloparsecs of their larger namesakes. In addition, these arms are only traced by dust and do not exhibit the enhanced star formation and stellar surface density characteristic of galaxy-scale spiral density waves. The lack of star formation and absence of a detectable NIR surface density enhancement suggests that grand design nuclear spirals either do not trace significant enhancements in the dust surface density or they have sufficient shear to inhibit star formation. Estimates of the dust surface density increase in the arms by Martini & Pogge (1999) supports the former scenario, although this does not constrain the amount of shear in the dust lanes.

Many galaxies with grand design nuclear spirals have additional circumnuclear dust, often in the form of spiral arm fragments, in the interarm region between the grand design spiral arms (e.g. NGC 4303, NGC 6814). We still classified galaxies as grand design nuclear spirals provided that the symmetric, two-arm structure was more prominent than the more irregular features in their interarm region. A common feature of many of these spirals (and the additional types we define below) is that the dust structures on one half of the circumnuclear disk are not as distinct as those in the other half, e.g. NGC 6890. As the division between the high and low contrast halves of the circumnuclear disk always coincides with the position angle of the host galaxy, we attribute this change in contrast to the inclination of the galaxy. In several cases, this effect is so strong that only a hint of the second arm is apparent, yet we still classify a galaxy as a grand design nuclear spiral if a 180 degree rotation of the first arm would clearly align with any structure on the other side of the disk, as is the case for NGC 2639.

### 3.1.2. *Tightly Wound Nuclear Spiral (TW)*

Many galaxies with clear nuclear dust spirals lack either the clear symmetry of grand design spirals, two dust lanes, or both. We have separated these galaxies into two classes based upon the pitch angle of the nuclear spiral features. We classified spirals with small pitch angles as tightly wound (TW) and spirals with larger pitch angles as loosely wound (LW). The dividing line in pitch angle corresponds roughly to Hubble type Sab. Tightly wound nuclear spirals generally maintain their coherence for one or more complete rotations about the nucleus, e.g. NGC 2985 (Figure 33) and NGC 4030. As is the case for grand design and other nuclear spirals, these arms do not appear to trace circumnuclear star formation,

nor are they apparent in NIR surface photometry.

### 3.1.3. *Loosely Wound Nuclear Spiral (LW)*

All of the remaining galaxies with coherent nuclear spirals, but with larger pitch angle (comparable to the pitch angles exhibited by Hubble types Sb and later), are grouped into the class of loosely wound nuclear spirals. While these arms exhibit similar coherence as the tightly wound nuclear spirals, there are always several clear spiral arms in loosely wound nuclear spirals, e.g. NGC 6951 (Figure 33) and NGC 4941, whereas the tightly wound nuclear spirals often have such sufficiently small pitch angles that it is difficult to discern the number of spiral arms present. Although the LW nuclear spirals are well separated, all of the spiral arms in a given galaxy appear to have comparable pitch angles and imply the same sense of rotation. Another common feature of LW spiral arms is that they are nearly always too loosely wound to make a complete rotation about the nucleus, whereas the tightly wound nuclear spirals typically make one or more complete rotations. This is not an obvious physical difference between the two types, however, as often signal-to-noise (e.g. NGC 3486), the NICMOS field of view (e.g. NGC 7392), or larger scale structures in the host galaxy (e.g. NGC 6951) limit the apparent radial extent of the LW spirals.

### 3.1.4. *Chaotic Nuclear Spiral (CS)*

Many galaxies exhibit evidence for one or more spiral arm fragments or dust arcs that suggest spiral structure, yet they lack the coherent structure over a large range in radius exhibited by the three classes described above. We classified these galaxies as chaotic nuclear spirals because they still show evidence for some spiral structure, though more reminiscent of the spiral features in irregular galaxies than in any of the traditional spiral galaxy classes. As in the case of the other types of nuclear dust spirals, the dust lanes also do not have star formation, which is not the case for the spiral arm fragments seen in Irregulars. The chaotic spirals include dust spirals that are broken into many fragments (e.g. NGC 6221) or do not fill the entire circumnuclear disk (e.g. NGC 2460; Figure 33). In order to be included in this class, however, they do need to possess at least two spiral arms that suggest the same sense of rotation. For example, NGC 3368 has at least two spiral arm fragments with the same sense of rotation, whereas NGC 4260, which we do not classify as a chaotic nuclear spiral, has at best one arm fragment. Instead, we classify NGC 4260 as a member of the chaotic class defined in the next subsection.

### 3.1.5. Chaotic Circumnuclear Dust (C)

These galaxies have clearly discernible, and often considerable, circumnuclear dust, yet without unambiguous evidence for spiral structure. While there are a few galaxies that suggest spiral features, such as NGC 6946 (Figure 33) or NGC 2336, in both of these cases there are features of nearly equal size and contrast that could be due to spiral arms in a disk with the opposite sense of rotation. This class is in effect a catch-all for any galaxies that show no evidence for spiral structure, yet a larger sample could merit the division of this class into several distinct groups. For example, a number of these galaxies have straight dust lanes that completely cross the nucleus, such as IC 5267 and NGC 3627. Other galaxies are at relatively high inclination and have several straight dust lanes crossing the nucleus on one half, e.g. NGC 4939, NGC 5033 and NGC 5970. If these galaxies were not so highly inclined relative to the line of sight, they might be classified as nuclear spirals. Several other galaxies with high inclination simply have a large cloud of dust on what is presumably the near side of the disk, e.g. NGC 4258 and NGC 6300, rather than many lanes of dust.

### 3.1.6. No Structure (N)

The final class corresponds to galaxies with no dust structure in the circumnuclear region. Galaxies in this class, e.g. NGC 1398 (Figure 33) and NGC 357, do not show any dust structures within at least the central few hundred parsecs. For most of these galaxies there is also no evidence for nonuniform dust at larger radii. However, the case of NGC 628 illustrates the complication caused by the large distance distribution of the full sample. In this galaxy the central region is essentially featureless, yet outside of approximately 200 parsecs radius there is significant spiral dust structure. Nevertheless we have classified this galaxy as having no structure as the well-resolved central region is apparently free of dust lanes.

## 3.2. Notes on the Classification Process

The nuclear classifications for each galaxy are provided in the last column of Table 3. Each galaxy was classified independently by two of us (PM and MR) after we agreed on the classification scheme described above and a set of prototypes for each class. The galaxies given above as examples of each class include the prototypes used for the classification. There were disagreements for nearly half of the galaxies. This high rate of disagreement is some cause for concern given the subjective nature of this process, yet upon closer scrutiny nearly

all of the sources of conflict were between similar classes, such as between the chaotic spirals and chaotic or between chaotic spirals and loosely wound spirals. A blind reclassification of all of the sources of conflict led to resolution of most of the cases, which we attribute to our increased familiarity with the classification scheme. The remaining conflicts were resolved in binding arbitration (provided by JM).

Galaxies with  $R_{25} > 0.35$  ( $\sim 70$  degrees) were considered too highly inclined for a reliable classification. They have been labeled as high inclination (HI) systems in Table 3. There is a great deal of dust in these high inclination systems and occasionally nuclear spiral structure is visible, e.g. NGC 1320. For these galaxies we have provided an additional classification after the HI in the table, although most just show chaotic dust structures. For inclinations greater than  $R_{25} = 0.30$  the fraction of galaxies classified as chaotic starts to increase noticeably and therefore only galaxies with  $R_{25} < 0.30$  are included in the detailed analysis described in Paper II.

Many of these galaxies have high contrast dust features present on half of the color map and little or no structure on the opposite half. This appears to be due to the inclination of the host galaxy and can be used, as noted by Hubble (1943), to break the degeneracy between the near and far sides of a galaxy. We assumed that lower contrast or the absence of dust features on one half of a circumnuclear disk was due to inclination alone and classified these cases as if similar dust structures were visible on both sides of the disk. For several galaxies, such as NGC 3393 or NGC 3458, the center of the galaxy fell near the edge of the NICMOS image and therefore only half of the galaxy is present in the color map. In these instances, and in others where the signal-to-noise of the NIR image was significantly worse than the visible image, we also used the WFPC2 ( $V$ ) image to aid in the classification. In the Appendix we provide more detail on the classifications for individual galaxies.

## 4. Circumnuclear Dust Structure

### 4.1. Nuclear Activity

In Figure 34 we plot histograms of the fraction of active and inactive galaxies in each of the classes described above, as well as histograms of their distribution in heliocentric velocity ( $v$ ),  $B$  luminosities ( $M_B$ ), Hubble types (T), size (fraction of  $D_{25}$  within the  $20''$  field of view), and inclination ( $R_{25}$ ). Each set of histograms is normalized such that a given bin reflects the fraction of the total active or inactive sample within that bin. The number on top of each histogram then gives the actual number of galaxies in that bin. The total number of galaxies in each panel does not add up to the 123 galaxies in the entire sample as

there are typically several galaxies which fall outside the range of each histogram.

The first histogram in Figure 34 shows that nuclear spiral structure is a very common feature in active galaxies as 52 of the 64 active galaxies (with  $R_{25} < 0.3$ ) in this sample, or 80%, fall into one of the four classes of nuclear spiral structure defined above. Nuclear spirals of some form are also found in the majority of the inactive galaxies we observed: 23 of the 39 inactive galaxies, or approximately 60% of the full sample. This sample size greatly exceeds the number studied in our previous work, in which we suggested that nuclear spirals could remove sufficient angular momentum to fuel nuclear activity.

The remaining five histograms in the figure illustrate some of the potential biases that could affect the relative distributions of the active and inactive galaxies. From the distribution of host galaxy types it is apparent that the active galaxies are slightly biased toward an earlier mean Hubble type than the inactive galaxies. The distribution in  $M_B$  and  $v$  shows that the active galaxies are on average also brighter and more distant than the inactive galaxies. The large number of distant active galaxies is partially due to the inclusion of the CfA Seyferts, many of which are even more distant than the upper limit of  $6000 \text{ km s}^{-1}$  for the last bin shown in Figure 34. The lowest two panels show the size and inclination distributions. The active and inactive samples clearly have different size distributions. The angular size of the active galaxies are systematically smaller than the inactive galaxies, which shows that their greater mean distance more than offsets the fact that they are in brighter, presumably larger galaxies. The inclination distributions are similar for both samples. These many differences between the host galaxy properties of the active and inactive galaxies preclude any physical interpretation of the differences in the distributions of their circumnuclear dust classifications. In a future paper we will create subsamples of active and inactive galaxies without differences in their host galaxy properties and investigate the differences in their circumnuclear dust morphology in detail.

In several AGN the spiral nuclear dust lanes also appear to have segments illuminated by ionization cones emerging from the active nucleus. The most striking example is Mrk 573 in which the grand design nuclear spiral appears to make two rotations about the nucleus, with 4 segments illuminated in emission in a double biconical form (Quillen et al. 1999). Several other galaxies also show dust lanes in absorption that become emission in a cone-shaped region centered on the nucleus, particularly Mrk 1066 and NGC 788. This may also be the case in NGC 3393, which has spectacular S-shaped emission filaments inside the ionization cone (Pogge 1997; Cooke et al. 2000). Unfortunately, the  $H$  observation missed the nucleus and there is only a  $V - H$  color map of one of the ionization cones, but the filaments on the ends of this emission become dust lanes at larger radii and outside the ionization cone. Studies of both Mrk 573 (Tsvetanov & Walsh 1992; Pogge & De Robertis 1995; Capetti et

al. 1996) and NGC 3393 (Cooke et al. 2000) debate the relative importance of bow shocks and anisotropic nuclear ionization in the formation of these structures. Following Quillen et al. (1999), who studied 4 galaxies, we find additional evidence that in at least some of these galaxies a significant fraction of the gas in the extended narrow-line regions is ambient gas photoionized *in situ* by the active nucleus.

## 4.2. Bars

Figure 35 shows a similar set of histograms for the barred and unbarred galaxies in the sample. The distribution of host properties for the barred and unbarred galaxies are much more similar than for the active and inactive galaxies, although the unbarred samples are slightly earlier Hubble type, fainter, and more distant than the barred galaxies. Given these similarities, the distribution of the barred and unbarred galaxies into the different circumnuclear dust classes can provide real physical insight into the interaction of a large scale bar and the circumnuclear ISM, and these distributions do show some striking trends. The most prominent trend is that grand design nuclear spirals are only present in barred galaxies. There are 19 barred galaxies, or 27% of the sample, with grand design nuclear spirals, yet no unbarred galaxies. Given the fraction of unbarred galaxies in the sample, we would expect there to be eight unbarred galaxies with grand design nuclear spirals if this form of circumnuclear structure were independent of the presence of a large scale bar.

Straight dust lanes in strong, large-scale bars have been observed in galaxies such as NGC 1300 or NGC 7479. Simulations of barred galaxies show that shock fronts develop in the interstellar medium in strong bars (Prendergast 1983; Athanassoula 1992). These shocks can extend inwards as a grand-design spiral, depending on the properties of the potential and ISM, and cause dissipation when gas flows across them (Maciejewski et al. 2002). Simulations of gas flow in bars have shown that the angle between the bar and the dust lanes depends on the strength of the bar, where the dust lanes in the strongest bars are parallel to the bar’s semimajor axis (Athanassoula 1992). These dust lanes have the greatest shear, and consequently both the largest inflow and no associated star formation. Dust lanes in weaker bars (e.g. which on average correspond to type “SAB” in the RC3 catalog, although with significant scatter Buta & Block 2001) have less shear and some bars, such as in NGC 1566 (Comte & Duquennoy 1982), have star formation in their dust lanes. Several of the galaxies (NGC 4253, NGC 5135, NGC 5383, and NGC 7130) in this sample with dust lanes and grand design nuclear spirals also have star formation associated with the large scale bar’s dust lanes, which indicates that grand design nuclear dust spirals are not only found in strong bars. There are also barred galaxies with straight dust lanes that do not form grand design

nuclear spirals, such as NGC 4314 and NGC 6951, where the bar dust lanes end in rings. Estimates or direct observations of gas flow along the dust lanes in bars have been made for NGC 1097 (Quillen et al. 1995) and NGC 7479 (Regan, Vogel, & Teuben 1997). Recent, higher-resolution simulations have shown that the infalling material may become sheared by differential rotation within the Inner Lindblad Resonance of the bar or smoothed by a high sound speed (Englmaier & Shlosman 2000). This differential rotation creates a symmetric, two-arm spiral like the grand design nuclear spiral class.

Englmaier & Shlosman (2000) used their models to demonstrate how the pitch angle and coherence of the nuclear dust spirals depends on the central mass concentration and the pressure in the ISM, which is parametrized by a single value for the sound speed in their simulations. Models with greater central concentrations have more tightly wound arms, as do models with lower sound speeds. There is a wide range of pitch angle among the grand design nuclear spirals shown in Figure 1, which offer the opportunity to test the predictions of these simulations in detail. For example, the grand design nuclear spiral arms in NGC 1530 or NGC 5643 have larger pitch angles than those in NGC 1300 or Mrk 573. As noted above, the observations of grand design nuclear spirals show that their circumnuclear disks are generally filled with finer dust structures in regions that are not dominated by the large, two-arm spiral. The presence of these smaller, flocculent spiral structures mixed with the dominant, two-arm spiral is a clear difference between the observations of grand-design spirals and the simulations of Englmaier & Shlosman (2000), who only produce the two-arm spiral. This difference may be due to the use of a single sound speed to characterize the ISM in their simulations as filamentary structure is seen in multiphase ISM models (Wada & Norman 1999, 2001). Filamentary structure is also seen in multiphase ISM models which include a weak bar potential (Wada & Koda 2001), where the introduction of a multiphase ISM causes smooth spiral shocks to break down into parsec-scale, fine structure.

A second trend apparent in the nuclear class distribution is that the tightly wound nuclear spiral class appears to be much more common in unbarred galaxies than barred galaxies. There are eight unbarred galaxies with tightly wound nuclear spirals, or 26% of the sample, yet only three barred galaxies, or 4% of the sample, have tightly wound spirals. As barred galaxies outnumber unbarred galaxies by approximately three to one, and there was no obvious selection bias in favor or against circumnuclear structure in galaxies with or without large scale bars, this also appears to be real and not the spurious result of a combination of selection effects.

### 4.3. Nuclear Rings

In our sample of 123 galaxies we find 14 galaxies with a ringlike structure in the 20'' fields shown in Figure 1. Eight are cases of strong nuclear rings that have both current star formation and may also have an older stellar population. In these eight galaxies the basic morphology of the star formation and dust is the same: the star formation is clumpy and the star formation occurs outside of the dust ring. Five of the galaxies show the ring almost equally on both sides of the galaxy (NGC 1667, NGC 2273, NGC 3351, NGC 4314, and NGC 6951) and three galaxies (NGC 1672, NGC 5427, and NGC 6890) show the star formation clearer on one side of the galaxy and the dust clearer on the other side of the galaxy. In all the cases, the dust morphology is clumpy with the dust fragments implying a spiral-like shape. The sense of the spiral pattern in the dust is in the same sense as the rotation of the nuclear ring, assuming that the gas in the bar dust lanes curves into the rings (Piner, Stone & Teuben 1995). There also seems to be a tendency for the most active region of star formation to be between the dust ring and where the bar dust lanes joins the nuclear ring.

Four additional galaxies appear to have old stellar rings that are visible in both the *V* and *H* images. Two of these rings do not appear to have any associated dust: ESO138-G1 and Mrk 477, and two have dust lanes immediately interior to the ring: NGC 1300 and NGC 3081. The final two galaxies have bright star formation rings, one a very small nuclear starburst ring in NGC 864 and the other the larger starburst ring in NGC 7469. The properties of the galaxies with rings are summarized in Table 4 and additional information for several of these rings, many of which were previously studied from the ground by Buta & Crocker (1993), are provided in the Appendix.

## 5. Summary

We have presented *HST* observations of circumnuclear dust structure in a large sample of nearby galaxies. The color maps which trace this dust structure show that the nuclear dust spirals reported previously are the most common morphological feature in the circumnuclear region of spiral galaxies, irrespective of the presence or absence of an active nucleus or a large-scale bar. We have defined a set of four different classes of nuclear spiral structure that together encompass the main morphological features of nuclear spiral structure. There are in addition many galaxies that show no evidence of nuclear spiral structures and these galaxies have either very chaotic circumnuclear dust or no clearly discernible dust structure in their circumnuclear environment.

While the entire sample is too heterogeneous for a detailed examination of the frequency of nuclear spiral structure in active and inactive galaxies beyond the statement that it is a common feature of both types, there are several results, including two clear differences between barred and unbarred galaxies, that should not be affected by the various selection effects in this sample:

1. Only galaxies with large scale bars exhibit grand design nuclear spiral structure. Where high-quality data on larger scales is available, the two arms of the grand design nuclear spiral connect to the dust lanes on the leading edges of the large scale bar. As these cases demonstrate that some large scale bars can remove sufficient angular momentum to transport matter to within at least tens of parsecs of the nucleus, they provide qualitative support to the hypothesis that some large scale bars can directly fuel nuclear activity. However, these dust lanes are also found in galaxies that are not known to harbor AGN.
2. Tightly wound nuclear spiral arms are more likely to be found in unbarred galaxies than barred galaxies.
3. Several active galaxies with prominent ionization cones, most notably Mrk 573, Mrk 1066, and NGC 788, show that the emission line gas is the same material that forms the spiral dust lanes in the circumnuclear region. These dust lanes, traced by their absorption of stellar light, become bright emission regions where they cross the opening angle of the ionization cone from the nucleus.

In a future paper we will compare a subsample of active galaxies to an inactive, control sample matched in Hubble type, luminosity, heliocentric velocity, size, and inclination to determine if there are any differences in the circumnuclear dust structures between active and inactive galaxies. We will also employ a similar sample-matching strategy to verify these differences between the circumnuclear dust structures of barred and unbarred galaxies to extend the results described above.

Support for this work was provided by NASA through grant numbers SN-7330, GO-7867, and SN-8597 from the Space Telescope Science Institute, which is operated by the Association of Universities for Research in Astronomy, Inc., under NASA contract NAS5-26555. PM was supported by a Carnegie Starr Fellowship. We acknowledge several suggestions from the referee that have improved this manuscript, and thank Witold Maciejewski for some helpful comments. This research has made use of the NASA/IPAC Extragalactic Database (NED) which is operated by the Jet Propulsion Laboratory, California Institute of Technology, under contract with the National Aeronautics and Space Administration.

### A. Notes on Individual Objects

Below we provide details on why we applied a particular classification to each galaxy, whether or not the final classification was very uncertain, and note other interesting features in the circumnuclear dust structure.

ESO137-G34 (HI) – This Seyfert 2 is too highly inclined for an accurate classification, but it appears to possess a great deal of chaotic, circumnuclear dust including a dust lane extending across the images. The emission studied by Ferruit, Wilson, & Mulchaey (2000) is also clearly visible in the color map.

ESO138-G1 (C) – The most prominent feature of this galaxy is the smooth stellar ring, first observed by Ferruit, Wilson, & Mulchaey (2000), with a radius of approximately 1.1 kpc. There are no young star clusters or other structures in the ring. The bright, blue emission to the immediate southeast of the nucleus was studied by Ferruit, Wilson, & Mulchaey (2000) who argue that it is either scattered nuclear light from the Seyfert 2 nucleus or produced by young, hot stars.

IC2560 (LW) – The loosely wound nuclear dust spiral within the central 500 parsecs appear to form two, resolved dust arms that connect to the large scale bar. The white circle immediately south of the nucleus is the NIC2 coronagraphic spot.

IC5063 (C) – Although the circumnuclear dust structure is classified as chaotic, the straight dust lanes crossing to the north of the nucleus suggest that they could have a spiral morphology if viewed at a smaller inclination. Host galaxy dust may be responsible for its Seyfert 2 classification as the peak nuclear brightness in  $V$  and  $H$  are not coincident. There are also pronounced ionization cones extending to the east and west of the nucleus.

IC5267 (C) – There is a straight, north-south dust lane that crosses within  $1''$  of the nucleus and extends for over a kiloparsec. This dust lane and a neighboring feature with the same orientation give this galaxy its chaotic classification. These dust lanes appear similar to those expected in a nearly edge on galaxy, yet this galaxy is not highly inclined to the line of sight.

Mrk334 (LW) – While there is clear circumnuclear spiral morphology in this galaxy, its distance and bright nuclear source make it difficult to resolve structure within a few hundred parsecs of the nucleus.

Mrk461 (LW) – The coherence and pitch angle of the nuclear dust spirals make this a good example of a loosely wound nuclear spiral, although the contrast of the arms relative to the interarm region is not large. The nuclear spiral arms are more obvious on the near side than the far side of the galaxy.

Mrk471 (GD) – There are straight dust lanes along this galaxy’s large scale bar galaxy visible in both the  $V$  image and color map and they enter the circumnuclear region approximately perpendicular to the nuclear bar candidate discussed by Martini et al. (2001). The arms appear to curve inwards into a grand design nuclear spiral at these smaller scales, but the large distance of this galaxy precludes a detailed examination of the circumnuclear structure.

Mrk477 (LW) – This is one of the most distant galaxies in the sample and it is difficult to resolve much structure in the circumnuclear region. The loosely wound classification is based on much larger spatial scales than used for most of the galaxies and may not be representative of the circumnuclear structure.

Mrk573 (GD) – The grand design, nuclear dust spiral in this Seyfert is particularly striking as these dust lanes are lit up in emission where they cross the ionization cone from the active nucleus. The inner part of these spiral arms also appear to trace the leading edges of the nuclear bar, as discussed by Quillen et al. (1999) and Martini et al. (2001).

Mrk1066 (LW) – The peak brightness in the  $V$  and  $H$  images are slightly offset, which suggests that dust is obscuring the direct line of sight to the active nucleus. At larger scales these is a multiarm, flocculent spiral. The inner region of these dust lanes appears to be photoionized by the the AGN.

Mrk1210 (TW) – The tightly wound nuclear dust spiral is very regular and the individual dust lanes can be traced for over a full rotation about the nucleus.

NGC214 (LW) – There is a dramatic change in the dust structure between the central kiloparsec and larger scales. The circumnuclear region is relatively smooth except for a few dust lanes, while at larger scales the arms are much more fragmented, fill the galaxy disk, and have some associated star formation. The position angle of the ring-shaped transition region between the circumnuclear disk and larger scales is offset approximately 30 degrees from the position angle of the host galaxy.

NGC357 (N) – There is essentially no resolved circumnuclear dust in the central kiloparsec. While the nucleus is near the edge of the  $H$  image, the  $V$  image shows that the surface density is also smooth in the regions not visible in the color map. A few extremely low contrast dust features are present immediately south of the nucleus, but they are negligible compared to the contrast in any galaxy not in the N class.

NGC404 (C) – This LINER is one of the nearest galaxies in the sample and the  $H$  image has a mottled appearance due to the resolved giant stars. This complicates the identification of dust lanes and therefore the nuclear classification, but the dust distribution still appears chaotic. The  $V - I$  color map shown in Pogge et al. (2000) also supports this classification

and is less affected by resolved stars.

NGC628 (N) – While there is no evidence for dust structure within  $\sim 200$  pc of the nucleus, there are clear nuclear dust spirals at larger radii. If this galaxy were a factor of two or more distant, the empty central region might have been sufficiently poorly resolved to merit classification as a loosely wound or chaotic spiral.

NGC788 (LW) – There are some emission line regions in the central few hundred parsecs, and these emission structures are coincident with where the dust lanes cross the ionization cone.

NGC864 (LW) – There is a remarkably small circumnuclear starburst ring with a radius of slightly less than 100 parsecs. The blue light from this starburst appears to dominate the visible light from the nucleus.

NGC1068 (CS) – This extremely well-studied galaxy has numerous short dust lanes in a spiral pattern, but these arms do not have the coherence of the loosely wound nuclear spirals. We therefore classify this as a chaotic spiral.

NGC1144 (TW) – The large distance of this galaxy makes it difficult to classify the circumnuclear structure. On the observed scales, down to a limiting resolution of about 500 parsecs, it appears to be a tightly wound spiral.

NGC1241 (GD) – This is a well defined, if inclined, example of a grand design dust spiral. These arms appear to fragment somewhat in the central few hundred parsecs, although the main two arms are still visible down to these smallest scales.

NGC1275 (C) – There is a great deal of star formation in the circumnuclear region of this galaxy, as well as no coherent pattern to the dust.

NGC1300 (GD) – This very well known, strongly barred galaxy is one of the prototypes of the grand design nuclear dust spiral class. The dust lanes clearly connect to the dust lanes along the leading edges of the bar studied by Lindblad & Kristin (1996).

NGC1320 (HI/TW) – Although it is highly inclined, a tightly wound nuclear dust spiral is still clearly visible.

NGC1398 (N) – There is no dust structure at all and even the color map is extremely constant. The nucleus is only barely visible as a slightly bluer point on the otherwise flat color map.

NGC1530 (GD) – The classification for this galaxy is somewhat questionable. At large scales, down to approximately 500 parsecs, there is a grand design nuclear spiral and some

additional spiral arm fragments filling the rest of the circumnuclear disk. At smaller radii these arm fragments appear to have increasing contrast relative to the grand design spiral arms to the extent that it appears like a tightly wound spiral at the smallest radii.

NGC1638 (N) – There is no evidence for any dust structures within the central kiloparsec of this galaxy. Even at larger scales, there only appear to be a few small star formation regions with some associated dust.

NGC1667 (LW) – The star forming ring at approximately two kiloparsecs is composed of many spiral arm fragments intermixed with young star clusters. Inside of the ring the circumnuclear disk is substantially smoother and the few spiral dust lanes present do not fill the disk.

NGC1672 (LW) – The ring of star formation is crossed by many dust lanes. These dust lanes extend inwards into a loosely wound nuclear dust spiral that is significantly more prominent on the near side of the galaxy. The peak nuclear brightness is offset between the  $V$  and  $H$  images, which suggests that the Seyfert 2 classification may be due to dust obscuration.

NGC1961 (TW) – This peculiar galaxy has a multiarm, tightly wound nuclear spiral. There appear to be a few star clusters to the north of the nucleus, which may be the far side of the galaxy based on the contrast in the circumnuclear dust.

NGC2146 (C) – The many chaotic dust lanes in this galaxy are parallel to the semimajor axis of the host galaxy. While there are several sites of star formation, there is no obvious nucleus in the circumnuclear region.

NGC2179 (TW) – This is an excellent examples of a tightly wound nuclear dust spiral. It appears to begin as a two arm spiral near the nucleus, but then at larger scales the two dust lanes merge into a one arm spiral that remains coherent for at least three revolutions about the nucleus.

NGC2273 (CS) – The bright ring at the center, described by van Driel & Buta (1991), is clearly connected to dust lanes at larger radii. In the color map the emission line regions are not as prominent as in the  $V$  image, and the dust lanes do not form a coherent spiral. The narrowband images in Ferruit, Wilson, & Mulchaey (2000) clearly trace the line emission in this ring and show it is a star formation ring, rather an extended narrow line region.

NGC2276 (CS) – This is one of the galaxies in which we disputed the nuclear classification. There is only one obvious dust spiral arm in the  $V - H$  color map, although this is mostly because the nucleus is near the edge of the  $H$  image. The  $V$  image clearly shows several additional dust spiral arms to the south.

NGC2336 (C) – At large scales there is a clear, multiarm spiral, although within the central kiloparsec the dust is significantly less coherent. There are only a few, scattered dust lanes with low contrast that do not imply a sense of rotation and therefore this galaxy is not classified as a nuclear dust spiral.

NGC2460 (CS) – This galaxy has many scattered nuclear spiral features that do not maintain sufficient coherence to be classified as anything but a chaotic spiral.

NGC2639 (GD) – This is an excellent example of a grand design nuclear spiral, although the inclination of the host galaxy and dust geometry make the second spiral arm difficult to trace. As what few features present maintain the symmetry of the higher contrast arm, we classify this galaxy as a grand design spiral.

NGC2903 (C) – The well-known ‘hot spot’ galaxy has a large number of resolved circumnuclear star clusters, although there is only one dust lane with sufficient curvature to suggest spiral structure. Because there are no other, similar features, this is not classified as a nuclear dust spiral.

NGC2985 (TW) – This is one of the prototypes of the tightly wound nuclear spiral class and is also shown in Figure 33. While the nuclear spiral does appear to branch into additional dust lanes at larger radii, the main spiral arm remains coherent.

NGC3032 (LW) – This is one of the few examples of a nuclear dust spiral with associated star formation and there are several sites of star formation scattered throughout the circumnuclear disk. Given the high density of dust lanes, it is not possible to determine if these sites of star formation lead or trail the dust features, although the fact that they have the same pitch angle as the neighboring dust lanes suggests they are connected. The central region of the  $V$  image is saturated, although even outside this saturated region the circumnuclear disk is very blue.

NGC3079 (HI) – This well-known LINER is too highly inclined for any structure in the circumnuclear dust to be reliably classified.

NGC3081 (GD) – This is one of the best examples of a resonance ring galaxy known and the nuclear ring described by Buta & Purcell (1998) lies between the two Inner Lindblad Resonances. This ring is well-resolved as a dust ring in the color map and interior to the ring the dust lanes form a symmetric, two arm spiral. These dust lanes are somewhat unusual, however, as they appear to have nearly right angles where they meet the nuclear bar discussed by Wozniak et al. (1995) and Mulchaey, Regan, & Kundu (1997). Ferruit, Wilson, & Mulchaey (2000) suggest that there is star formation in both the nuclear ring and the two spiral arms.

NGC3145 (CS) – While classified as a chaotic spiral, this galaxy could also meet the criteria of the loosely wound spiral class. There are several spiral dust lanes that stretch completely across the color map, although since they extend off the color map it is not possible to trace out how long they remain coherent.

NGC3227 (C) – The nucleus in  $V$  is very saturated, although it is not so bright at  $H$  that it overwhelms the circumnuclear region. While there is considerable dust present, even down to small scales, it does not take an obvious spiral form.

NGC3300 (N) – The colormap for this early-type galaxy is completely featureless, with the exception of a faint and blue nuclear point source.

NGC3351 (C) – The bright starburst ring dominates the appearance of the circumnuclear region. Within the ring there is a great deal of dust structure, although it does not take on a spiral form.

NGC3362 (N) – While bright, starforming spiral arms are prominent at large scales, there are no obvious dust structures in the central kiloparsec. The only feature in the circumnuclear region is a blue structure in the colormap that is probably due to emission from the narrow line region.

NGC3368 (CS) – The dust lanes in this galaxy have very large pitch angles, although they are too incoherent to be classified as a loosely wound spiral.

NGC3393 (CS) – This galaxy has a spectacular, spiral-shaped ionization cone that appears morphologically similar to the one in Mrk 573 (Pogge 1997). Unfortunately, the NICMOS observation just missed the nucleus and the color map only shows half of the circumnuclear region. Based on this half, and the  $V$  image, there appears to be a nuclear spiral, although the contrast is insufficient to determine if the dust lanes and ionization cone are coupled as they are in Mrk 573.

NGC3458 (N) – The circumnuclear region is completely featureless and only shows a very faint and blue nuclear point source.

NGC3486 (LW) – While this galaxy appears to have a weak grand design spiral at larger radii, in the central hundred parsecs these dust lanes fragment into a multiarm spiral. This galaxy was therefore classified as a loosely wound, rather than grand design type.

NGC3516 (LW) – This bright AGN has a number of spiral dust arms to the north of the nucleus, along with several large, diffuse emission line regions at larger radii. To the south there is relatively little dust structure in the circumnuclear region, although this may be due to inclination.

NGC3627 (C) – The high inclination of this relatively nearby galaxy makes it difficult to discern the circumnuclear structure at distances much larger than a few hundred parsecs. The central region is dominated by several straight dust lanes that are parallel to the host galaxy semimajor axis.

NGC3718 (C) – The nucleus almost completely vanishes in the  $V - H$  color map, as also shown for  $V - I$  by Pogge et al. (2000), and the dust structure around the nucleus does not imply the presence of any center of symmetry.

NGC3786 (LW) – Most of the visible dust is in a fragmented set of spiral arms to the north of the nucleus and on the near side of the galaxy. In the immediate vicinity of the nucleus the circumnuclear region is relatively blue, which may be due to scattered light from the nucleus or an emission line region.

NGC3865 (CS) – The lack of any dust on the far side of the galaxy disk makes it difficult to determine the coherence of the dust lanes, although the large amount of fragmentation at approximately a kiloparsec from the nucleus suggests that this spiral is chaotic.

NGC3982 (GD) – There is a grand design nuclear spiral in the central kiloparsec, although some of the other spiral dust lanes in the circumnuclear region have nearly comparable contrast.

NGC4030 (TW) – This galaxy has a spectacular, tightly wound nuclear spiral that matches the criteria for acoustic turbulence extremely well as the dust spirals fill the disk at all radii and decrease in contrast near the nucleus. This is one of the prototypes of the tightly wound nuclear spiral class.

NGC4117 (LW) – The main, prominent dust lane parallel to the semimajor axis dominates the circumnuclear dust, yet at low contrast this arm appears to make an entire revolution about the nucleus. This galaxy is relatively highly inclined.

NGC4143 (LW) – The circumnuclear dust structure is very low contrast, yet at least three dust spirals are still visible. While no circumnuclear star formation is visible, the LINER nucleus is visible as a faint, blue point source.

NGC4151 (LW) – The bright nucleus in both  $V$  and  $H$  make it difficult to observe circumnuclear dust structure in the central hundred parsecs, yet at larger scales there are several spiral dust arms with large pitch angle.

NGC4253 (GD) – This is a Seyfert galaxy with grand design nuclear dust spirals extending to the unresolved nuclear region, although due to the distance and bright nuclear point source, the smallest resolved radii correspond to about 300 parsecs. The dust lanes along

the leading edge of the large scale bar, particularly to the east, show star formation in the dust lane along the bar. The presence of this star formation is characteristic of weak bars.

NGC4254 (CS) – Although some spiral structure is present, it is very chaotic. There is some circumnuclear star formation scattered between the dust spirals, but they are not obvious associated with them.

NGC4258 (HI) – The inclination of this galaxy is too high to classify the circumnuclear dust structure. The near side of the galaxy is obscured by a great deal of dust, while there is no clear dust structure visible on the far side. It is also sufficiently nearby that the giant stars are resolved, which give the color map its mottled appearance. The  $V - I$  color map shown in Pogge et al. (2000) is less affected by resolved stars and indicates structure is present in the circumnuclear emission-line gas.

NGC4260 (C) – Dust structures are visible in the circumnuclear region, but they are not of sufficient contrast to classify easily. Those present do not imply any sense of rotation; we therefore classify this as a chaotic spiral.

NGC4303 (GD) – The prominent grand design nuclear dust spirals connect to the dust lanes along the large-scale bar. As noted by Colina & Wada (2000), these two main dust spirals are composed of many smaller dust lanes and they find that the star formation in the circumnuclear disk is due to gravitational instabilities.

NGC4314 (LW) – Benedict (1993) have extensively studied this galaxy and its bright, star forming ring. The ring includes a great deal of dust interior to the star formation. At larger scales there are two dust lanes that extend to the large-scale bar, while interior to the ring there are a number of nuclear dust spiral arms with large pitch angle.

NGC4380 (CS) – The dust spirals in this galaxy appear very flocculent. There are spiral arm fragments throughout the circumnuclear region, yet they continuously cross one another and reconnect.

NGC4388 (HI/C) – While there is a copious amount of dust, the inclination is too great for a meaningful classification.

NGC4395 (C) – This galaxy is almost too nearby to classify. At  $H$  the brightest stars are resolved, while makes it difficult to trace the circumnuclear dust structure in the colormap. There are a few amorphous shapes, however, along with some emission coincident with the active nucleus and other star formation.

NGC4569 (C) – There are clear dust structures present, yet no obvious spiral structure and this may be due to the moderate inclination of the galaxy. Pogge et al. (2000) also noted

the chaotic circumnuclear dust in their  $V - I$  color map. The round feature to the upper right in the NIR image and colormap are due to the NIC2 coronagraph.

NGC4593 (TW) – This galaxy has a tightly wound, one-arm nuclear spiral. It is somewhat unusual in that no other dust features outside of the one dust spiral are visible in the central kiloparsec. The circle to the right in the  $H$  image and colormap is an artifact of the NIC2 coronagraph.

NGC4725 (C) – The nuclear dust structures are very low contrast in this galaxy and those visible do not form any obvious spiral pattern.

NGC4939 (C) – The narrow line emission extends to the east and west, nearly perpendicular to the galaxy’s semimajor axis. The straight dust lanes parallel to the semimajor axis extend across the frame, although the field of view is insufficient to see if they form any spiral structure.

NGC4941 (LW) – This is a prototype of the loosely wound spiral class and also illustrates the effect of galaxy inclination on the relative contrast between dust features on the near and far sides of the galaxy.

NGC4968 (C) – Any dust structure on the far side of the circumnuclear region is essentially washed out, and this makes it difficult to determine if the dust visible on the near side forms a spiral pattern. Southeast of the nucleus is a bluer region in the color map and this corresponds to the extended emission observed by Ferruit, Wilson, & Mulchaey (2000), which may be the ionization cone.

NGC5005 (C) – CO observations by Sakamoto, Baker, & Scoville (2000) of this highly inclined LINER find  $10^9 M_{\odot}$  of gas within the central five arcseconds and both the  $V - H$  and the  $V - I$  color map of Pogge et al. (2000) show that there is a large amount of chaotic, circumnuclear dust. The nucleus at  $V$  is very indistinct, although the  $H$  band image shows that the nucleus is approximately coincident with the northernmost emission feature at  $V$ . The peak at  $H$  is still south of the location of the radio and CO peak shown by Sakamoto, Baker, & Scoville (2000).

NGC5033 (C) – While this galaxy was considered to have a nuclear dust spiral by Martini & Pogge (1999), inclination effects make it difficult to determine if these dust lanes actually form spiral structure.

NGC5054 (LW) – There is some star formation in the circumnuclear disk, particularly to the south and west of the nucleus, but these star formation regions are not obviously associated with any of the many nuclear dust spirals.

NGC5064 (TW) – In spite of its relatively high inclination, the tightly wound nuclear dust spiral is apparent on both the near and far side of the circumnuclear disk.

NGC5135 (GD) – There is a clear, grand design spiral at larger radii with some associated star formation along the leading edges of the dust arms. This star formation suggests that the bar is relatively weak (Athanasoula 1992). Within the central kiloparsec the spiral becomes much less ordered and the classification is consequently more uncertain. There also appears to be a great deal of circumnuclear star formation.

NGC5252 (CS) – This colormap is relatively low signal to noise outside of the central kiloparsec, yet two spiral arm fragments are visible within the circumnuclear region. The structure map shown in Pogge & Martini (2002) shows that this chaotic spiral has a flocculent form. There is also a small emission region to the immediate northeast of the nucleus.

NGC5256 (C) – This chaotic, interacting system has no organized structure in the circumnuclear dust. The peak nuclear brightness at  $V$  and  $H$  are offset, which suggests the line of sight to the nucleus may be completely obscured at  $V$ .

NGC5273 (CS) – The small nuclear spiral in this galaxy almost takes the form of a nuclear dust ring, although the arms do not quite form a circle. There are also some low contrast dust features at larger radii.

NGC5283 (CS) – There is very little circumnuclear dust present and the central several hundred parsecs are dominated by emission regions. At slightly larger radii there are some dust structures to the south of the nucleus.

NGC5347 (GD) – The two, symmetric dust lanes form a very well-defined grand design nuclear dust spiral, although the modest distance and Seyfert nucleus obscure these dust lanes before they make a full revolution about the nucleus.

NGC5383 (GD) – This galaxy, studied in detail by Sheth et al. (2000), has a grand design nuclear dust spiral that gradually decreases in prominence at smaller radii. There is a great deal of star formation associated with the dust lanes as they emerge from the inner edge of the large scale bar, particularly to the south, which suggests a weak bar (Athanasoula 1992).

NGC5427 (LW) – This galaxy is unusual as it appears to have star formation along the leading edges of a two arm, symmetric dust spiral. However, these arms are the continuation of the main disk, Sc grand design spiral pattern. Interior to these arms, at less than approximately 700 parsecs radius, there are four or five nuclear dust spirals and we therefore classify this galaxy as loosely wound, rather than grand design.

NGC5506 (HI/LW) – This galaxy has too high an inclination for reliable classification, although the dust lanes present to the south of the nucleus suggest a dust spiral.

NGC5548 (TW) – The extremely prominent nucleus of this Seyfert 1 at both  $V$  and  $H$  obscure the central five hundred parsecs with diffraction rings and other PSF artifacts. On larger scales, a tightly wound spiral is apparent and this spiral may change from a one arm to a two arm spiral at a radius of about a kiloparsec.

NGC5614 (TW) – The tightly wound nuclear dust spiral in the central kiloparsec becomes less coherent at larger radii and branches into additional spiral dust lanes.

NGC5643 (GD) – This well-defined, symmetric grand design nuclear dust spiral is another prototype of its class. While there are other dust spirals present in the circumnuclear region, the two main dust arms are wider and have greater contrast. The peak of nuclear brightness at  $V$  and  $H$  are slightly offset from one another, which is presumably due to dust.

NGC5674 (CS) – There appears to be a blue, barlike feature oriented nearly east-west in the color map, however Martini et al. (2001) showed that this feature is not present at  $H$  and is likely an artifact of the two, prominent dust lanes to the north and south of the nucleus.

NGC5691 (C) – This galaxy has a great deal of distributed, circumnuclear star formation, although very few dust lanes. The nucleus, even at  $H$ , is not distinct.

NGC5695 (LW) – This galaxy could arguably be also classified as a chaotic spiral as there are a number of dust lanes in the circumnuclear region with no connection to the curved dust lanes of the spiral.

NGC5929 (CS) – Most of the circumnuclear dust is amorphous, although there are two dust spirals to the south that imply the same sense of rotation.

NGC5953 (TW) – There are a large number of fragmented spiral dust arms with low pitch angle and unlike the other tightly wound nuclear dust spirals in the sample, these arms appear to have associated star formation.

NGC5970 (C) – This may be a nuclear dust spiral observed at sufficiently high inclination that the spiral shape is not apparent. There are a number of straight dust lanes parallel to the host galaxy semimajor axis, yet they do not obvious wrap around the nuclear region.

NGC6221 (CS) – The circumnuclear dust has a quite chaotic appearance, yet there are clear spiral arm fragments, particularly to the east. This galaxy is therefore one of our prototypes of the chaotic spiral class.

NGC6300 (C) – This galaxy is difficult to classify as the nucleus falls in a corner of the  $H$

image. There is a great deal of dust visible in the colormap, and the  $V$  image shows that this dust extends to the south, yet it is dominated by a large cloud of dust rather than any filamentary structure. A two arm spiral is apparent at larger scales than shown in these frames.

NGC6384 (C) – There is very little circumnuclear dust and the dust lanes are nearly straight. This may be due to inclination, but as only one of these dust lanes has any curvature it does not meet the requirements for a nuclear dust spiral.

NGC6412 (C) – There is a very bright, radial filament of star formation extending nearly due north of the nucleus and about 600 parsecs in length. The circumnuclear dust around it is very fragmented and it is not obviously associated with the star formation filament.

NGC6744 (C) – Because the nucleus is near the corner of the  $H$  image it is difficult to make out much structure in the circumnuclear region. There are several, distinct dust features, but they form no coherent structure.

NGC6814 (GD) – The grand design nuclear spiral is the most obvious feature in the circumnuclear region, although there are several additional dust lanes at larger radii. This is unusual as most of the grand design spirals are wider and higher contrast at larger radii and become fragmented closer to the nucleus.

NGC6890 (GD) – This is another prototype of the grand design nuclear spiral class and it illustrates the effect of inclination in enhancing and suppressing the dust contrast on the near and far sides of the galaxy, respectively.

NGC6946 (C) – There is a great deal of dust in the circumnuclear region of this spiral galaxy, yet no spiral pattern. This galaxy is one of the prototypes of the chaotic class.

NGC6951 (LW) – This galaxy has two dust lanes along its large scale bar and the southern one is clearly visible in the color map. The dust lanes end at the circumnuclear starburst ring, however, and inside of the ring there appears to be a loosely wound spiral rather than a grand design. This galaxy is a prototype of the loosely wound nuclear spiral class.

NGC7096 (N) – There may be two, very low contrast dust lanes in the central kiloparsec, although these features are much weaker than for the other galaxies with clear, circumnuclear dust structure. The nucleus is visible as a very faint, blue point source.

NGC7126 (TW) – While the tightly wound nuclear dust spiral is lower contrast on the far side of the galaxy, the dust lanes are still visible for several rotations about the nucleus.

NGC7130 (GD) – This is a good example of a galaxy whose large scale bar is clearly transporting material to within several hundred kiloparsecs of the nucleus. The dust lanes from

the large scale bar have some star formation on their leading edges, indicative of a weak bar, and there appear to be several knots of star formation in the very center.

NGC7177 (CS) – Almost all of the circumnuclear dust structures are to the south of the nucleus and several of the dust lanes imply the same sense of rotation.

NGC7392 (LW) – The symmetric, two arm nuclear dust spiral suggests appears similar to the grand design nuclear spiral class, yet these two dust arms are not higher contrast than other dust lanes in the circumnuclear region.

NGC7469 (TW) – The most noticeable feature of this galaxy is the bright circumnuclear starburst ring, followed by the prominent Seyfert 1 nucleus. Outside of the ring there is a tightly wound nuclear dust spiral, although it is difficult to determine if this structure continues inside the ring.

NGC7496 (C) – There is a hint of a spiral dust arm to the southeast, yet the remainder of the circumnuclear region is sufficiently amorphous that we classify it as chaotic.

NGC7582 (HI/C) – There is a great deal of star formation in the central kiloparsec, although the high inclination makes it difficult to determine whether or not the star formation is connected to the dust lanes.

NGC7674 (GD) – There are two clear dust lanes entering the circumnuclear region from the large scale bar, yet the great distance and bright nuclear point source makes it difficult to resolve dust lanes in the central kiloparsec, although they appear to have a slight curve at the smallest radii observable.

NGC7682 (LW) – It is difficult to reliably classify this galaxy due to its large distance. There are two weak dust arms that hint at a grand design structure, but due to their low contrast and absence of obvious symmetry we classify it as loosely wound. The ionization cones extending to the north and south are quite obvious in the colormap as two blue cones.

NGC7716 (CS) – Because the nucleus is close to the edge of the  $H$  image it is difficult to get a detailed picture of the circumnuclear dust morphology. There is a weak spiral arm that extends to the north, although to the south there are only a few scattered dust clumps.

NGC7743 (LW) – There are several dust lanes with large pitch angle that imply the same sense of rotation, although these dust lanes do not appear to extend more than approximately 500 parsecs from the nucleus.

NGC7814 (HI) – This nearly edge on galaxy has a striking dust lane across the nucleus that remains prominent in the NIR.

UGC12138 (GD) – The two, curved dust lanes along the leading edges of the host galaxy bar curve inwards after half of a rotation about the circumnuclear region. Within the central several hundred parsecs the bright nuclear source obscures any smaller-scale structure.

UGC6100 (LW) – There are spiral dust lanes within the central two kiloparsec that form a coherent, loosely wound nuclear spiral. In the inner few hundred parsecs there is an emission line region that is probably associated with the narrow line region.

UM146 (LW) – The signal to noise in the  $H$  image makes it difficult to identify dust structures outside the central kiloparsec, but the circumnuclear region appears to be dominated by a two arm spiral. Because it is difficult to determine the symmetry of this spiral, it was not classified as a grand design nuclear spiral. The two arm spiral is more obvious in the structure map shown by Pogge & Martini (2002).

## REFERENCES

- Anderson, K.S. 1970, ApJ, 162, 743
- Athanassoula, E. 1992, MNRAS, 259, 345
- Benedict, G.F, et al. 1993, AJ, 105, 1369
- Bica, E. & Alloin, D. 1987, A&AS, 70, 281
- Bohuski, T.J., Fairall, A.P., & Weedman, D.W. 1978, ApJ, 221, 776
- Burbidge, E.M. & Burbidge, G.R. 1962, ApJ, 135, 694
- Buta, R. & Crocker, D.A. 1993, AJ, 105, 1344
- Buta, R. 1995, ApJS, 96, 39
- Buta, R. & Purcell, G.B. 1998, AJ, 115, 484
- Buta, R. & Block, D.L. 2001, ApJ, 550, 243
- Caldwell, N., Rose, J.A., & Dendy, K. 1999, AJ, 117, 140
- Capetti, A., Axon, D.J., Macchetto, F., Sparks, W.B., & Boksenberg, A. 1996, ApJ, 469, 554
- Carollo, C.M., Stiavelli, M., & Mack, J. 1998, AJ, 116, 68

- Ciardullo, R., Rubin, V.C., Ford, W.K., Jr., Jacoby, G.H., & Ford, H.C. 1988, *AJ*, 95, 438
- Colina, L. & Wada, K. 2000, *ApJ*, 529, 845
- Comte, G. & Duquennoy, A. 1982, *A&A*, 114, 7
- Cooke, A.J., Baldwin, J.A., Ferland, G.J., Netzer, H., & Wilson, A.S. 2000, *ApJS*, 129, 517
- da Costa, L.N., Pellegrini, P.S., Nunes, M.A., Willmer, C., & Latham, D.W. 1984, *AJ*, 89, 1310
- Dahari, O. 1985, *ApJS*, 57, 643
- de Bruyn, A.G. & Sargent, W.L.W. 1978, *AJ*, 83, 1257
- De Robertis, M.M., & Osterbrock, D.E. 1986, *ApJ*, 301, 98
- de Vaucouleurs, G., de Vaucouleurs, A., Corwin, H.G., Jr., Buta, R., Paturel, G., & Fouque, P. 1991, *Third Reference Catalogue of Bright Galaxies (New Your: Springer-Verlag) (RC3)*
- Eastmond, T.S. & Abell, G.O. 1978, *PASP*, 90, 367
- Elmegreen, D.M. & Elmegreen, B.G. 1984, *ApJS*, 54, 127
- Elmegreen, B.G., Elmegreen, D.M., Brinks E., Yuan, C., Kaufman, M., Klarić, M., Montenegro, L., Struck, C., & Thomasson, M. 1998, *ApJ*, 503, L119
- Elmegreen, D.M., Elmegreen, B.G., & Eberwein, K.S. 2002, *ApJ*, 564, 234
- Englmaier, P. & Shlosman, I. 2000, *ApJ*, 528, 677
- Fairall, A.P. 1986, *MNRAS*, 218, 453
- Fairall, A.P. 1988, *MNRAS*, 230, 69
- Ferrarese, L. & Merritt, D. 2000, *ApJ*, 539, L9
- Ferrarese, L., Pogge, R.W., Peterson, B.M., Merritt, D., Wandel, A., & Joseph, C.L. 2001, *ApJ*, 555, L79
- Ferruit, P., Wilson, A.S., & Mulchaey, J. 2000, *ApJS*, 128, 139
- Friedli, D. & Martinet, L. 1993, *A&A*, 277, 27
- Fukuda, H., Wada, K., & Habe, A. 1998, *MNRAS*, 295, 463

- Gebhardt, K. et al. 2000, ApJ, 543, L5
- Gebhardt, K. et al. 2001, AJ, 122, 2469
- Graham, J.A. et al. 1997, ApJ, 477, 535
- Hewitt, A. & Burbidge, G. 1991, ApJS, 75, 297
- Ho, L.C., Filippenko, A.V., & Sargent, L.W. 1997b, ApJS, 112, 315
- Hubble, E.P. 1943, ApJ, 97, 112
- Huchra, J.P., Wyatt, W.F., & Davis, M. 1982, AJ, 87, 1628
- Huchra, J., Davis, M., Latham, D., & Tonry, J. 1983, ApJS, 52, 89
- Huchra, J. & Burg, R. 1992, ApJ, 393, 90
- Keel, W.C., Kennicutt, R.C., Jr., Hummel, E., & van der Hulst, J.M. 1985, AJ, 90, 708
- Koski, A.T. 1978, ApJ, 223, 56
- Knapen, J.H., Beckman, J.E., Heller, C.H., Shlosman, I., de Jong, R. S. 1995, ApJ, 454, 623
- Krist, J.E. & Hook, R.N. 1999, The Tiny Tim User's Guide (Baltimore: STScI)
- Laine, S.; Knapen, J. H.; Perez-Ramirez, D.; Doyon, R.; Nadeau, D. 1999, MNRAS, 302, L33
- Laine, S., Shlosman, I., Knapen, J.H., & Peletier, R.F. 2002, ApJ, *accepted*
- Lindblad, P.A.B. & Kristen, H. 1996, A&A, 313, 733
- Lucy, L.B. 1974, AJ, 79, 745
- Maciejewski, W., Teuben, P.J., Sparke, L.S., & Stone, J.M. 2002, MNRAS, 329, 502
- Maiolino, R. & Reike, G.H. 1995, ApJ, 454, 95
- Malkan, M.A., Gorjian, V., & Tam, R. 1998, ApJS, 117, 25
- Markarian, B.E. 1977, A&A, 58, 139
- Martini, P. & Pogge, R.W. 1999, AJ, 118, 2646
- Martini, P., Pogge, R.W., Ravindranath, R. & An, J.H. 2001, ApJ, 562, 139

- Martini, P., Regan, M.W., Mulchaey, J.S., & Pogge, R.W. 2002, *ApJ*, *in preparation* (Paper II)
- Márquez, I. et al. 1999, *A&AS*, 140, 1
- Márquez, I. et al. 2000, *A&A*, 360, 431
- McElroy, D.B. 1983, *ApJ*, 270, 485
- McLeod, K.K. & Rieke, G.H. 1995, *ApJ*, 441, 96
- Montenegro, L.E., Yuan, C., & Elmegreen, B.G. 1999, *ApJ*, 520, 582
- Morris, M. & Serabyn, E. 1996, *ARA&A*, 34, 645
- Mulchaey, J.S., Wilson, A.S., & Tsvetanov, Z. 1996, *ApJS*, 102, 309
- Mulchaey, J.S. & Regan, M.W. 1997, *ApJ*, 482, 135
- Mulchaey, J.S., Regan, M.W., & Kundu, A. 1997, *ApJS*, 11, 299
- Oey, M.S. & Kennicutt, R.C. 1993, *ApJ*, 411, 137
- Osterbrock, D.E. & Dahari, O. 1983, *ApJ*, 273, 478
- Osterbrock, D.E. & Martel, A. 1993, *ApJ*, 414, 552
- Patsis, P.A. & Athanassoula, E. 2000, *A&A*, 358, 45
- Phillips, A.C., Illingworth, G.D., MacKenty, J.W., & Franx, M. 1996, *AJ*, 111, 1566
- Phillips, M.M. 1979, *ApJ*, 227, L121
- Phillips, M.M., Charles, P.A., & Baldwin, J.A. 1983, *ApJ*, 266, 485
- Piner, B.G., Stone, J.M. & Teuben, P.J. 1995, *ApJ*, 449, 508
- Pogge, R.W. & De Robertis, M.M. 2002, *ApJ*, 451, 585
- Pogge, R.W. 1997, in *Emission Lines in Active Galactic Nuclei: New Methods and Techniques*, ed. B.M. Peterson, F.-Z. Cheng, & A.S. Wilson, *ASP Conference Series*, 113, 378
- Pogge, R.W., Maoz, D., Ho, L.C., & Eracleous, M. 2000, *ApJ*, 532, 323
- Pogge, R.W. & Martini, P. 2002, *ApJ*, 569, *in press*

- Poulain, P., Nieto, J.-L., & Davoust, E. 1992, *A&AS*, 95, 129
- Prendergast, K.H. 1983, in *IAU Symp. 100, Internal Kinematics and Dynamics of Galaxies*, ed. E. Athanassoula (Dordrecht: Reidel), 215
- Quillen, A.C., Frogel, J.A., Kenney, J.D.P., Pogge, R.W., Depoy, D.L. 1995, *ApJ*, 441, 549
- Quillen, A.C., Alonso-Herrero, A., Rieke, M. J., McDonald, C., Falcke, H., & Rieke, G. H. 1999, *ApJ*, 525, 685
- Regan, M.W., Vogel, S.N., & Teuben, P.J. 1997, *ApJ*, 482, L143
- Regan, M.W. & Mulchaey, J.S. 1999, *AJ*, 117, 2676
- Richardson, W.H. 1972, *JOSA*, 62, 55
- Richstone, D.O., et al. 1998, *Nature*, 395, A14
- Saha, A. Sandage, A., Tammann, G.A., Labhardt, L., Macchetto, F.D. & Panagia, N. 1999, *ApJ*, 522, 802
- Sakamoto, K., Okumura, S.K., Ishizuki, S., & Scoville, N.Z. 1999, *ApJS*, 124, 403
- Sakamoto, K., Baker, A.J., & Scoville, N.Z. 2000, *ApJ*, 533, 149
- Sandage, A. 1978, *AJ*, 83, 904
- Sandage, A. & Bedke, J. 1994, *The Carnegie Atlas of Galaxies* (Publ. 638; Washington, DC: Carnegie Inst. Washington)
- Scoville, N.Z., Matthews, K., Carico, D.P., Sanders, D.B. 1988, *ApJ*, 327, L61
- Seyfert, C.K. 1943, *ApJ*, 97, 28
- Sheth, K., Regan, M.W., Vogel, S.N., & Teuben, P.J. 2000, *ApJ*, 532, 221
- Stauffer, J. 1982, *ApJ*, 262, 66
- Theureau, G., Bottinelli, L., Coudreau-Durand, N., Gouguenheim, L., Hallet, N., Loulergue, M., Paturel, G., & Teerikorpi, P. 1998, *A&AS*, 130, 333
- Thornley, M.D. 1996, *ApJ*, 469, 45
- Thronson, H.A., et al. 1989, *ApJ*, 343, 158

- Tonry, J.L., Dressler, A., Blakeslee, J.P., Ajhar, E.A., Fletcher, A.B., Luppino, G.A., Metzger, M.R., & Moore, C.B. 2001, *ApJ*, 546, 681
- Trager, S.C., Worthey, G., Faber, S.M., Burstein, D., & Gonzalez, J.J. 1998, *ApJS*, 116, 1
- Tsvetanov, Z. & Walsh, J.R. 1992, *ApJ*, 386, 485
- Tully, R.B. 1988, *Nearby Galaxies Catalog* (Cambridge: Cambridge Univ. Press)
- Tully, R.B., Shaya, E.J., & Pierce, M.J. 1992, *ApJS*, 80, 479
- Tully, R.B. Verheijen, M.A.W., Pierce, M.J., Huang, J.-S., & Wainscoat, R.J. 1996, *AJ*, 112, 2471
- van Dokkum, P.G. & Franx, M. 1995, *AJ*, 110, 2027
- van Dokkum, P.G. 2001, *PASP*, 113, 1420
- van Driel, W. & Buta, R.J. 1991, *A&A*, 245, 7
- Vaceli, M.S., Viegas, S.M., Gruenwald, R., & de Souza, R.E. 1997, *AJ*, 114, 1345
- Veron, M.P. 1981, *A&A*, 100, 12
- Veron-Cetty, M.-P., & Veron, P. 1986, *A&A*, 66, 335
- Virani, S.N., De Robertis, M.M., & Van Dalfsen, M.L. 2000, *ApJ*, 120, 1739
- Wada, K. & Norman, C.A. 1999, *ApJ*, 526, L13
- Wada, K. & Norman, C.A. 2001, *ApJ*, 547, 172
- Wada, K. & Koda, J. 2001, *PASJ*, 53, 1163
- Ward, M., Penston, M.V., Blades, J.C., & Turtle, A.J. 1980, *MNRAS*, 193, 563
- Wilson, A.S., Penston, M.V., Fosbury, R.A.E., & Boksenberg, A. 1976, *MNRAS*, 177, 673
- Wozniak, H., Friedli, D., Martinet, L., Martin, P., & Bratschi, P. 1995, *A&AS*, 111, 115
- Yahil, A., Tammann, G.A., & Sandage, A. 1977, *ApJ*, 217, 903
- Yuan, C., & Kuo, C.-L. 1998, *ApJ*, 497, 689

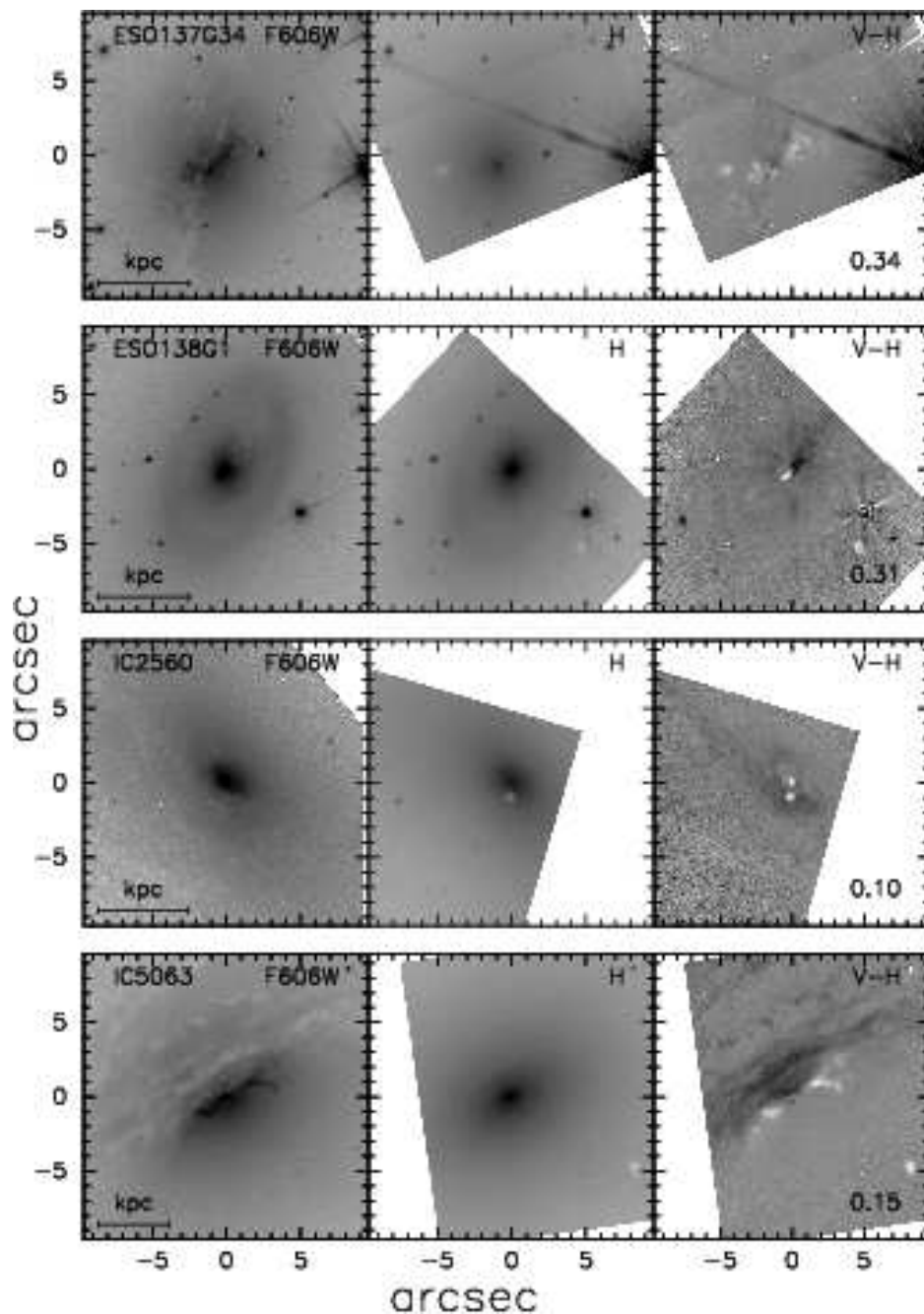


Fig. 1.—  $V$  and  $H$  images and  $V - H$  color maps of the galaxies, one galaxy per row. The  $V$  image was obtained through the WFPC2 filter named in the upper right of the left panel. The bar in the lower left of the left panel shows the projected spatial scale at the distance of the galaxy (for  $H_0 = 75 \text{ km s}^{-1} \text{ Mpc}^{-1}$ ). The middle panel shows the NICMOS F160W image. Those galaxies with smaller images were observed with Nicmos Camera 1; most galaxies were observed with Nicmos Camera 2. The right panel shows the  $V - H$  colormap, where dark on the greyscale corresponds to red and light to blue. All three panels are on a logarithmic greyscale, have a  $20''$  field of view, and are oriented such that North is up and East is to the left.

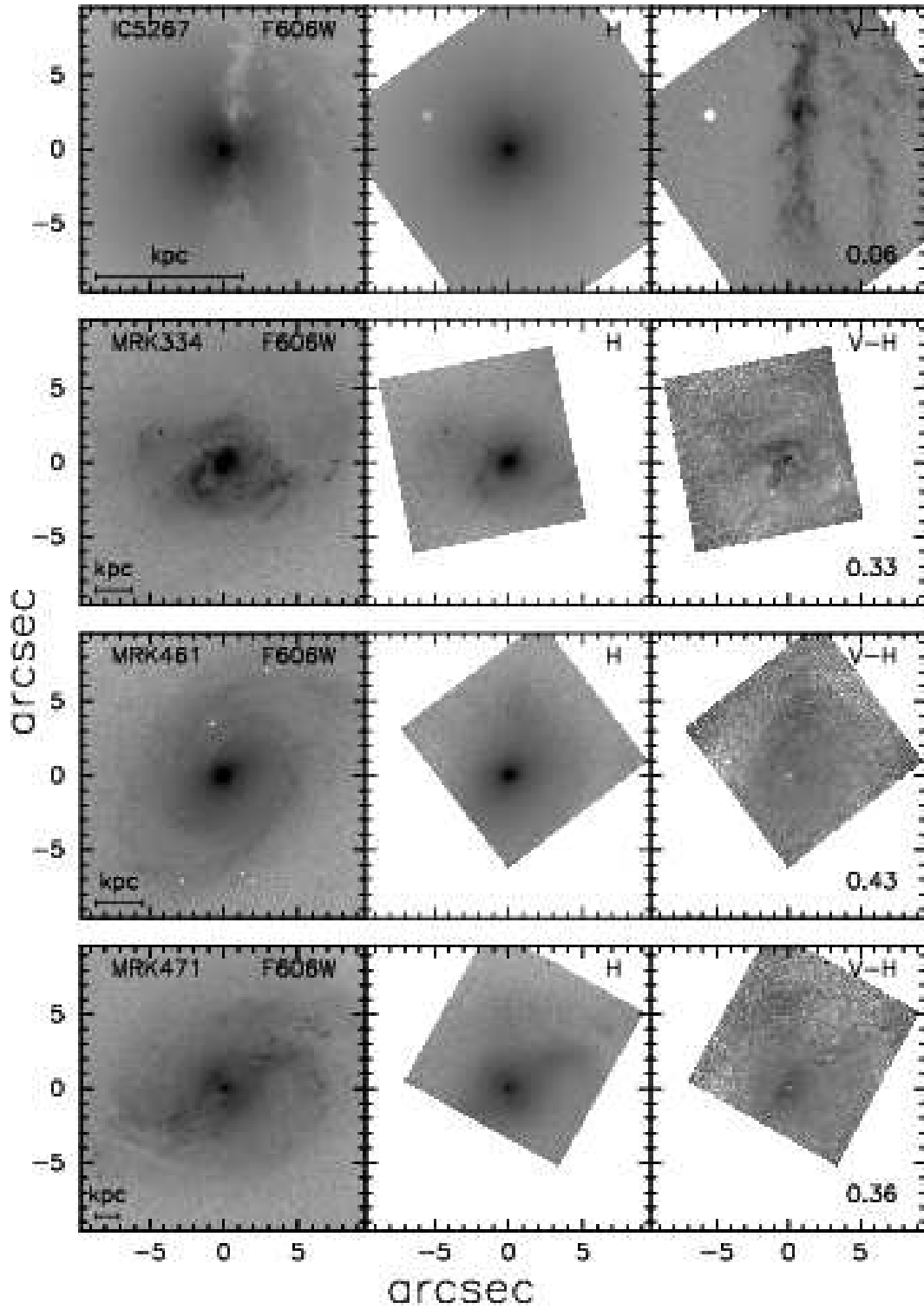


Fig. 2.— Figure 1 - *Continued*

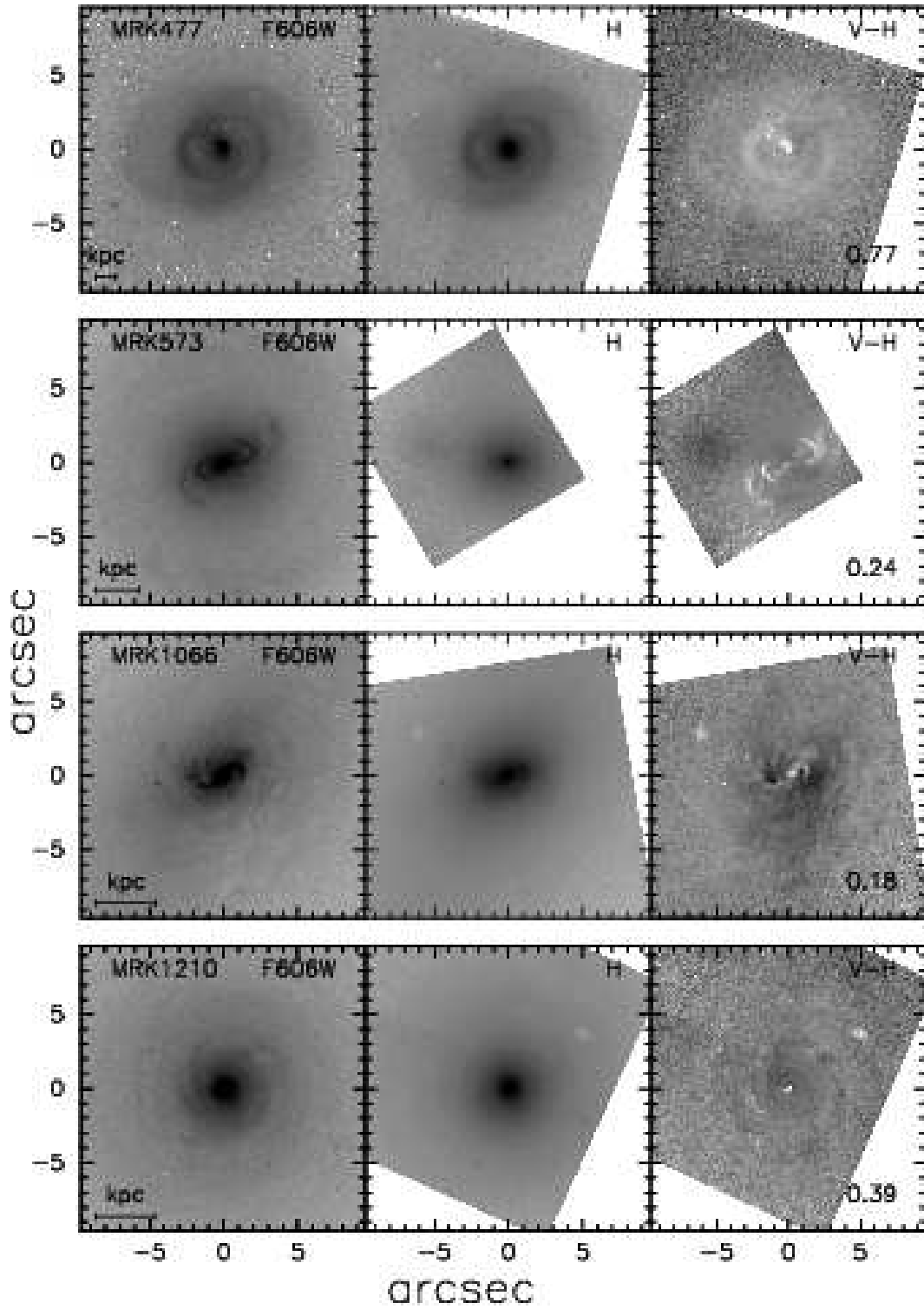


Fig. 3.— Figure 1 – *Continued*

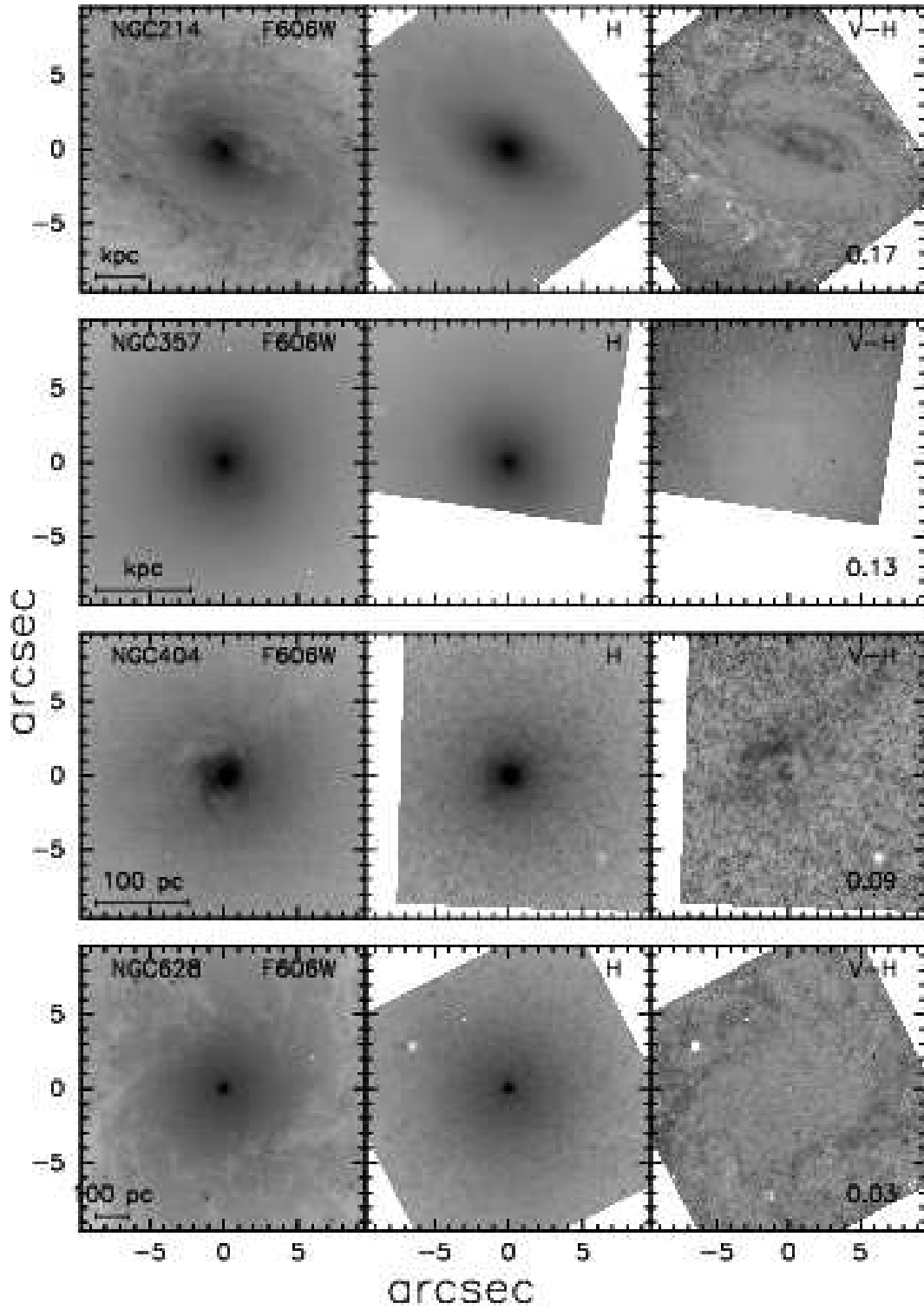


Fig. 4.— Figure 1 – *Continued*

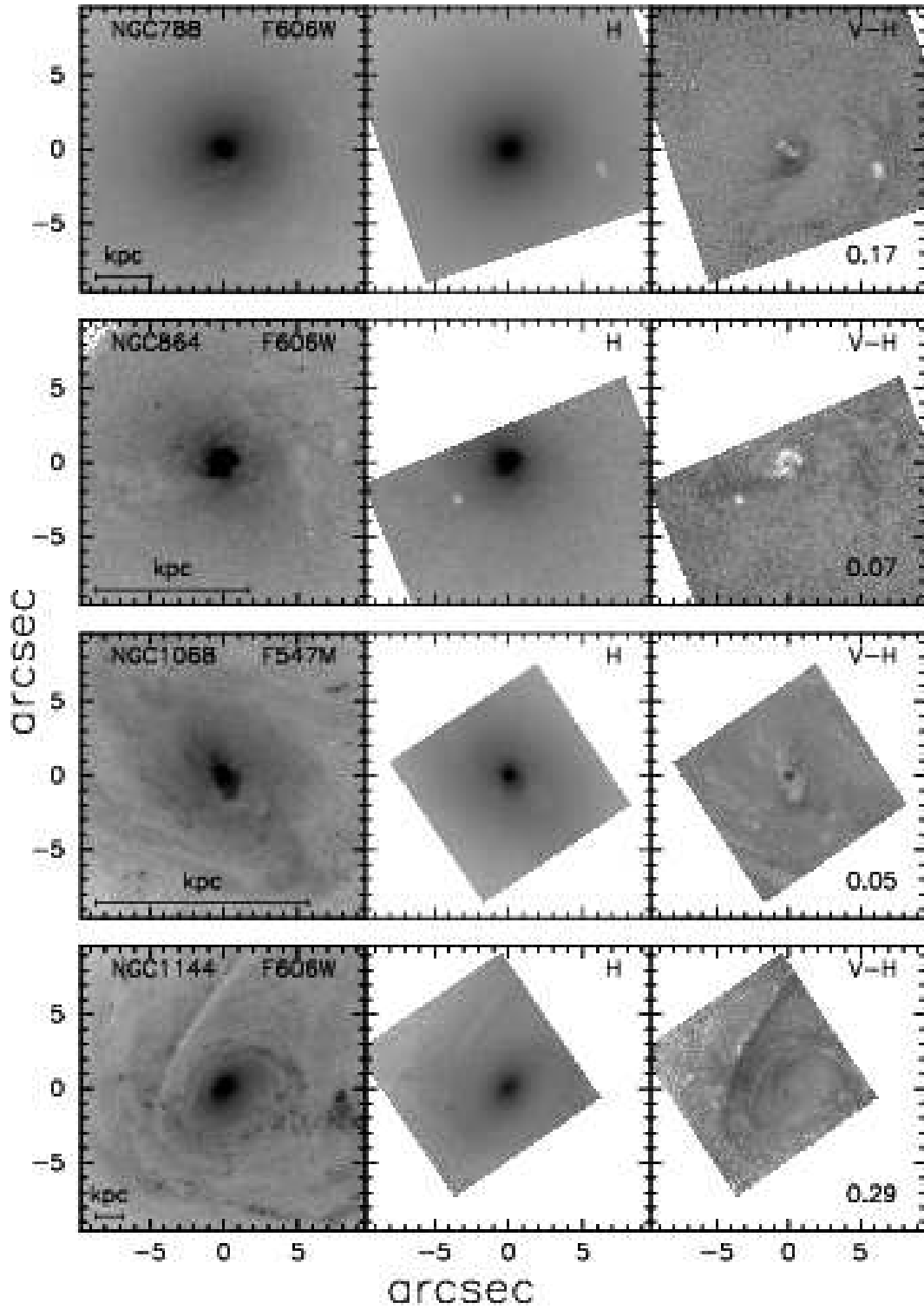


Fig. 5.— Figure 1 – *Continued*

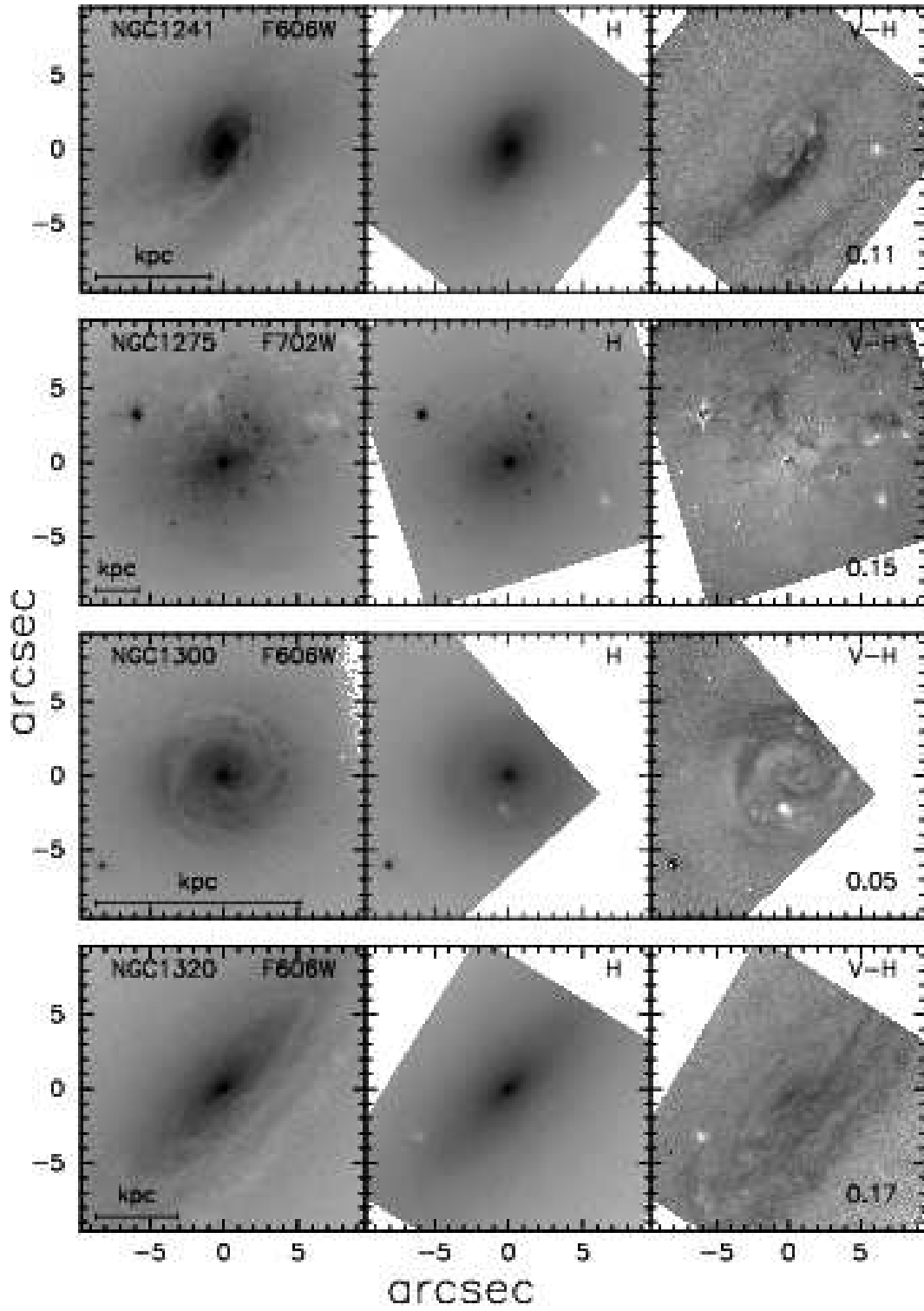


Fig. 6.— Figure 1 - *Continued*

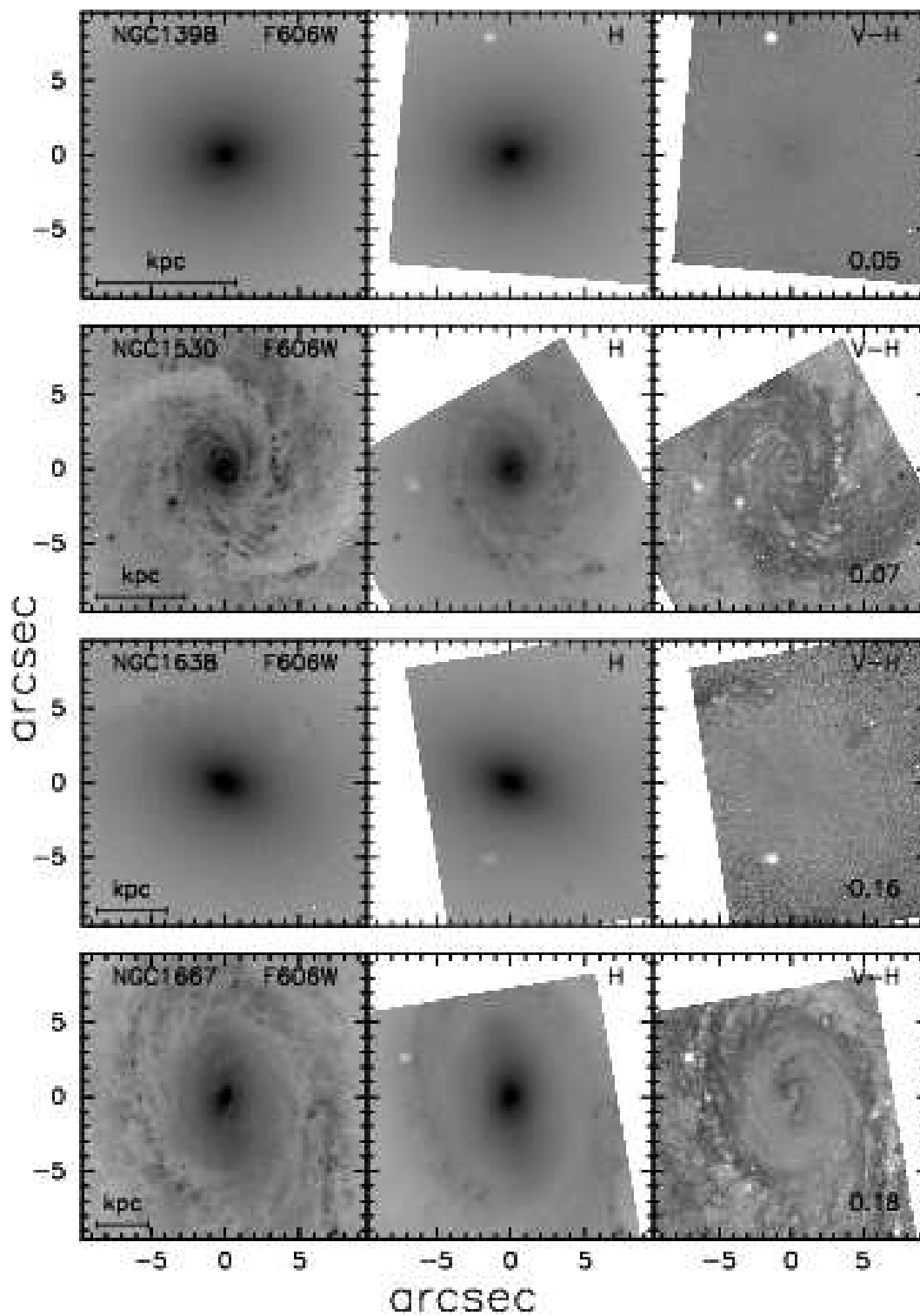


Fig. 7.— Figure 1 – *Continued*

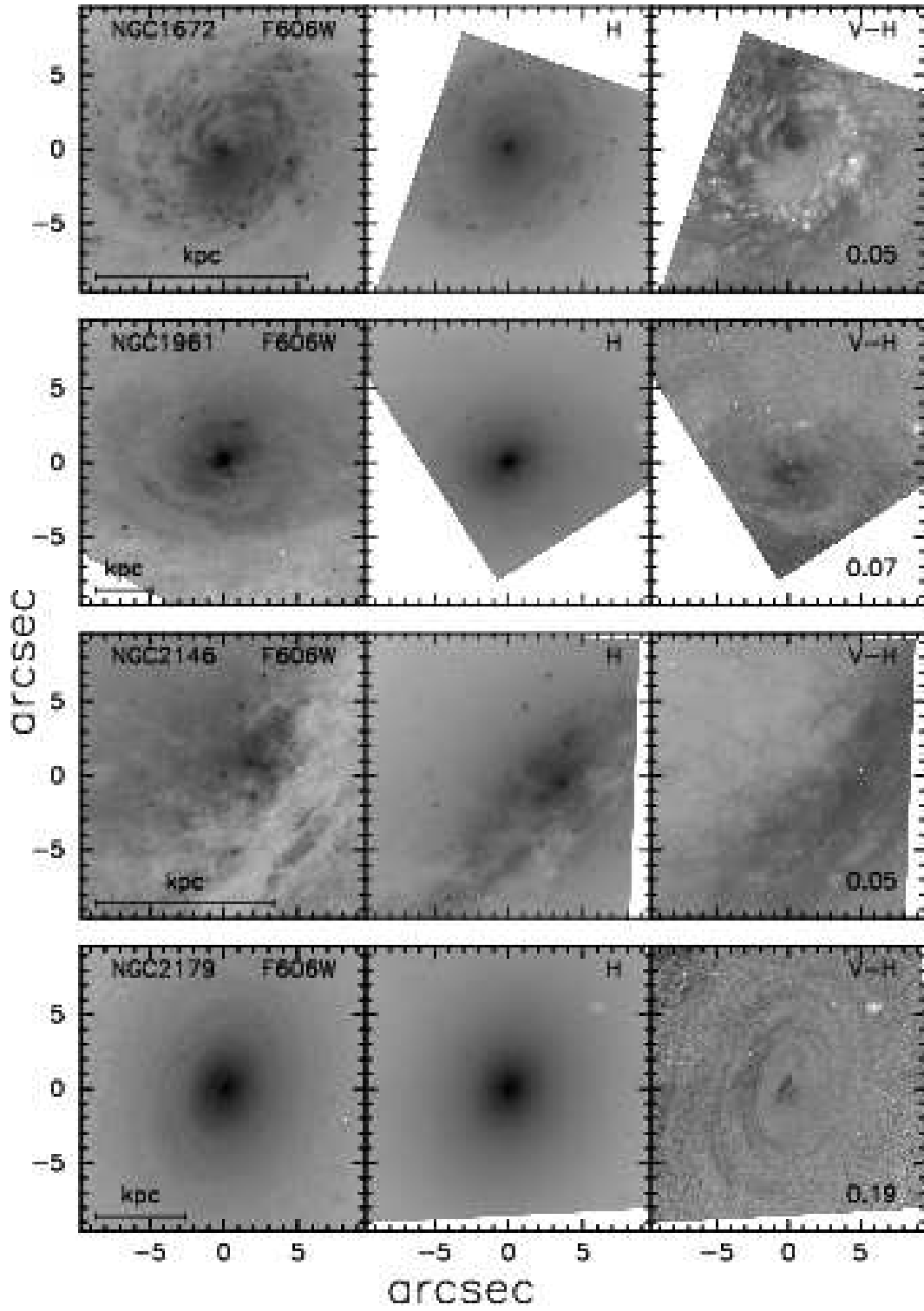


Fig. 8.— Figure 1 – *Continued*

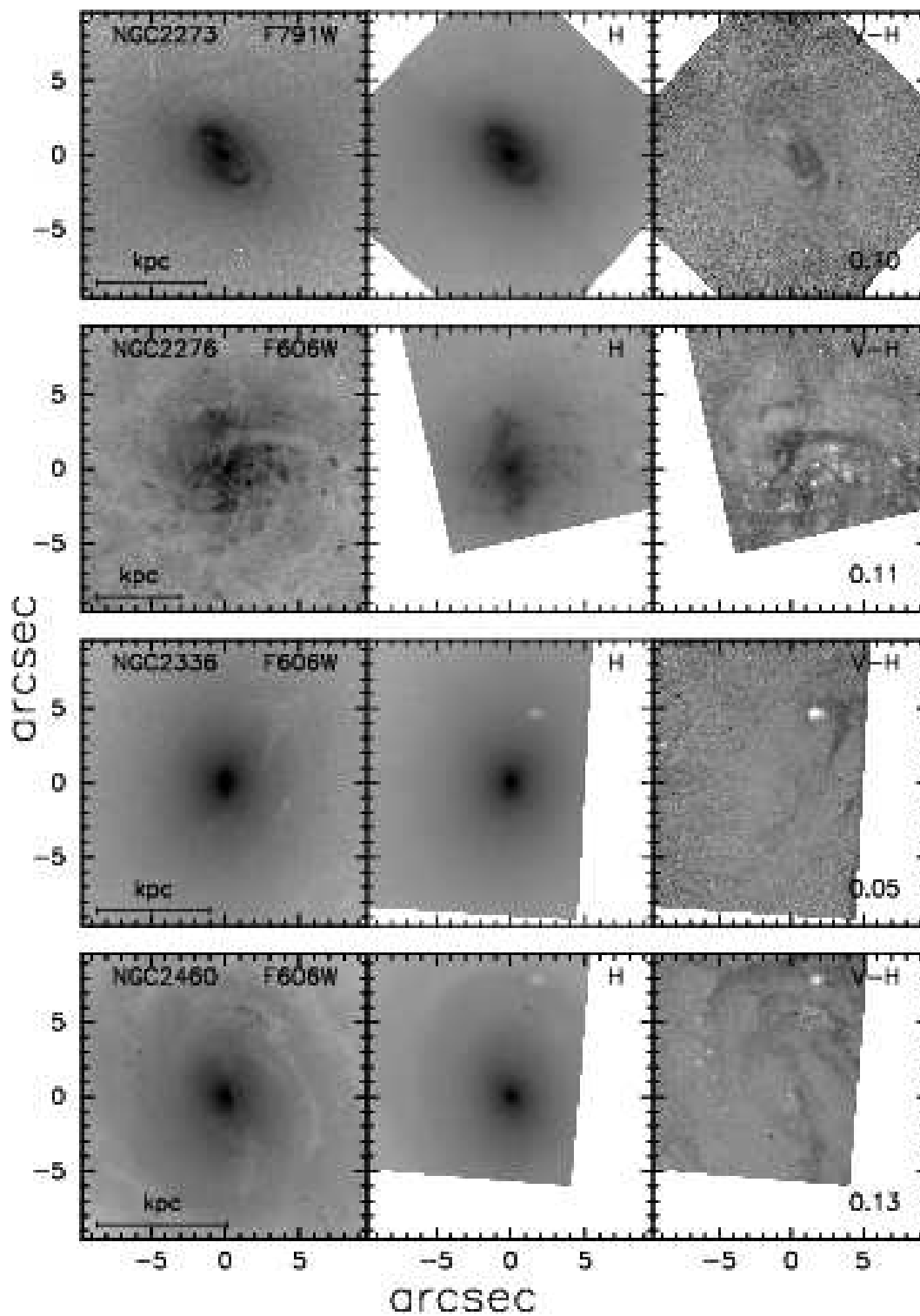


Fig. 9.— Figure 1 - *Continued*

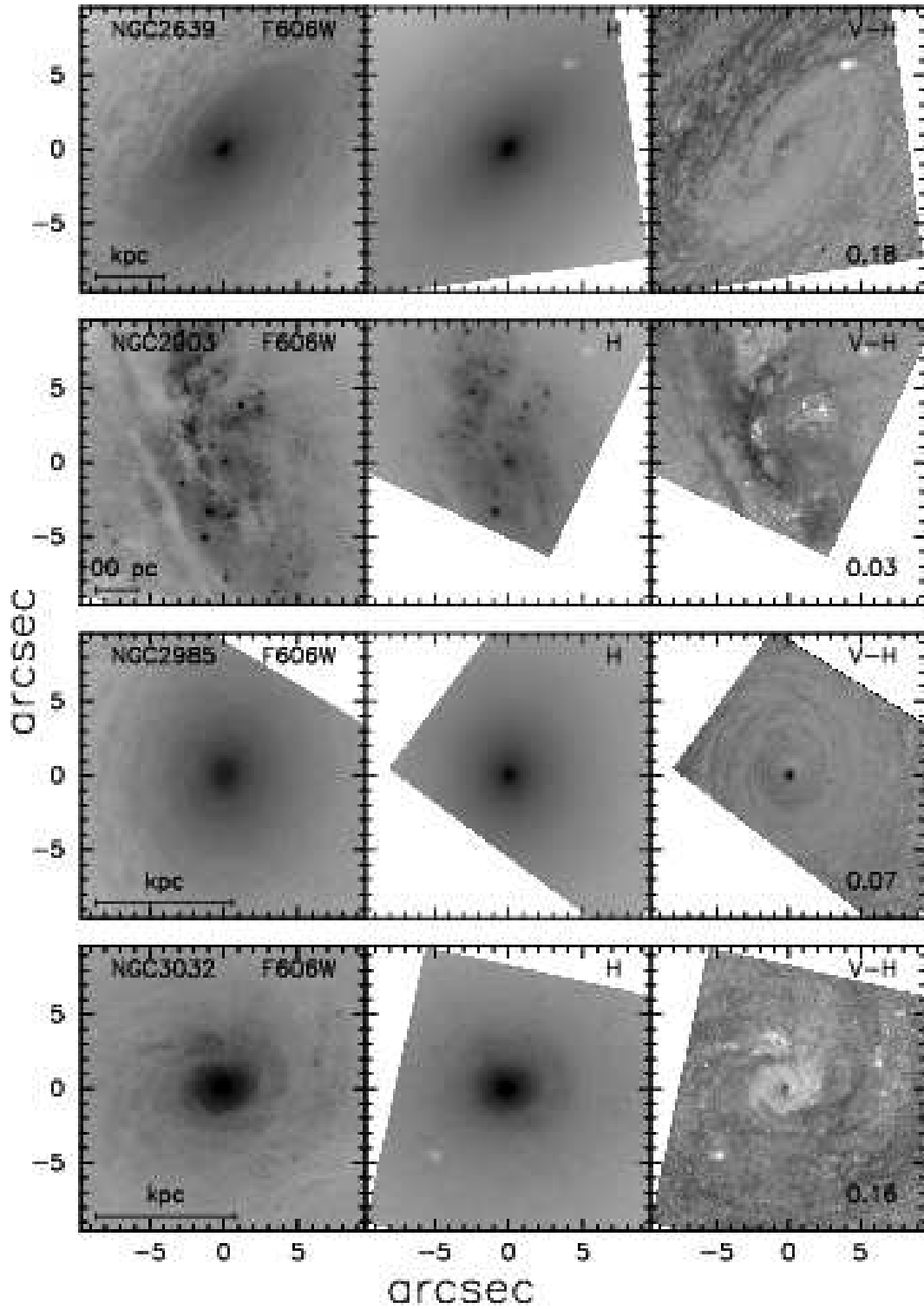


Fig. 10.— Figure 1 – *Continued*

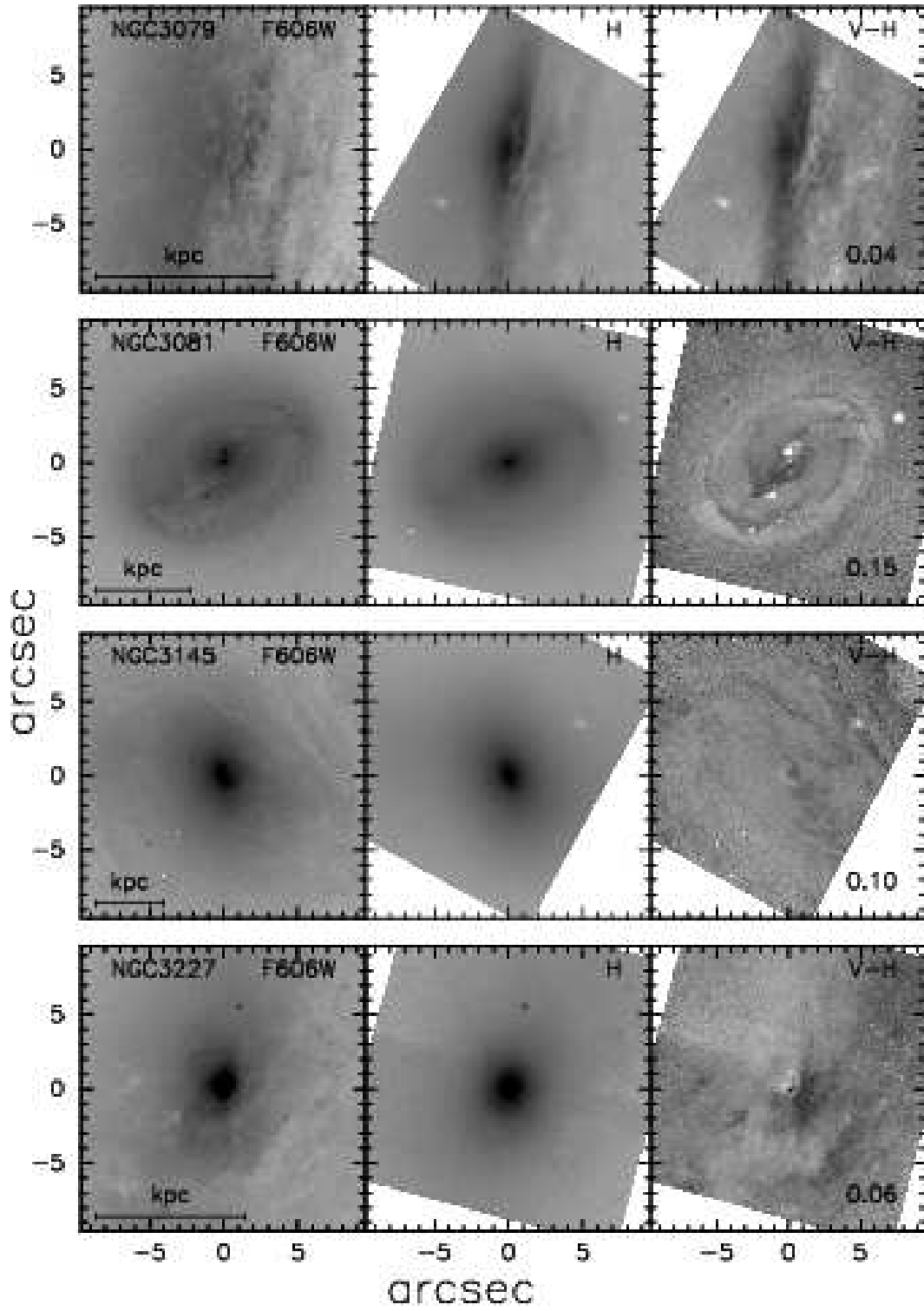


Fig. 11.— Figure 1 - *Continued*

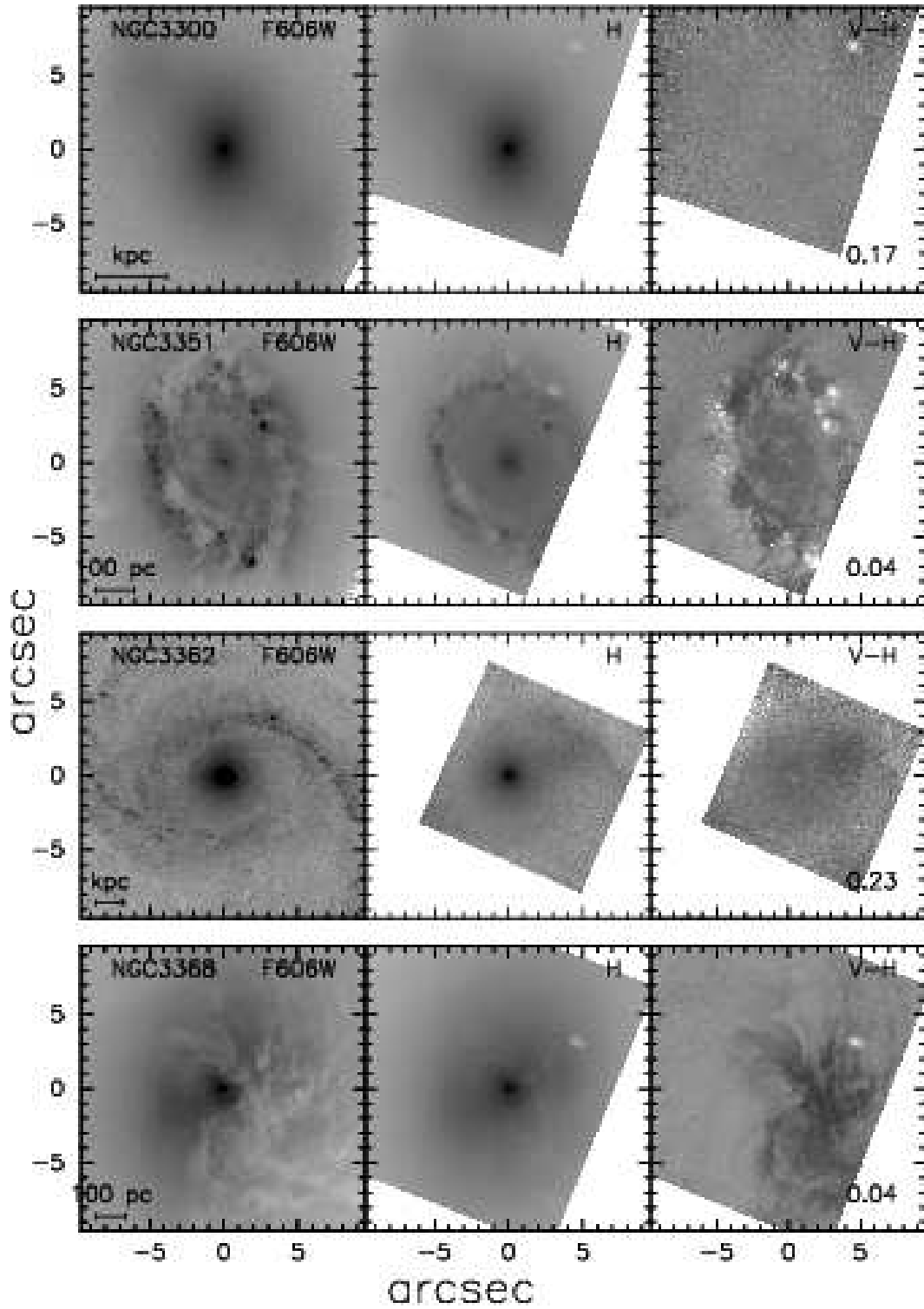


Fig. 12.— Figure 1 - *Continued*

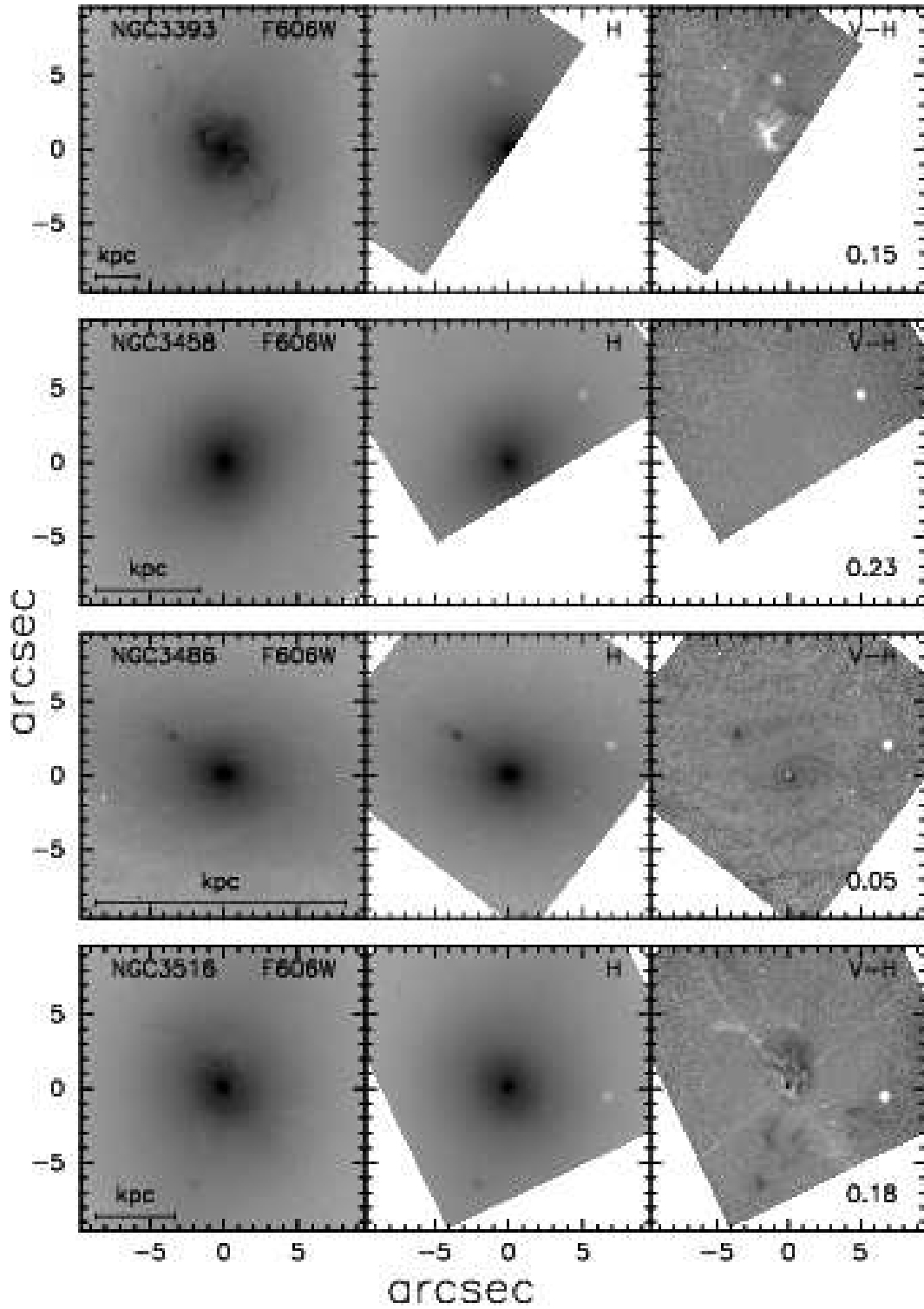


Fig. 13.— Figure 1 – *Continued*

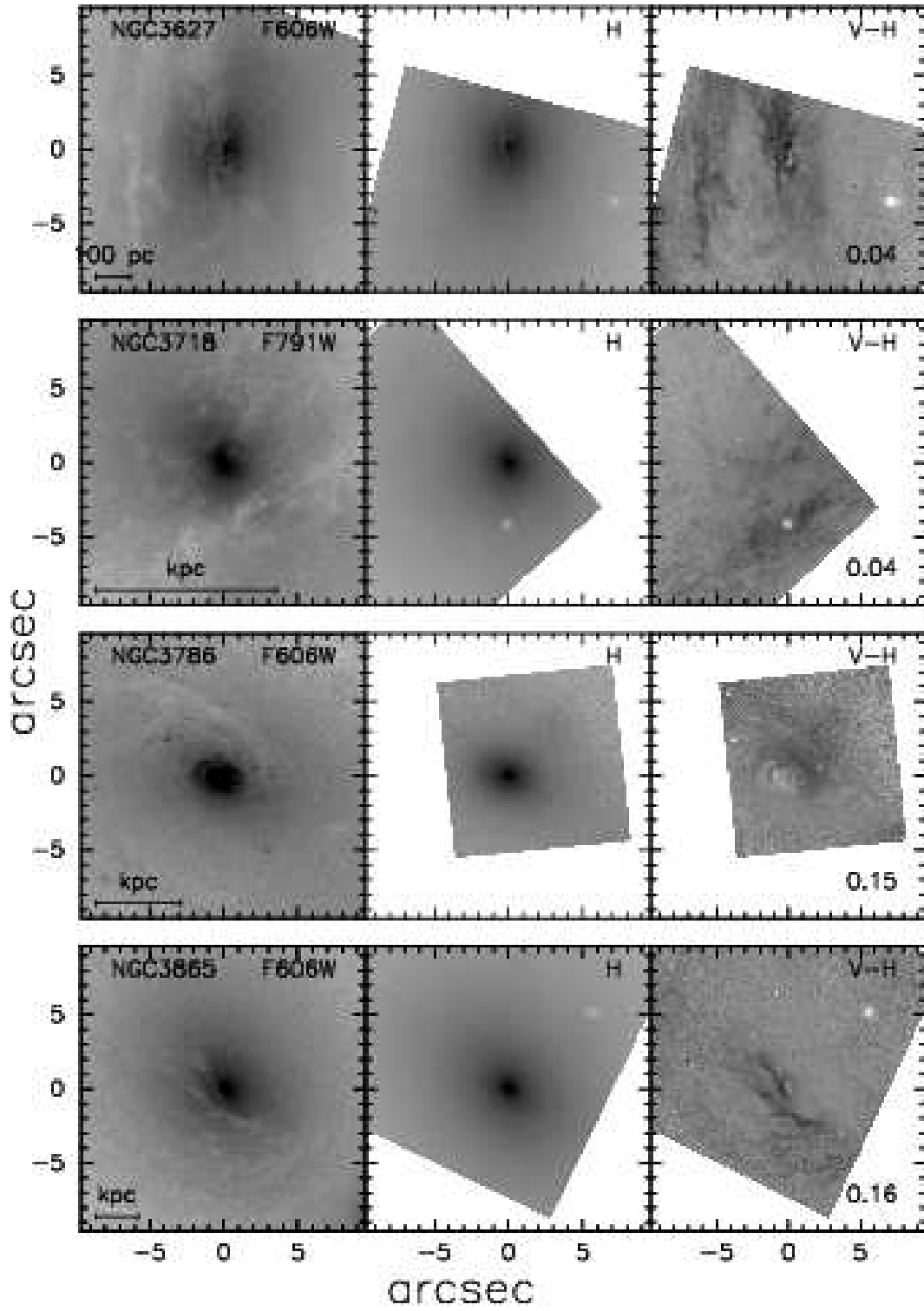


Fig. 14.— Figure 1 – *Continued*

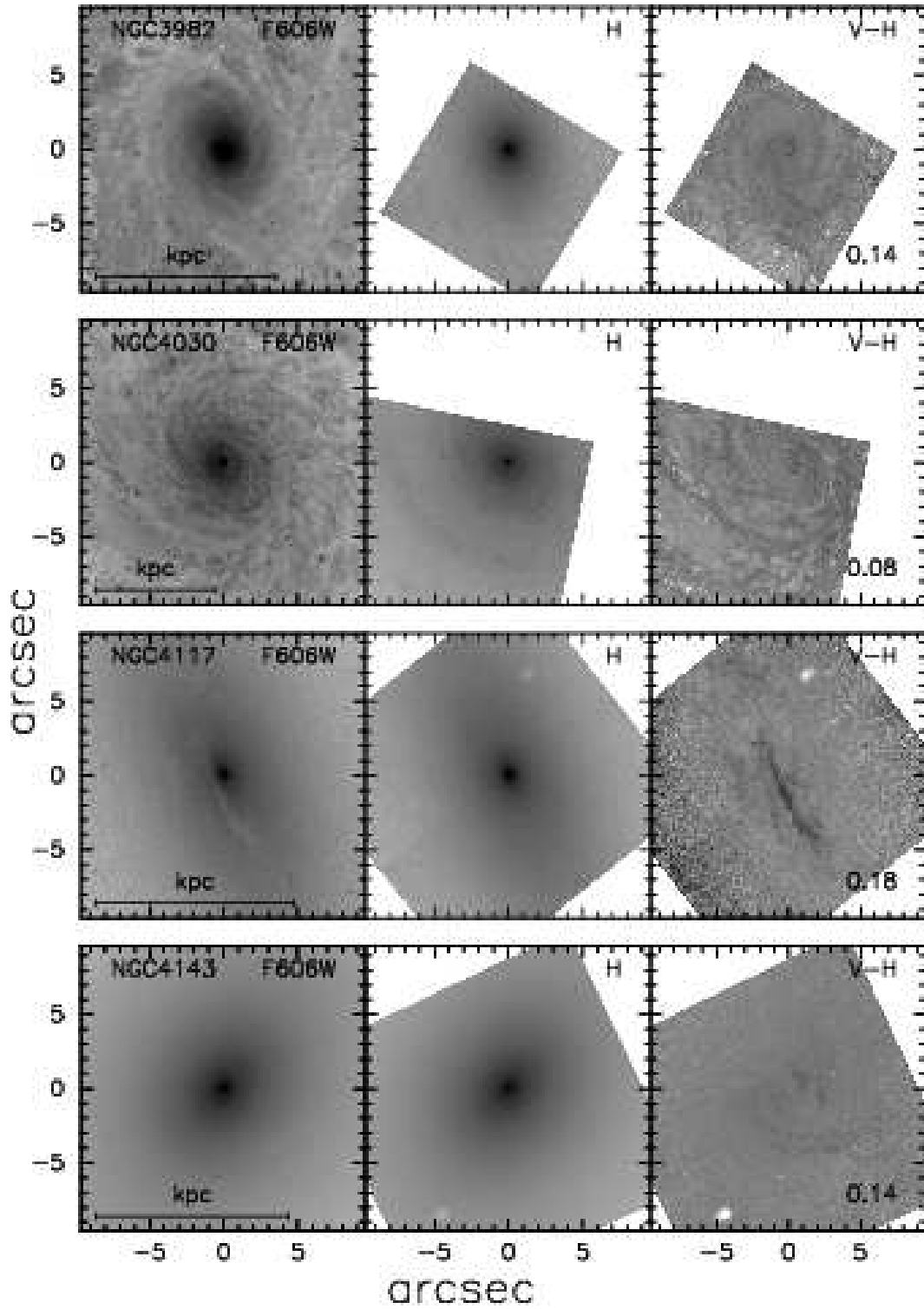


Fig. 15.— Figure 1 - *Continued*

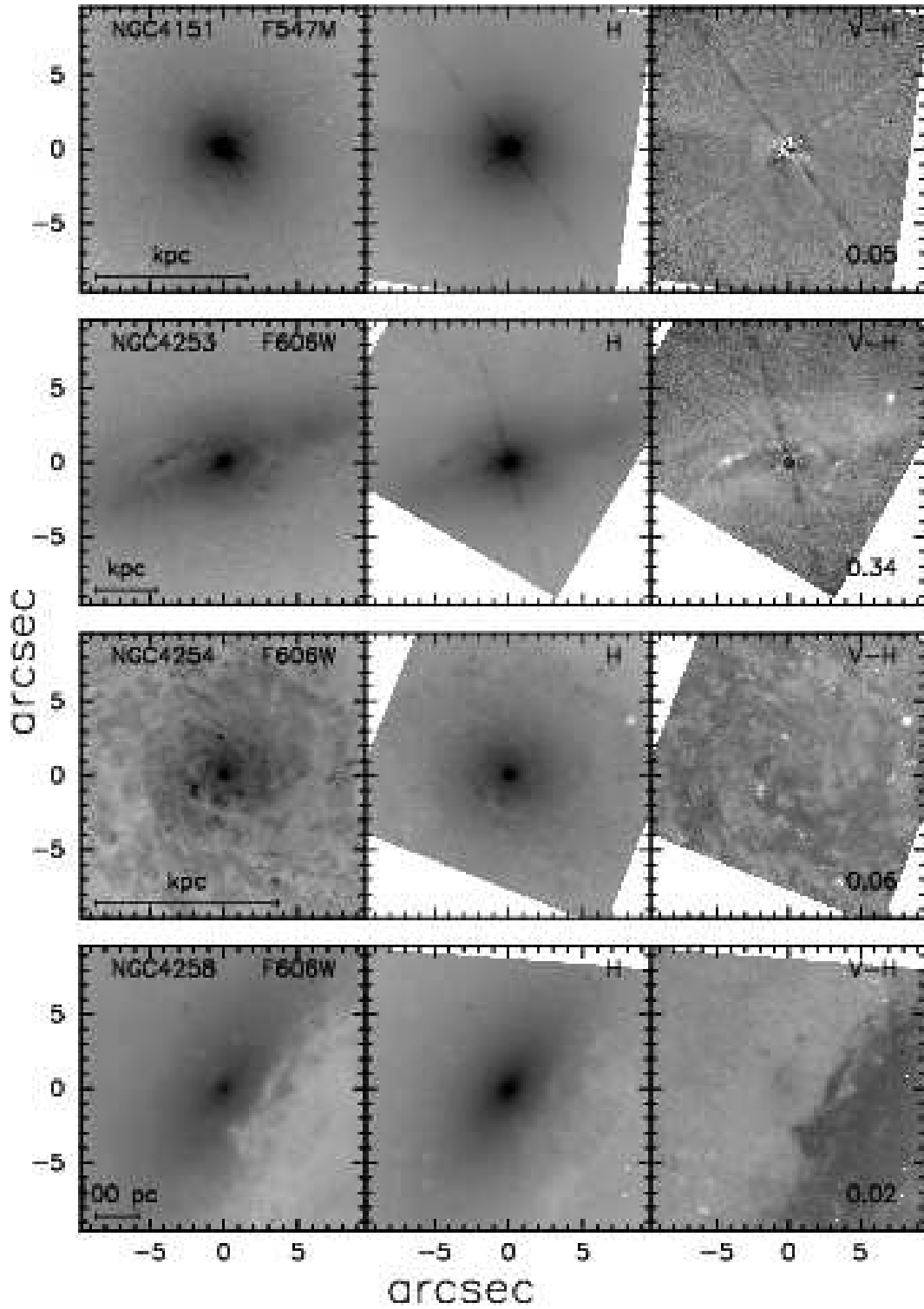


Fig. 16.— Figure 1 - *Continued*

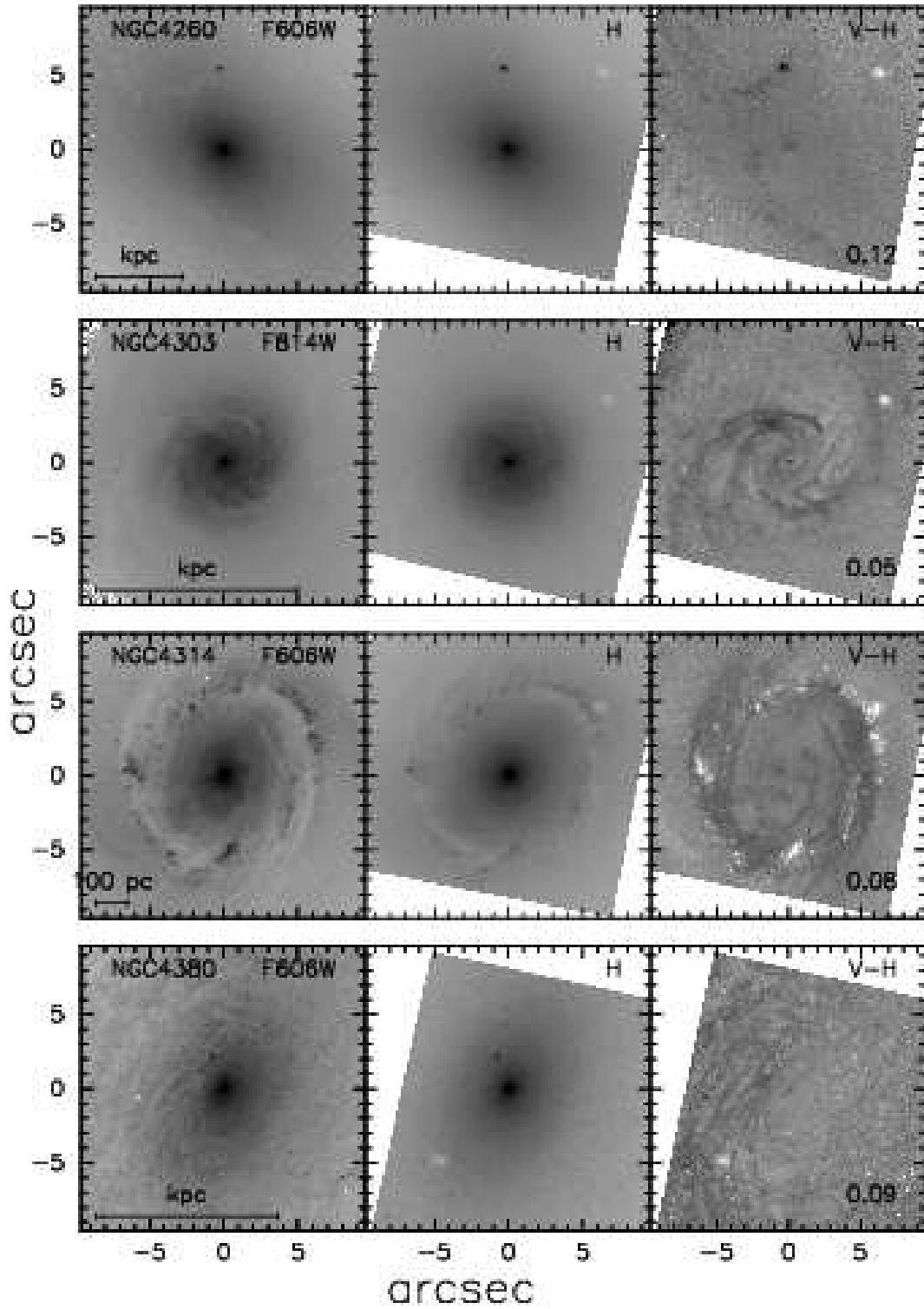


Fig. 17.— Figure 1 - *Continued*

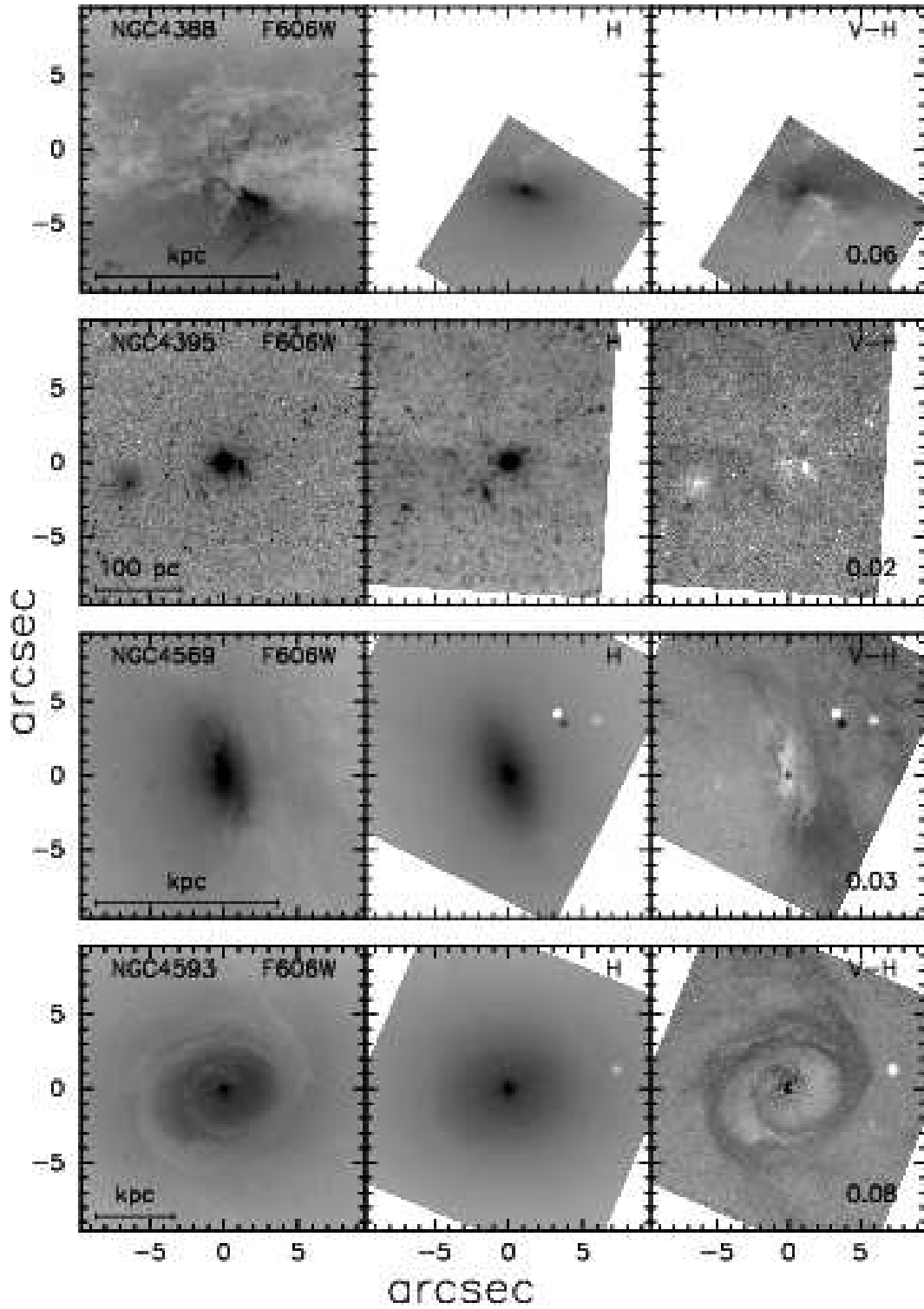


Fig. 18.— Figure 1 – *Continued*

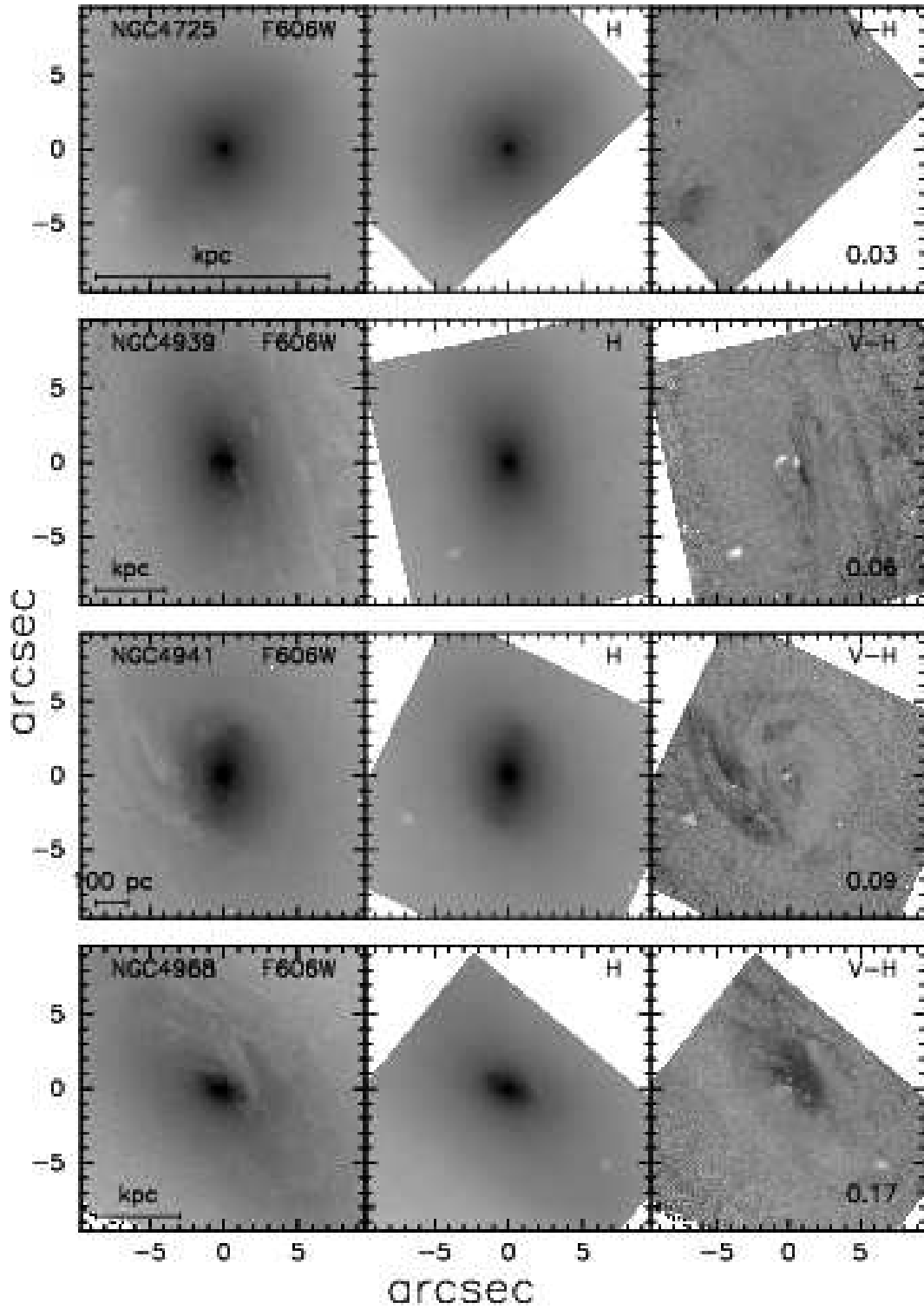


Fig. 19.— Figure 1 - *Continued*

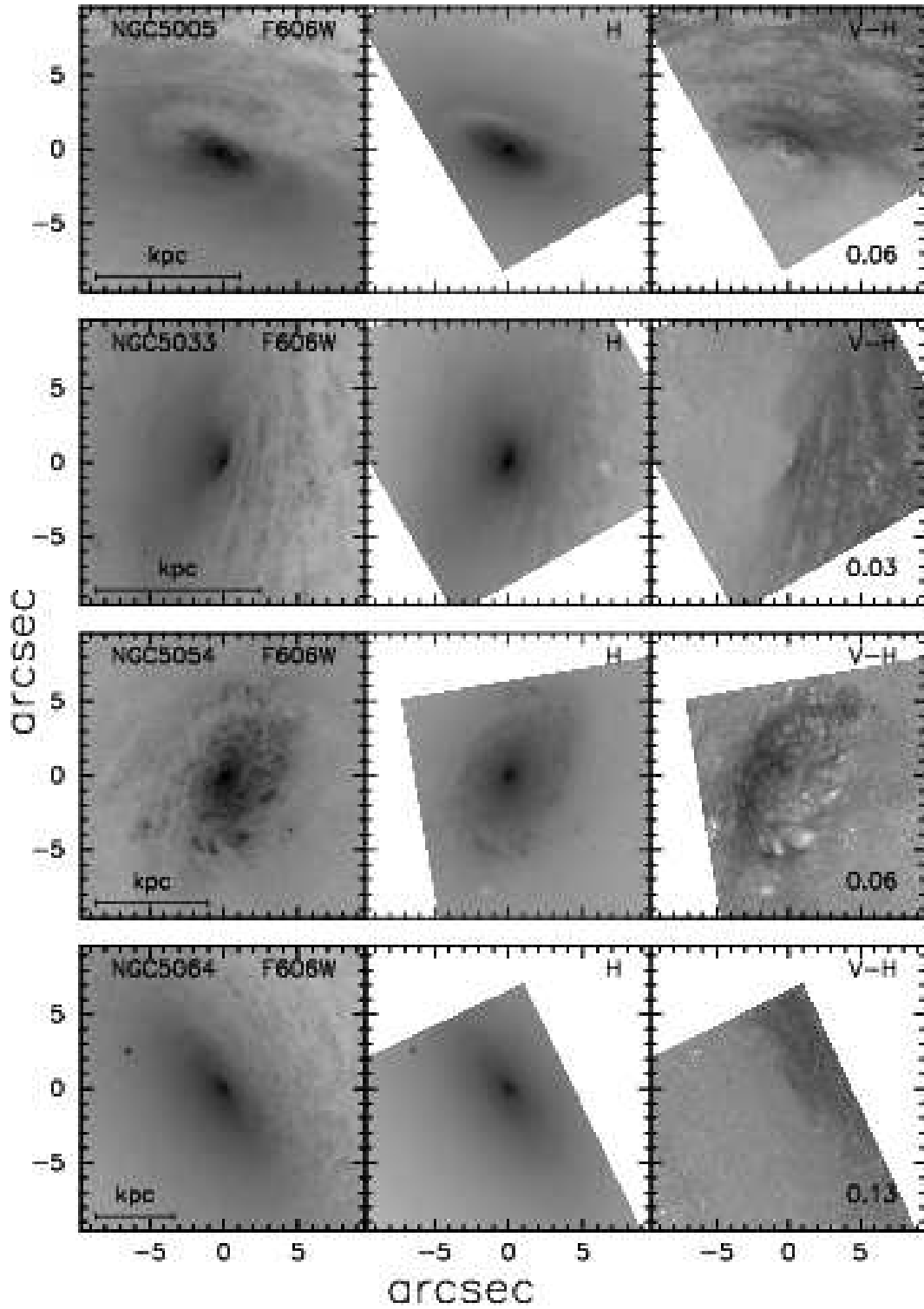


Fig. 20.— Figure 1 - *Continued*

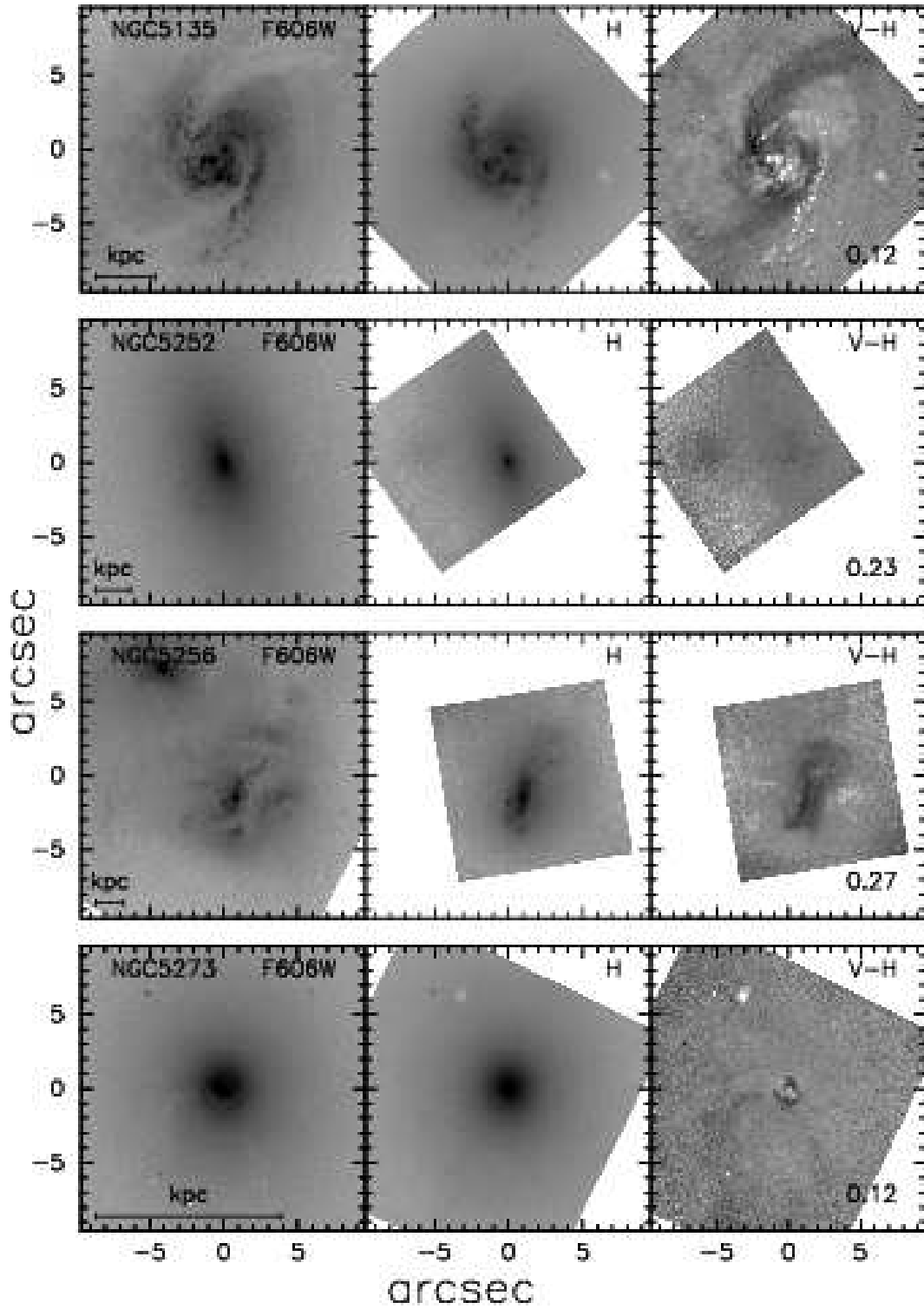


Fig. 21.— Figure 1 - *Continued*

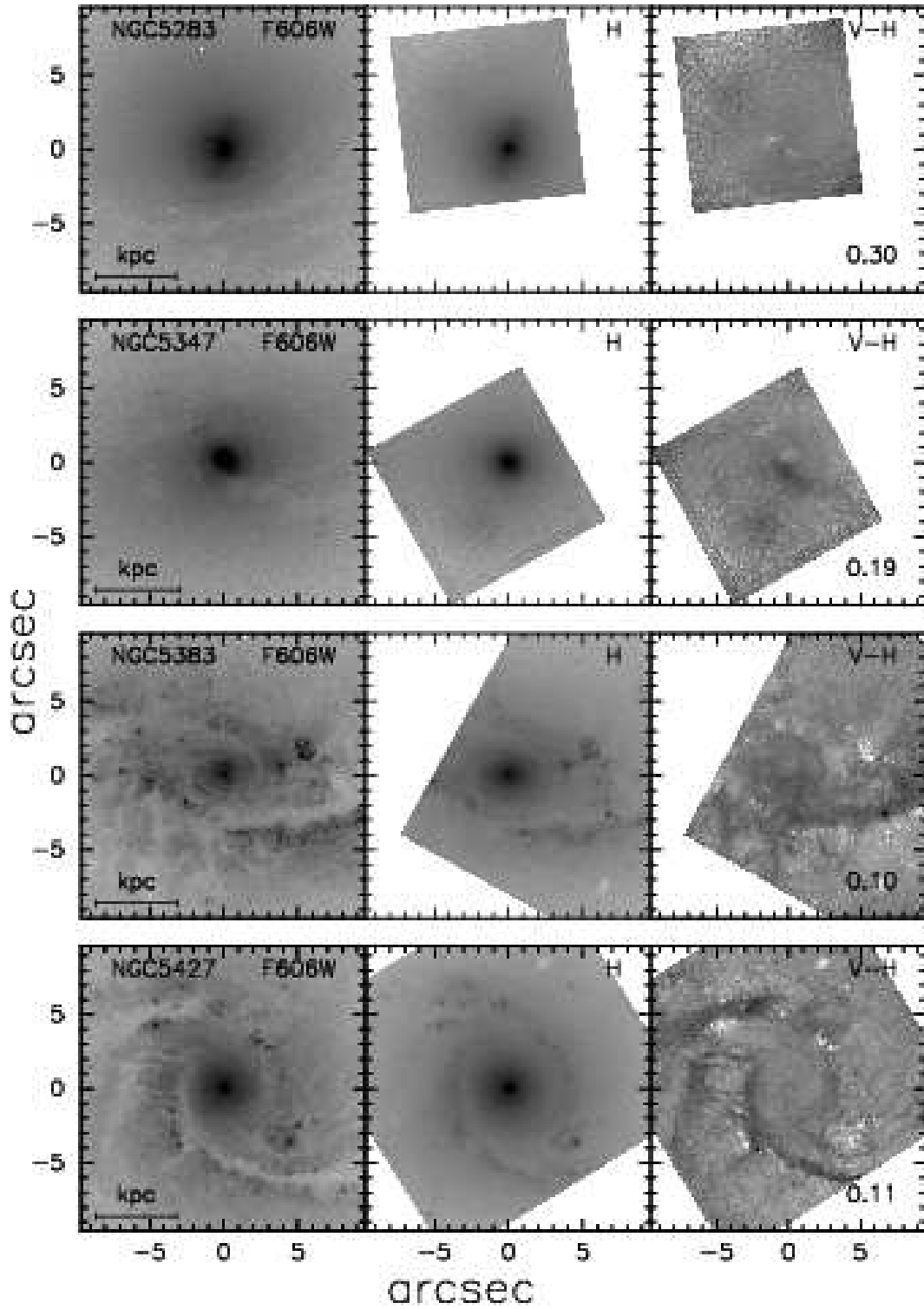


Fig. 22.— Figure 1 – *Continued*

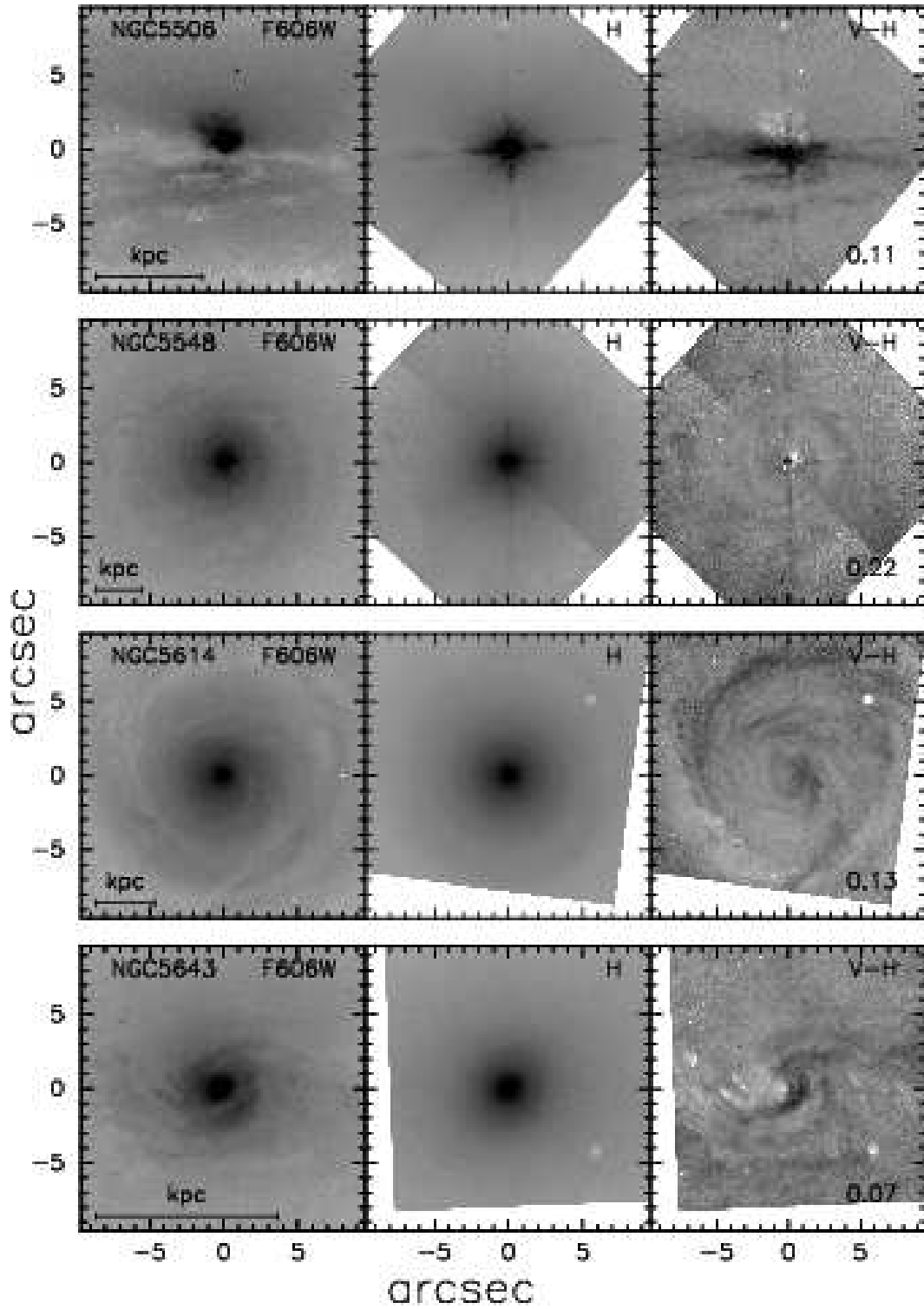


Fig. 23.— Figure 1 – *Continued*

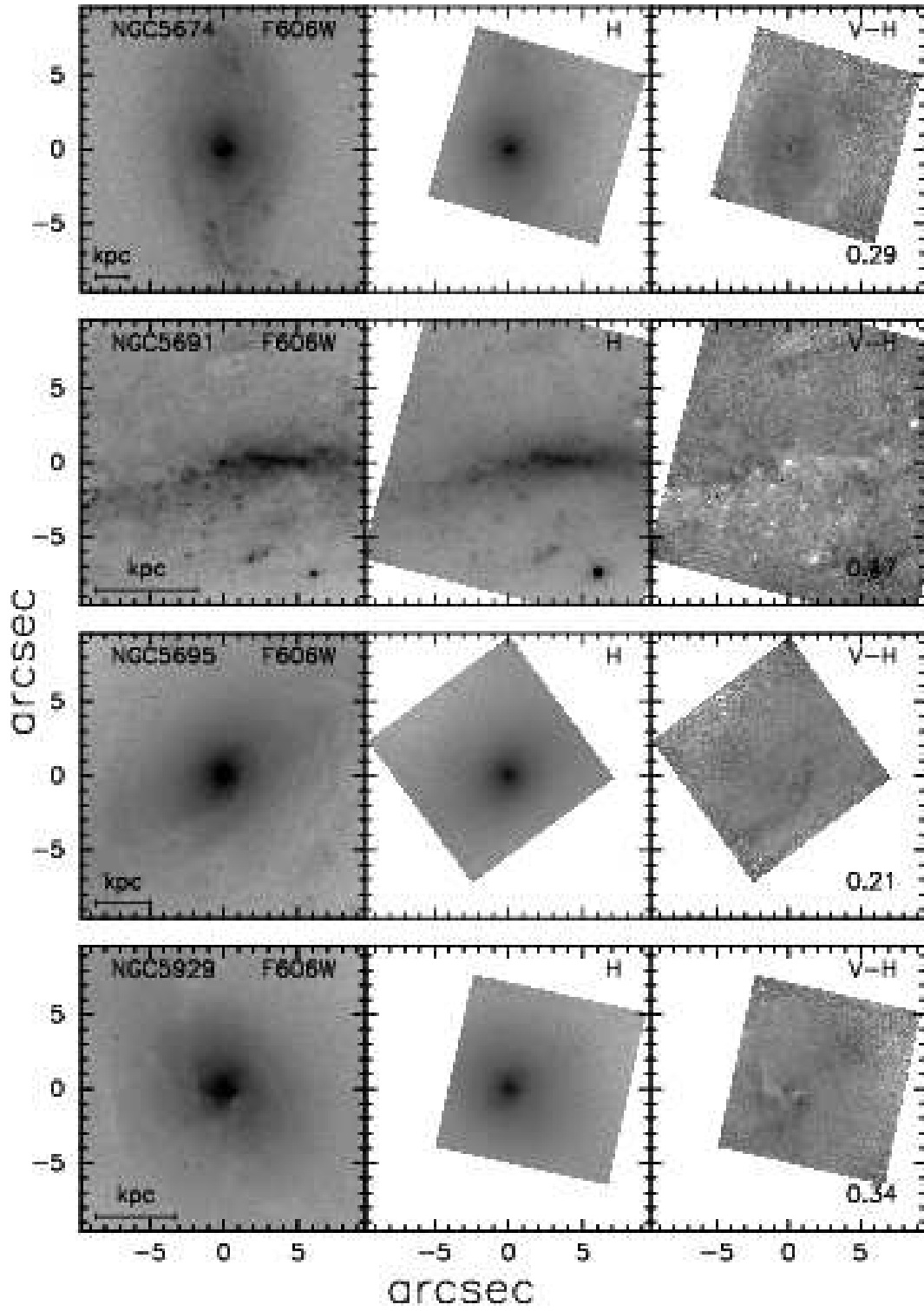


Fig. 24.— Figure 1 – *Continued*

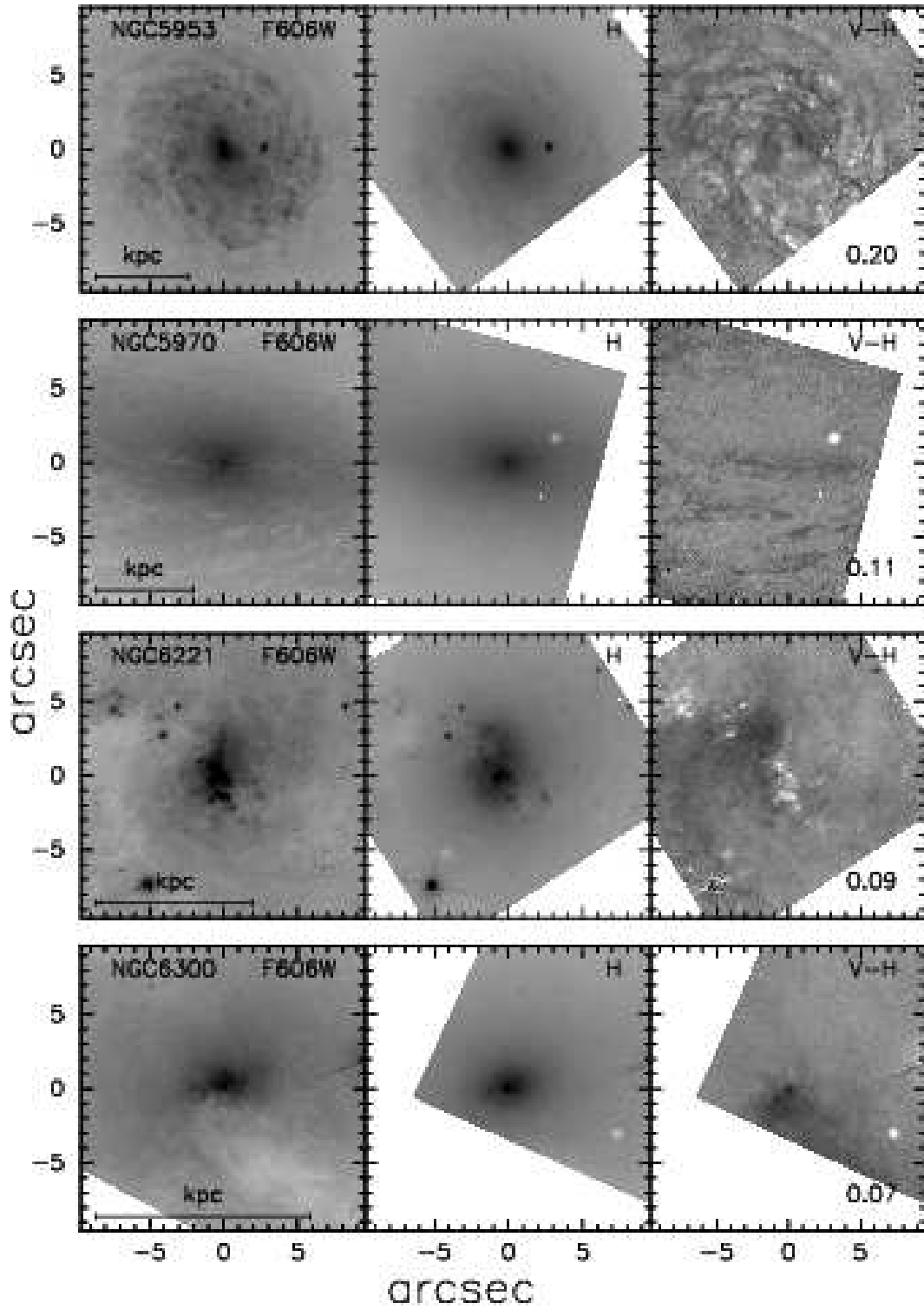


Fig. 25.— Figure 1 - *Continued*

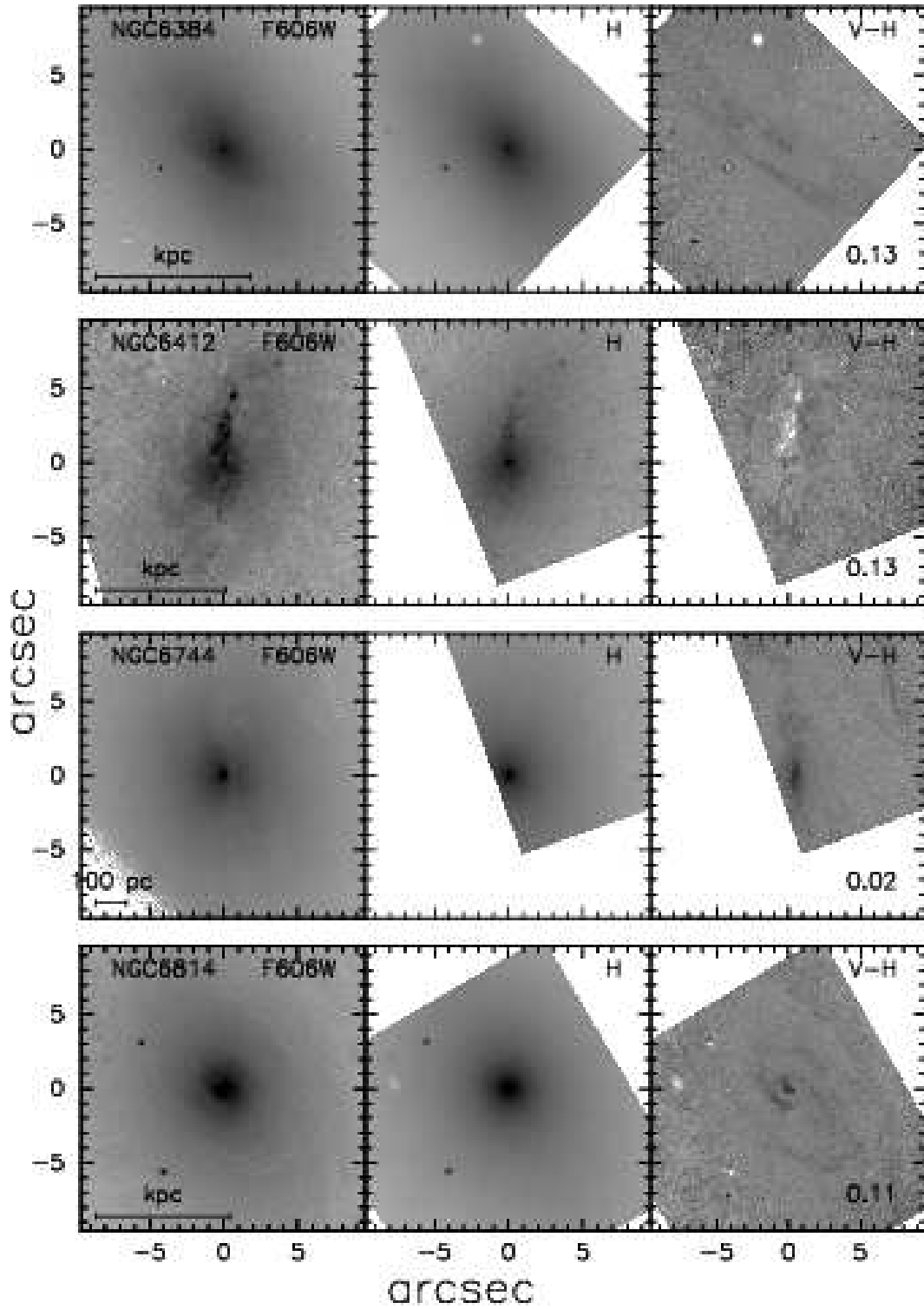


Fig. 26.— Figure 1 – *Continued*

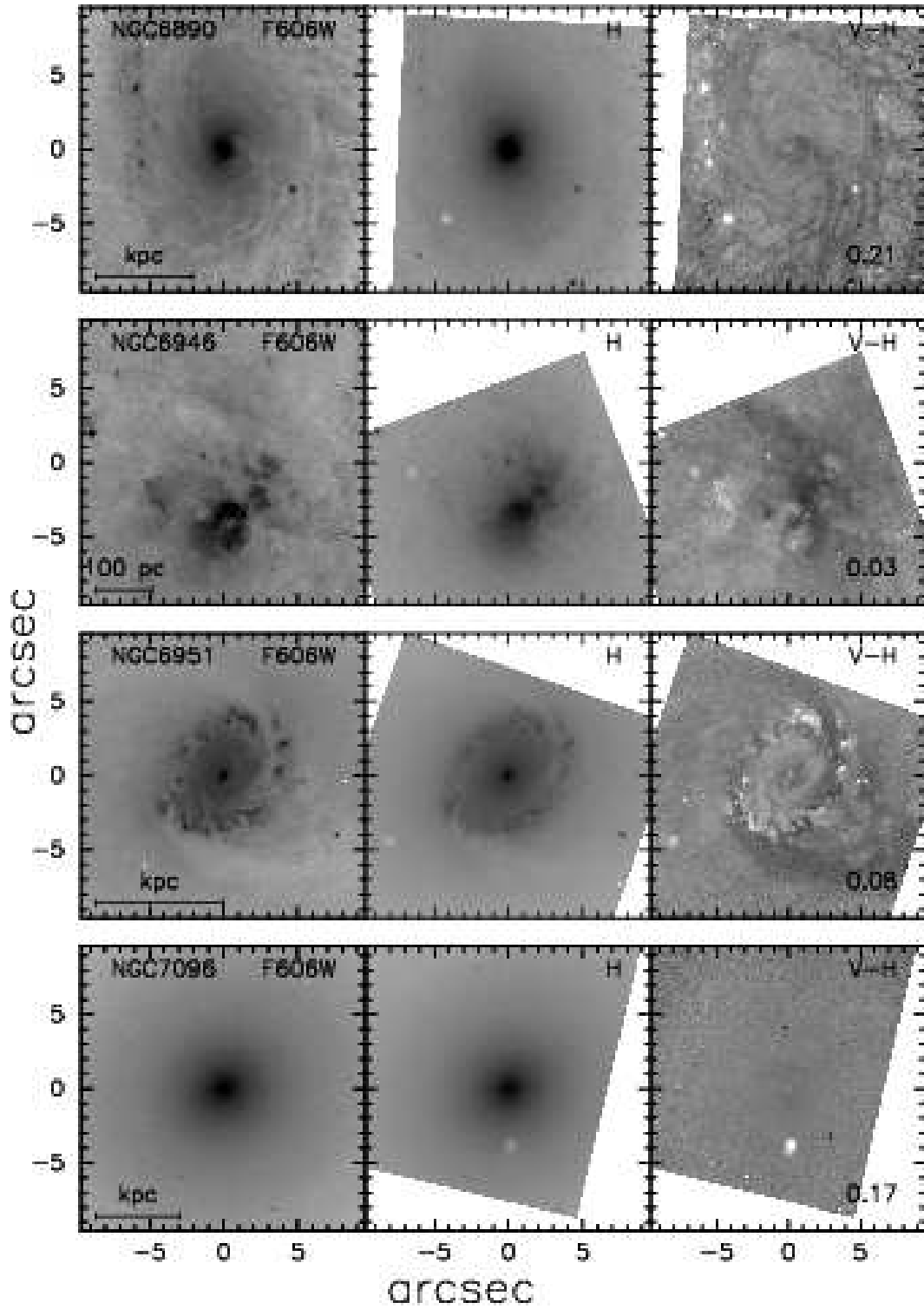


Fig. 27.— Figure 1 - *Continued*

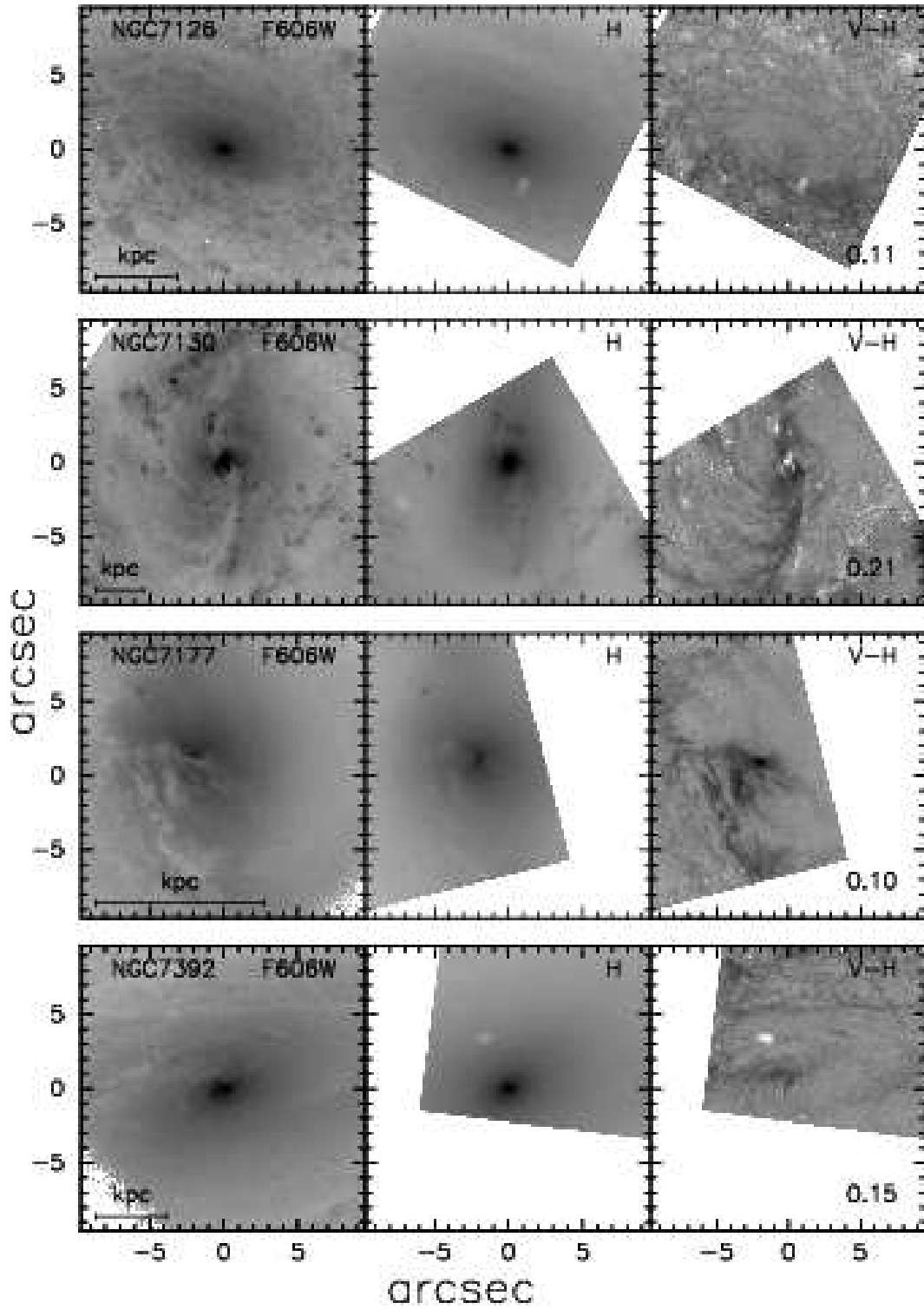


Fig. 28.— Figure 1 – *Continued*

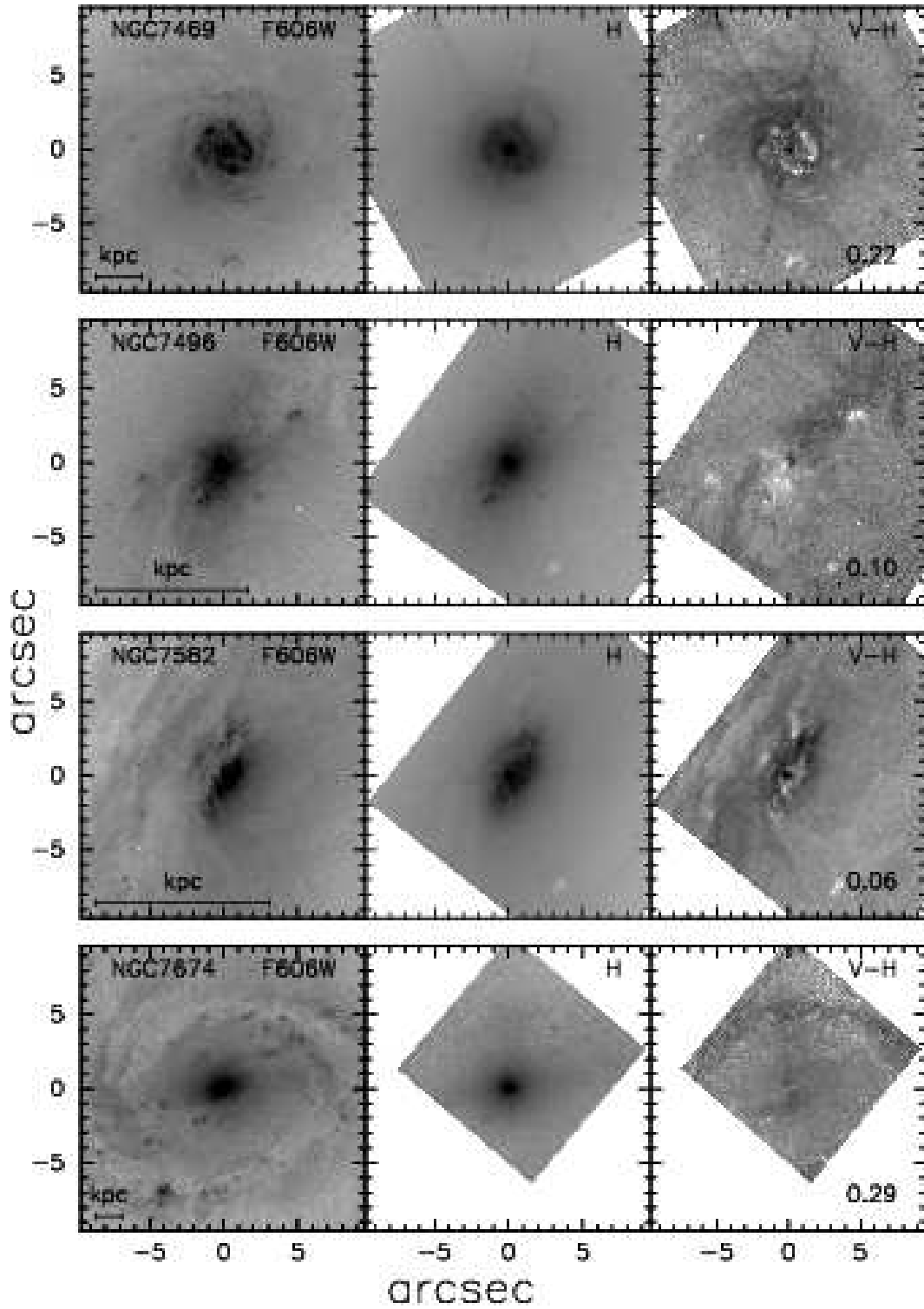


Fig. 29.— Figure 1 – *Continued*

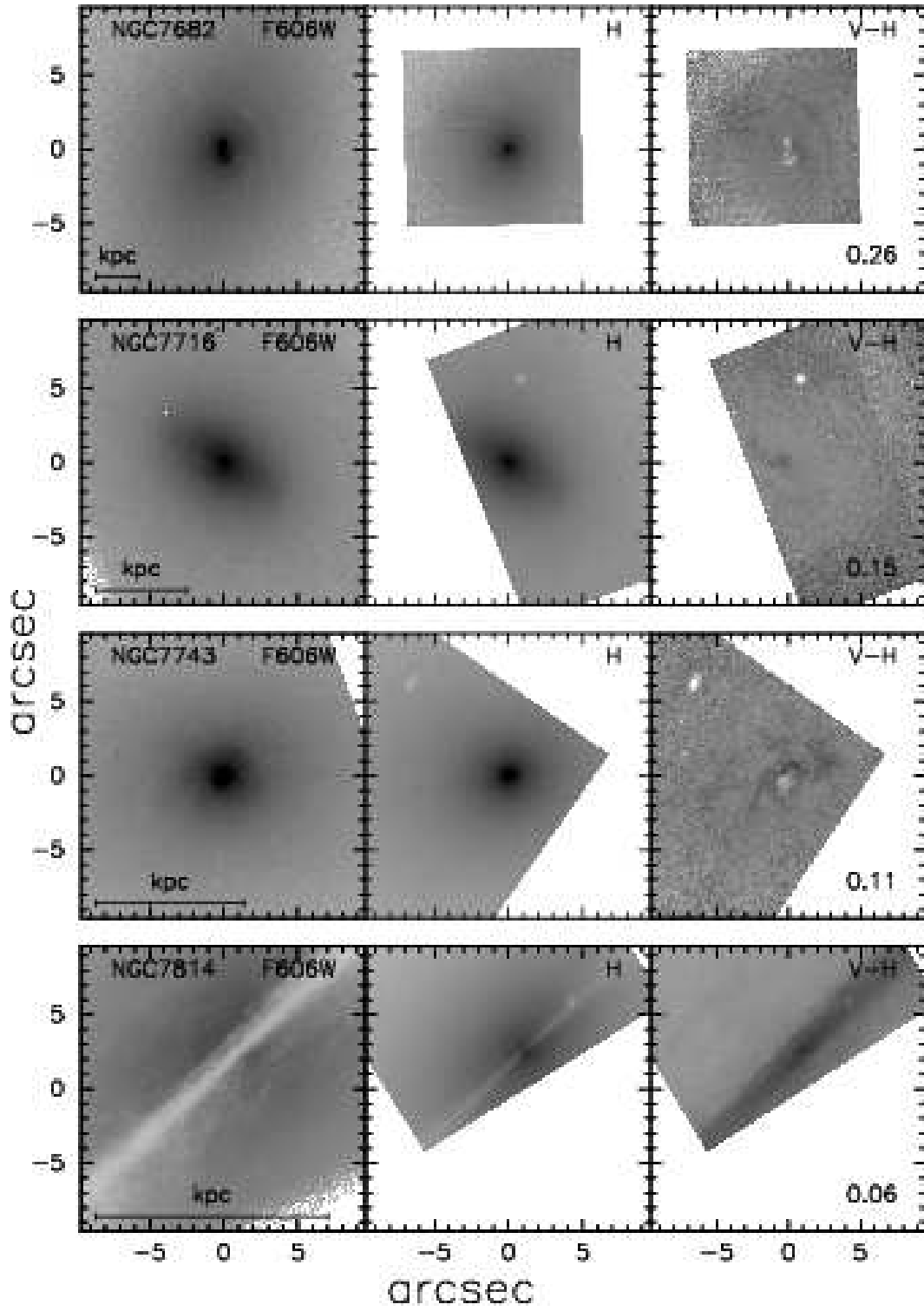


Fig. 30.— Figure 1 - *Continued*

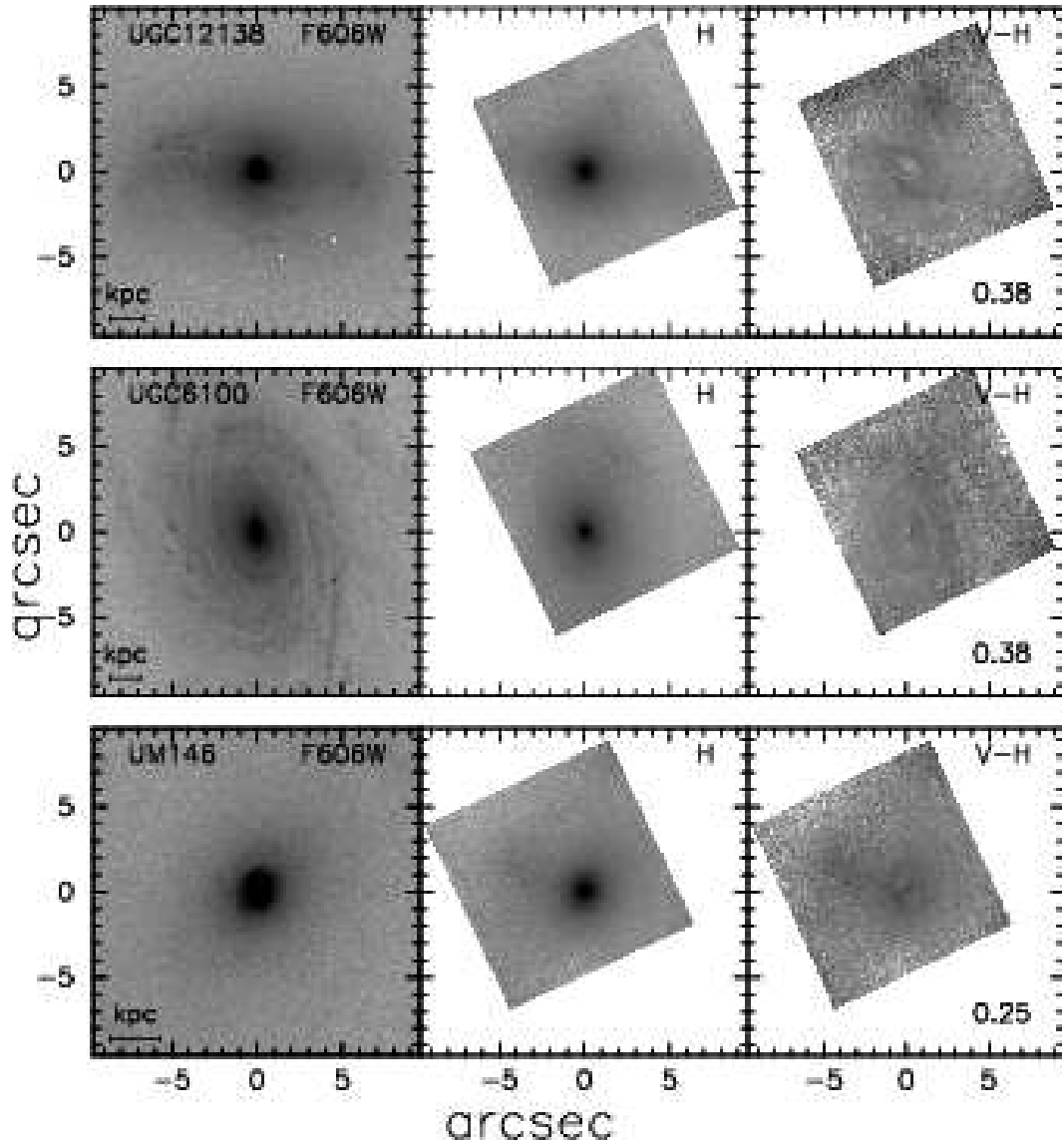


Fig. 31.— Figure 1 - *Continued*

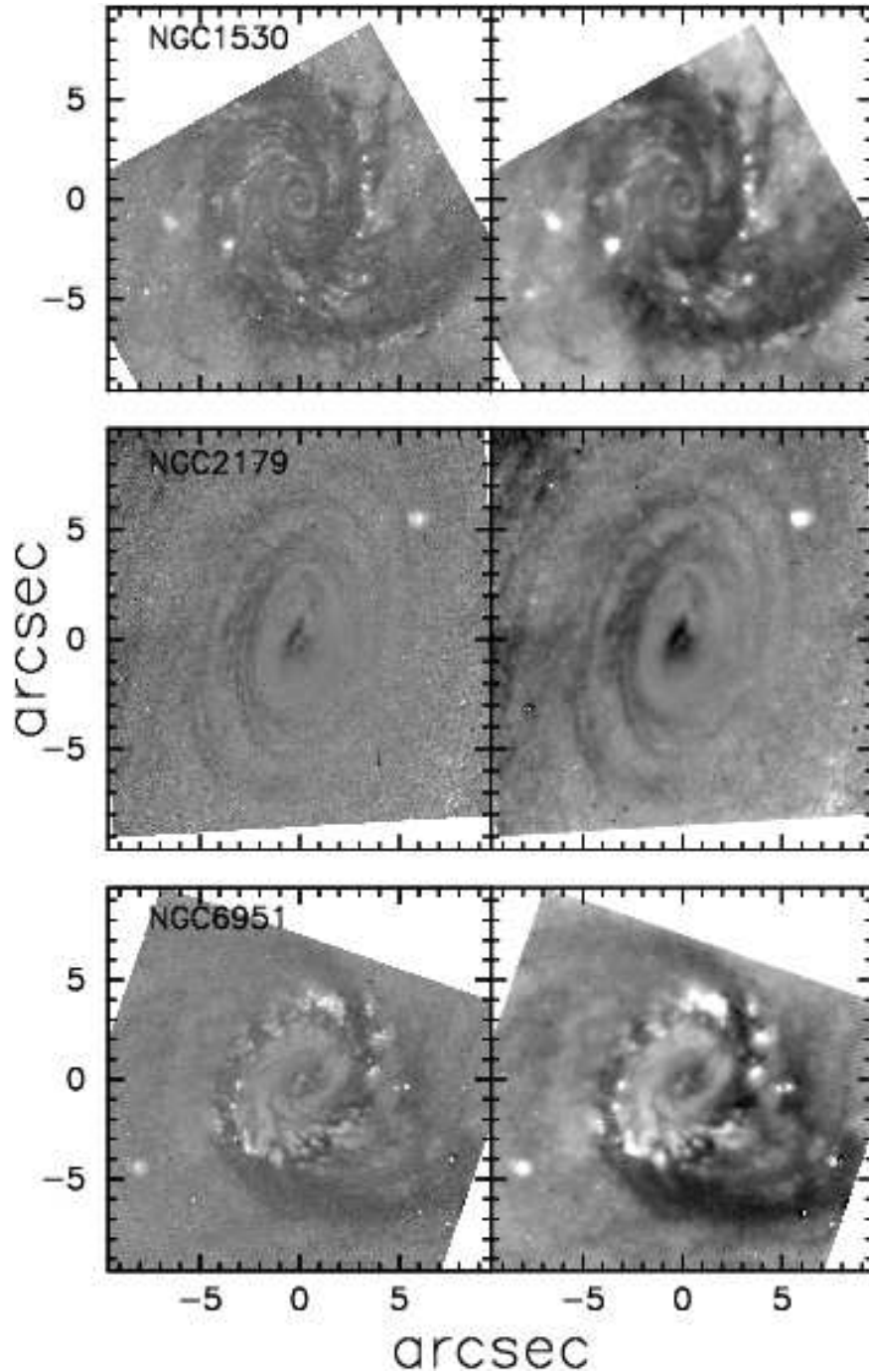


Fig. 32.— Demonstration of the effects of image convolution for three galaxies with nuclear dust spirals: NGC 1530 (GD), NGC 2179 (TW), and NGC 6951 (LW). The classification codes are described in §3.1. The left image shows the  $V - H$  colormap from Figure 1, the right image shows the same colormap constructed from a  $V$  image convolved with the  $H$  PSF and the  $H$  image convolved with the  $V$  PSF. Although the contrast of the dust lanes is poorer in the convolved images, the objects are still recognizable as members of these three different nuclear spiral classes. This figure further shows that the dust features in the unconvolved images are not spurious features caused by the angular resolution mismatch of the two filters.

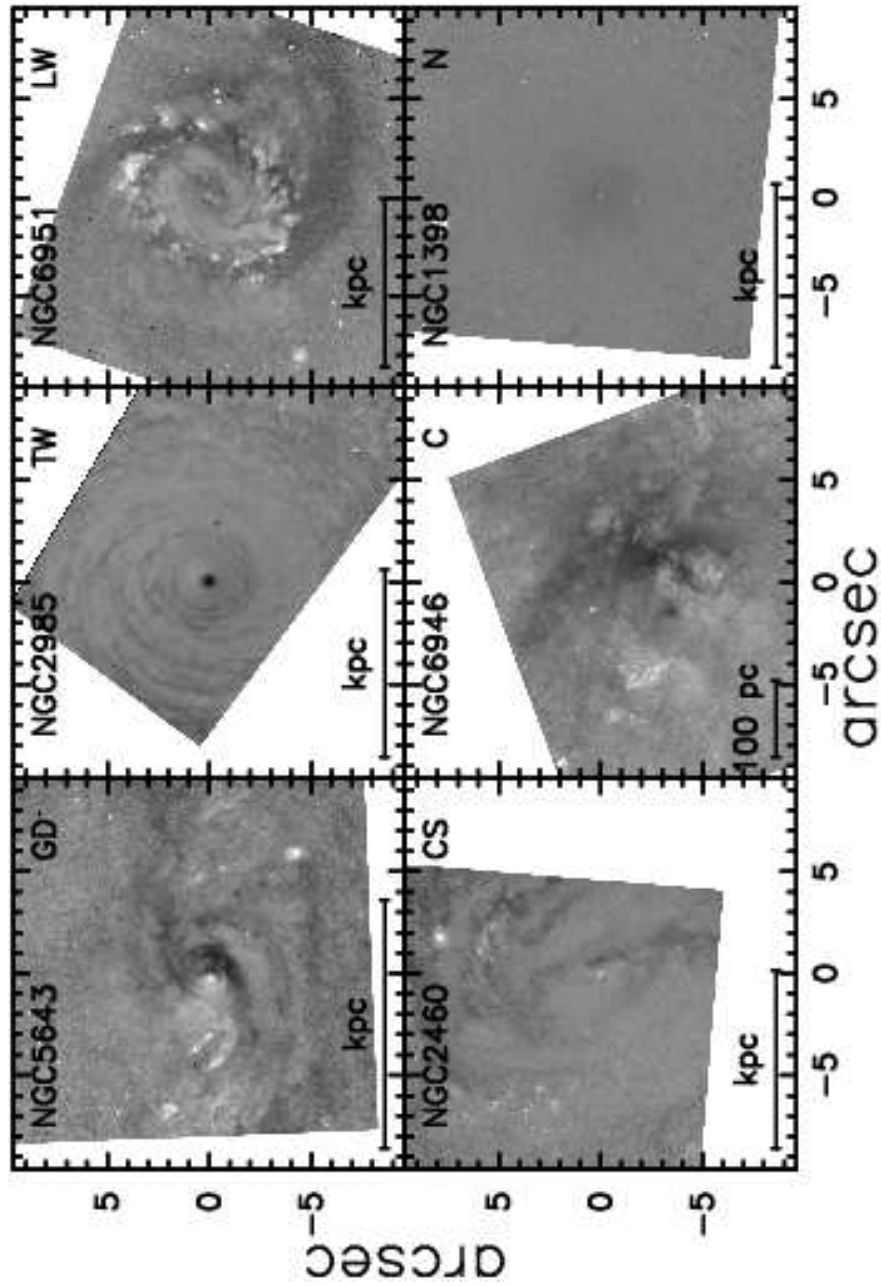


Fig. 33.— Examples of each of the nuclear classifications described in §3.1. The colormaps are the same as those shown in Figure 1 for NGC 5643 (GD: grand design nuclear spiral), NGC 2985 (TW: tightly wound), NGC 6951 (LW: loosely wound), NGC 2460 (CS: chaotic spiral), NGC 6946 (C: chaotic circumnuclear dust structure), and NGC 1398 (N: no obvious circumnuclear dust structure).

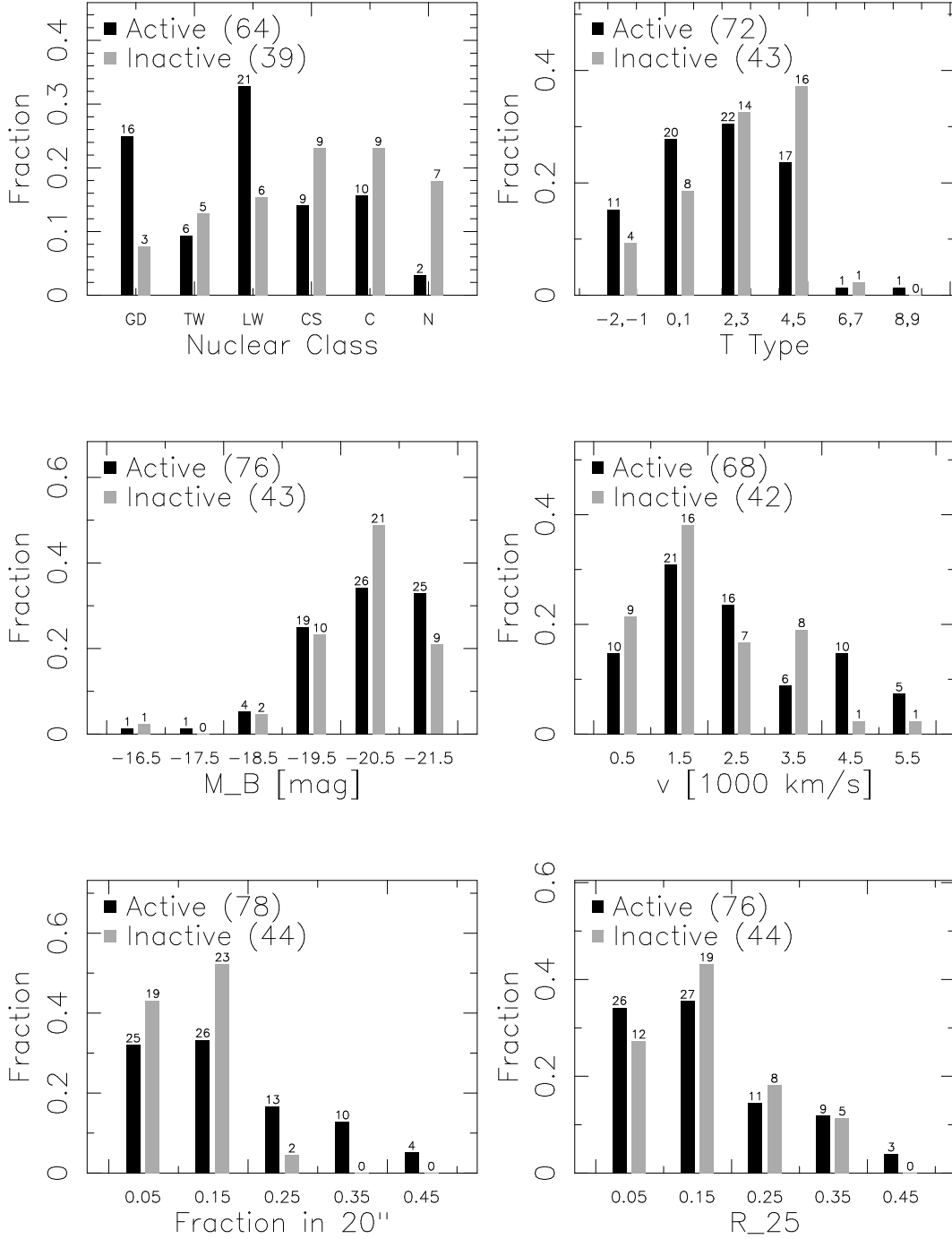


Fig. 34.— Distribution of the nuclear and host galaxy properties of the full sample of active and inactive galaxies observed with *HST*. The upper left histogram shows the distribution of these galaxies into the six nuclear classes defined in §3.1. The histogram bars are normalized to the total number of galaxies of each type and the number of galaxies in each class is given above the histogram bar. The remaining five histograms show the distribution of the Hubble type,  $B$  luminosity, heliocentric velocity, size, and inclination of the active and inactive galaxies. The total number of galaxies in each panel does not equal 123 as galaxies with  $R_{35} > 0.30$  were not include in the first panel and several individual galaxies fall outside the range of each of the bins shown.

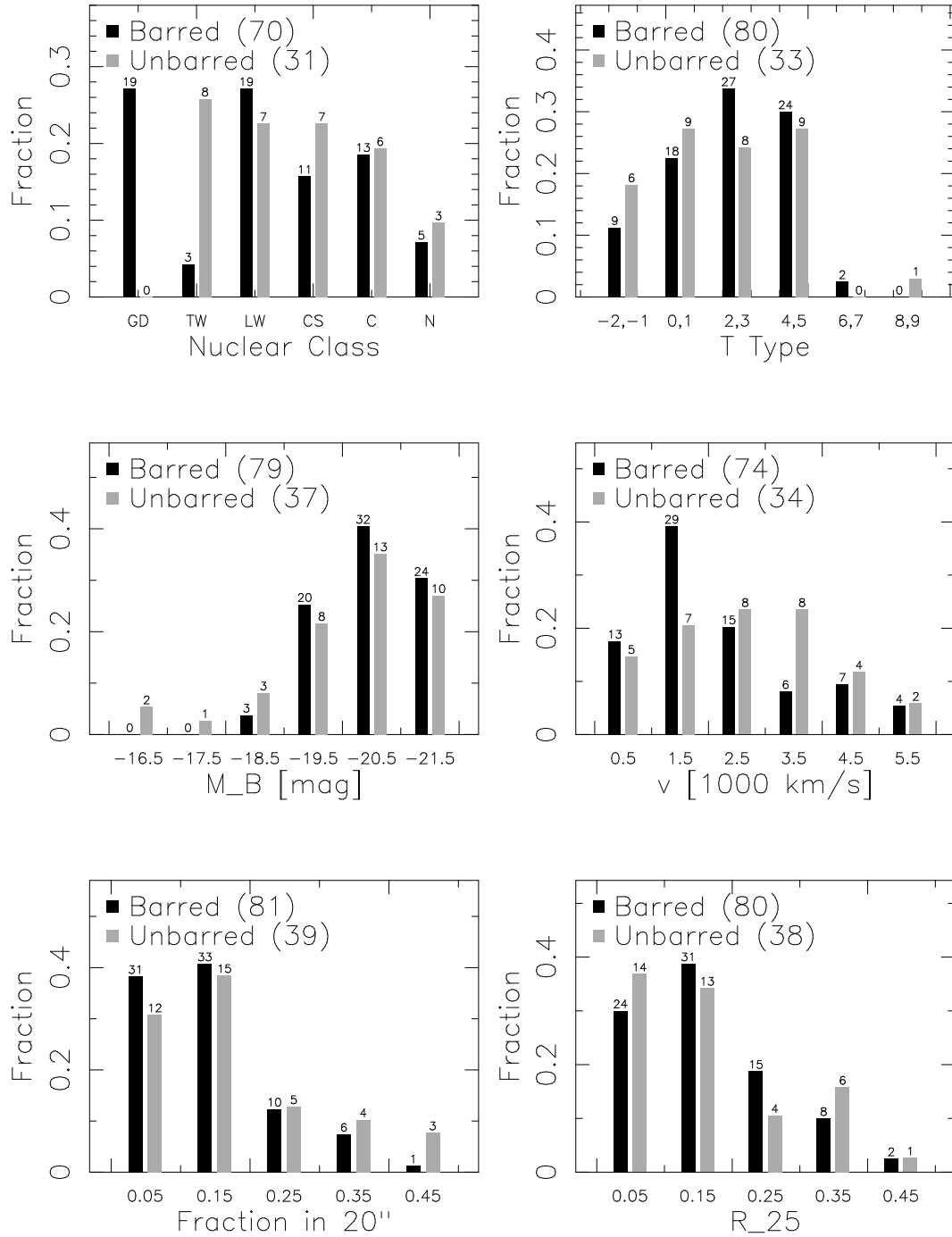


Fig. 35.— Same as Figure 34 for the barred and unbarred galaxies.

Table 1. Observations

Name	Aliases	V Prop ID	V Filter	H Prop ID
ESO 137-G34	-	5479	F606W	7330
ESO 138-G1	-	5479	F606W	7330
IC 2560	-	8597	F606W	7330
IC 5063	PKS 2048-572	5479	F606W	7330
IC 5267	-	8597	F606W	7330
Mrk 334	UGC 6	5479	F606W	7867
Mrk 461	UGC 8718	8597	F606W	7867
Mrk 471	UGC 9214	5479	F606W	7867
Mrk 477	IZw92	8597	F606W	7330
Mrk 573	UGC 1214	5479	F606W	7330
Mrk 1066	UGC 2456	5479	F606W	7330
Mrk 1210	UGC 4203	5479	F606W	7330
NGC 214	-	8597	F606W	7330
NGC 357	-	8597	F606W	7330
NGC 404	-	8597	F606W	7330
NGC 628	M74	8597	F606W	7330
NGC 788	-	5479	F606W	7330
NGC 864	-	8597	F606W	7330
NGC 1068	M77	8597	F606W	7215
NGC 1144	-	5479	F606W	7867
NGC 1241	-	5479	F606W	7330
NGC 1275	3C84,PersA	6228	F702W	7330
NGC 1300	-	8597	F606W	7330
NGC 1320	Mrk 607	5479	F606W	7330
NGC 1398	-	8597	F606W	7330
NGC 1530	-	8597	F606W	7330
NGC 1638	-	8597	F606W	7330
NGC 1667	-	5479	F606W	7330
NGC 1672	-	8597	F606W	7330
NGC 1961	-	8597	F606W	7330
NGC 2146	-	8597	F606W	7330
NGC 2179	-	8597	F606W	7330
NGC 2273	Mrk 620	6419	F791W	7172
NGC 2276	-	8597	F606W	7330
NGC 2336	-	8597	F606W	7330
NGC 2460	-	8597	F606W	7330
NGC 2639	-	5479	F606W	7330
NGC 2903	NGC 2905	8597	F606W	7330
NGC 2985	-	5479	F606W	7330
NGC 3032	-	5479	F606W	7330
NGC 3079	-	8597	F606W	7330
NGC 3081	-	5479	F606W	7330
NGC 3145	-	8597	F606W	7330
NGC 3227	-	5479	F606W	7172
NGC 3300	-	8597	F606W	7330
NGC 3351	M95	8597	F606W	7330
NGC 3362	-	5479	F606W	7867
NGC 3368	-	8597	F606W	7330

Table 1—Continued

Name	Aliases	V Prop ID	V Filter	H Prop ID
NGC 3393	-	5479	F606W	7330
NGC 3458	-	8597	F606W	7330
NGC 3486	-	8597	F606W	7330
NGC 3516	-	5479	F606W	7330
NGC 3627	M66	8597	F606W	7330
NGC 3718	-	6436	F791W	7330
NGC 3786	Mrk 744	5479	F606W	7867
NGC 3865	-	8597	F606W	7330
NGC 3982	-	5479	F606W	7330
NGC 4030	-	6359	F606W	7330
NGC 4117	-	8597	F606W	7330
NGC 4143	-	8597	F606W	7330
NGC 4151	-	5433	F547M	7215
NGC 4253	Mrk 766	5479	F606W	7330
NGC 4254	M99	8597	F606W	7330
NGC 4258	M106	8597	F606W	7230
NGC 4260	-	8597	F606W	7330
NGC 4303	M61	9042	F814W	7330
NGC 4314	-	8597	F606W	7330
NGC 4380	-	8597	F606W	7330
NGC 4388	Arp 120	8597	F606W	7867
NGC 4395	-	8597	F606W	7330
NGC 4569	-	8597	F606W	7331
NGC 4593	Mrk 1330	5479	F606W	7330
NGC 4725	-	8597	F606W	7330
NGC 4939	-	5479	F606W	7330
NGC 4941	-	8597	F606W	7330
NGC 4968	-	5479	F606W	7330
NGC 5005	-	8597	F606W	7330
NGC 5033	-	8597	F606W	7330
NGC 5054	-	8597	F606W	7330
NGC 5064	-	8597	F606W	7330
NGC 5135	-	5479	F606W	7330
NGC 5252	-	5479	F606W	7330
NGC 5256	Mrk 266SW	5479	F606W	7867
NGC 5273	-	8597	F606W	7330
NGC 5283	Mrk 270	5479	F606W	7867
NGC 5347	-	5479	F606W	7330
NGC 5383	-	8597	F606W	7330
NGC 5427	-	5479	F606W	7330
NGC 5506	Mrk 1376	5479	F606W	7330
NGC 5548	-	5479	F606W	7172
NGC 5614	-	8597	F606W	7330
NGC 5643	-	8597	F606W	7330
NGC 5674	-	5479	F606W	7867
NGC 5691	-	8597	F606W	7330
NGC 5695	Mrk 686	5479	F606W	7867
NGC 5929	-	5479	F606W	7330

Table 1—Continued

Name	Aliases	V Prop ID	V Filter	H Prop ID
NGC 5953	-	5479	F606W	7330
NGC 5970	-	8597	F606W	7330
NGC 6221	-	5479	F606W	7330
NGC 6300	-	5479	F606W	7330
NGC 6384	-	6359	F606W	7330
NGC 6412	-	8597	F606W	7330
NGC 6744	-	8597	F606W	7330
NGC 6814	-	5479	F606W	7330
NGC 6890	-	8597	F606W	7330
NGC 6946	-	8597	F606W	7330
NGC 6951	-	8597	F606W	7330
NGC 7096	-	8597	F606W	7330
NGC 7126	-	8597	F606W	7330
NGC 7130	IC 5135	5479	F606W	7330
NGC 7177	-	8597	F606W	7330
NGC 7392	-	8597	F606W	7330
NGC 7469	-	5479	F606W	7219
NGC 7496	-	8597	F606W	7330
NGC 7582	-	8597	F606W	7330
NGC 7674	Mrk 533	5479	F606W	7867
NGC 7682	-	5479	F606W	7867
NGC 7716	-	8597	F606W	7330
NGC 7743	-	8597	F606W	7330
NGC 7814	-	8597	F606W	7330
UGC 12138	2237+07	5479	F606W	7867
UGC 6100	A1058+45	5479	F606W	7867
UM 146	UGC 1395	5479	F606W	7867

Table 2. Literature Data and Sample Assignments

Name	D	References	pc/''	Bar	Note	References	AGN	References
ESO 137-G34	33.8	7	164	B	1	5	S2	27
ESO 138-G1	33.8	7	164	0	4	5	S2	26
IC 2560	34.4	7	167	B	1	1	S2	23
IC 5063	43.8	7	212	0	5	6	S2	10,13,18
IC 5267	21.0	1	102	0	5	6	No	24
Mrk 334	88.4	7	429	0	5	4	S1.8	20,29
Mrk 461	65.6	7	318	0	5	4	S2	28,29
Mrk 471	137.3	7	666	B	1	1	S1.8	7,29
Mrk 477	153.5	7	744	?	3	.	S2	7
Mrk 573	71.0	7	344	X	2	1	S2	9,29
Mrk 1066	50.9	7	247	B	1	1	S2	17
Mrk 1210	52.3	7	254	0	5	8	S2	27
NGC 214	63.9	7	310	X	2	1	No	16
NGC 357	32.1	1	156	B	1	6	No	24
NGC 404	3.3	6	16	0	5	8	No(L2)	30
NGC 628	9.7	1	47	0	5	8	No	30
NGC 788	55.7	7	270	0	5	6	S2	14
NGC 864	20.0	1	97	B	1	6	No	30
NGC 1068	14.4	1	70	B	1	2	S1.8	1,29,30
NGC 1144	116.4	7	564	B	1	1	S2	14,29
NGC 1241	26.6	1	129	B	1	1	S2	20
NGC 1275	73.0	7	354	0	5	3	S1.5	1,30
NGC 1300	15.0	2	73	B	1	1	No	2
NGC 1320	37.7	1	183	0	4	1	S2	22
NGC 1398	22.2	2	108	B	1	1	No	2,24
NGC 1530	36.6	1	177	B	1	1	No	2
NGC 1638	44.3	7	215	0	5	6	No	32
NGC 1667	60.3	7	292	B	1	6	S2	10,18
NGC 1672	14.5	1	70	B	1	1	S2	24
NGC 1961	55.2	7	268	0	5	8	No(L2)	30
NGC 2146	17.2	1	83	B	1	1	No	30
NGC 2179	34.2	1	166	0	4	1	No	10
NGC 2273	28.4	1	138	B	1	6	S2	14
NGC 2276	36.8	1	178	X	2	1	No	30
NGC 2336	27.2	2	132	X	2	1	S2	30
NGC 2460	23.6	1	114	B	1	8	No	29
NGC 2639	45.6	7	221	B	1	7	S1	14
NGC 2903	7.4	2	36	X	2	1	No	2,30
NGC 2985	22.4	1	109	0	4	1	No(T1.9)	30
NGC 3032	22.0	6	107	X	2	1	No	32
NGC 3079	17.3	2	84	B	1	1	S2	28,30
NGC 3081	32.5	1	158	D	1	6	S2	10,18
NGC 3145	45.5	7	221	B	1	1	No	19
NGC 3227	20.6	1	100	B	1	6	S1.5	1,29
NGC 3300	42.9	1	208	X	2	1	No	10
NGC 3351	10.1	4	49	B	1	1	No	30
NGC 3362	108.7	7	527	X	2	1	S2	14,29
NGC 3368	10.4	6	50	X	2	1	No	30

Table 2—Continued

Name	D	References	pc/'	Bar	Note	References	AGN	References
NGC 3393	73.0	7	354	B	1	6	S2	6
NGC 3458	29.5	1	143	X	2	1	No	10
NGC 3486	12.3	2	60	X	2	1	S2	30
NGC 3516	38.9	1	189	B	1	4	S1.2	1,30
NGC 3627	11.1	5	54	X	2	1	S2	30
NGC 3718	17.0	1	82	B	1	1	L1.9	30
NGC 3786	36.1	7	175	B	1	8	S1.8	14
NGC 3865	73.1	7	354	0	5	6	No	10
NGC 3982	17.0	1	82	B	1	6	S2	10,18
NGC 4030	25.9	1	126	0	5	8	No	24
NGC 4117	15.5	3	75	0	5	8	S2	14
NGC 4143	15.9	6	77	X	2	1	L1.9	30
NGC 4151	20.3	1	98	?	3	4,6	S1	1,28
NGC 4253	50.7	7	246	B	1	4	S1	5
NGC 4254	16.8	1	81	0	5	8	No	30
NGC 4258	7.3	6	35	X	2	1	S1.9	2,28,30
NGC 4260	35.1	1	170	B	1	1	No	8
NGC 4303	15.2	1	74	X	2	1	L	30
NGC 4314	9.7	1	47	B	1	1	No(L2)	2,30
NGC 4380	16.8	1	81	0	4	1	No	30
NGC 4388	16.8	1	81	0	5	4	S1.9	10,14,18,30
NGC 4395	3.6	1	17	0	5	4	S1.8	28,30
NGC 4569	16.8	1	81	X	2	1	No	30
NGC 4593	39.5	1	192	B	1	6	S1	9
NGC 4725	13.2	6	64	X	2	1	S2	30
NGC 4939	44.3	1	215	0	5	8	S2	24
NGC 4941	9.7	2	47	X	2	1	S2	15,20
NGC 4968	36.2	7	176	X	2	1	S2	23
NGC 5005	21.3	1	103	X	2	1	L1.9	2,30
NGC 5033	18.7	1	91	0	5	4	S1.5	15,29,30
NGC 5054	27.3	1	132	0	5	8	No	24
NGC 5064	39.5	1	192	0	5	8	L	24,31
NGC 5135	51.6	7	250	B	1	6	S2	10,18
NGC 5252	90.7	7	440	0	5	4	S1.9	6,14,29
NGC 5256	111.0	7	538	0	5	4	S2	17,29
NGC 5273	16.5	6	80	0	5	6	S1.5	14,29,30
NGC 5283	38.2	7	185	0	5	8	S2	5,29
NGC 5347	36.7	1	178	B	1	6	S2	10,18,29
NGC 5383	37.8	1	183	B	1	1	No	30
NGC 5427	38.1	1	185	0	5	6	S2	20
NGC 5506	28.7	1	139	?	3	.	S1.9	4
NGC 5548	66.4	7	322	0	5	6	S1	3
NGC 5614	52.5	7	255	0	5	8	No	21
NGC 5643	16.9	1	82	B	1	6	S2	10,18
NGC 5674	98.1	7	476	B	1	1	S1.9	14,29
NGC 5691	30.2	1	146	B	1	6	No	10
NGC 5695	56.9	7	276	B	1	4	S2	17,29
NGC 5929	38.5	1	187	0	5	8	S2	14,29

Table 2—Continued

Name	D	References	pc/''	Bar	Note	References	AGN	References
NGC 5953	33.0	1	160	0	4	1	S2	21
NGC 5970	31.6	1	153	B	1	1	No(T2/L2:)	30
NGC 6221	19.4	1	94	B	1	1	S2	11
NGC 6300	14.3	1	69	B	1	6	S2	10,18
NGC 6384	19.8	2	96	X	2	1	No(T2)	30
NGC 6412	23.5	1	114	B	1	6	No	30
NGC 6744	10.4	1	50	X	2	1	L	24,31
NGC 6814	22.8	1	111	B	1	6	S1.5	3,24
NGC 6890	31.8	1	154	B	1	6	S2	10,18
NGC 6946	5.5	1	27	X	2	1	No	30
NGC 6951	24.1	1	117	B	1	6	S2	2,30
NGC 7096	36.7	1	178	0	5	8	No	10
NGC 7126	37.5	1	182	0	4	1	No	10,24
NGC 7130	64.7	7	314	B	1	6	S2	10,18
NGC 7177	18.2	1	88	X	2	1	No(T2)	30
NGC 7392	43.0	7	208	B	1	9	No	25
NGC 7469	66.9	7	324	B	1	4	S1.2	1,3
NGC 7496	20.1	1	97	B	1	6	S2	24
NGC 7582	17.6	1	85	B	1	1	S2	12
NGC 7674	118.5	7	575	B	1	4	S2	17,29
NGC 7682	70.8	7	343	B	1	1	S2	14,29
NGC 7716	33.7	1	163	B	1	6	No	24
NGC 7743	20.7	6	100	B	1	1	S2	15,28,30
NGC 7814	13.2	6	64	0	4	1	No(L2::)	30
UGC 12138	102.8	7	498	B	1	1	S1.8	14,29
UGC 6100	117.6	7	570	0	5	4	S2	14,29
UM 146	71.6	7	347	B	1	4	S1.9	14

Note. — Literature data and references for the distance (col. 2), derived projected spatial scale (col. 4), bar (col. 5), and nuclear activity class (col. 8) for each galaxy in the sample. Distance references: (1) Tully (1988); (2) Tully, Shaya, & Pierce (1992); (3) Tully et al. (1996); (4) Graham et al. (1997); (5) Saha et al. (1999); (6) Tonry et al. (2001); (7) Yahil, Tammann, & Sandage (1977). Bar Notes: (1) Bar in RC3 or other survey; (2) weak bar in RC3; (3) Bar classification unknown; (4) unbarred at visible wavelengths, e.g. RC3; (5) unbarred in near-infrared image. All galaxies with flags 1 and 2 were included in the barred sample, those with class 4 or 5 were included in the unbarred sample. Galaxies in class 3 were not included in the bar discussion. Bar references: (1) RC3; (2); Scoville et al. (1988); (3) Poulain, Nieto, & Davoust (1992); (4) McLeod & Rieke (1995); (5) Mulchaey, Wilson, & Tsvetanov (1996); (6) Mulchaey, Regan, & Kundu (1997); (7) Márquez et al. (1999); (8) Laine et al. (2002); (9) Buta (1995). AGN references: (1) Seyfert (1943); (2); Burbidge & Burbidge (1962); (3) Anderson (1970); (4) Wilson et al. (1976); (5) Markarian (1977); (6) Bohuksi, Fairall, & Weedman (1978); (7) de Bruyn & Sargent (1978); (8) Eastmond & Abell (1978); (9) Koski (1978); (10) Sandage (1978); (11) Phillips (1979); (12) Ward et al. (1980); (13) Veron (1981); (14) Huchra, Wyatt, & Davis (1982); (15) Stauffer (1982); (16) Huchra et al. (1983); (17) Osterbrock & Dahari (1983); (18) Phillips, Charles, & Baldwin (1983); (19) da Costa et al. (1984); (20) Dahari (1985); (21) Keel et al. (1985); (22) De Robertis & Osterbrock (1986); (23) Fairall (1986); (24) Veron-Cetty & Veron (1986); (25) Bica & Alloin (1987); (26) Fairall (1988); (27) Hewitt & Burbidge (1991); (28) Huchra & Burg (1992); (29) Osterbrock & Martel (1993); (30) Ho et al. (1997); (31) Vaceli et al. (1997); (32) Trager et al. (1998). All galaxies with “No” in column 8 are considered to be inactive.

Table 3. Morphological Classifications

Name	RC3	T	$B_T$	$M_B$	$v$	D <sub>25</sub>	20''frac	R <sub>25</sub>	Nuc Class
ESO 137-G34	.S?....	0.0	10.1	-22.8	2747	0.98	0.35	0.45	HI/C
ESO 138-G1	.E?....	-3.0	13.3	-19.5	2740	1.02	0.32	0.30	C
IC 2560	PSBR3*	3.3	11.9	-20.8	2925	1.50	0.11	0.20	LW
IC 5063	.LAS+*	-0.8	12.6	-20.7	3402	1.33	0.16	0.17	C
IC 5267	.SAS0..	0.0	11.3	-20.3	1713	1.72	0.06	0.13	C
Mrk 334	.P.....	0.0	14.4	-20.4	6605	0.99	0.34	0.14	LW
Mrk 461	.S.....	0.0	14.3	-19.7	4894	0.87	0.45	0.13	LW
Mrk 471	.SB.1..	1.0	14.2	-21.5	10263	0.95	0.37	0.19	GD
Mrk 477	.S...*P	0.0	15.2	-20.7	11379	0.62	0.80	0.11	LW
Mrk 573	RLXT+*	-1.0	13.6	-20.7	5178	1.13	0.25	0.01	GD
Mrk 1066	RLBS+..	-1.0	13.0	-20.4	3605	1.24	0.19	0.25	LW
Mrk 1210	.S?....	1.0	14.2	-19.4	4046	0.91	0.41	0.00	TW
NGC 214	.SXR5..	5.0	12.6	-21.4	4533	1.27	0.18	0.13	LW
NGC 357	.SBR0*	0.0	12.6	-19.9	2541	1.38	0.14	0.14	N
NGC 404	.LAS-*	-3.0	10.9	-16.7	-48	1.54	0.10	0.00	C
NGC 628	.SAS5..	5.0	9.8	-20.2	656	2.02	0.03	0.04	N
NGC 788	.SAS0*	0.0	12.8	-20.9	4078	1.28	0.17	0.12	LW
NGC 864	.SXT5..	5.0	11.3	-20.2	1550	1.67	0.07	0.12	LW
NGC 1068	RSAT3..	3.0	9.5	-21.3	1109	1.85	0.05	0.07	CS
NGC 1144	.RING.B	-5.0	13.2	-22.1	8641	1.04	0.30	0.21	TW
NGC 1241	.SBT3..	3.0	12.1	-20.0	4030	1.45	0.12	0.22	GD
NGC 1275	.P.....	99.0	12.6	-21.7	5260	1.34	0.15	0.12	C
NGC 1300	.SBT4..	4.0	10.8	-20.1	16	1.79	0.05	0.18	GD
NGC 1320	.S..1*/	1.0	13.2	-19.7	2716	1.28	0.17	0.47	HI/TW
NGC 1398	PSBR2..	2.0	10.4	-21.3	1407	1.85	0.05	0.12	N
NGC 1530	.SBT3..	3.0	11.4	-21.3	2461	1.66	0.07	0.28	GD
NGC 1638	.LXT0?.	-2.3	12.8	-20.4	3320	1.30	0.17	0.13	N
NGC 1667	.SXR5..	5.0	12.4	-21.5	4547	1.25	0.19	0.11	LW
NGC 1672	.SBS3..	3.0	10.2	-20.6	1350	1.82	0.05	0.08	LW
NGC 1961	.SXT5..	5.0	11.0	-22.7	3930	1.66	0.07	0.19	TW
NGC 2146	.SBS2P.	2.0	10.6	-20.6	893	1.78	0.06	0.25	C
NGC 2179	.SAS0..	0.0	12.8	-19.8	2798	1.23	0.20	0.16	TW
NGC 2273	.SBR1*	0.5	12.0	-20.2	1840	1.51	0.10	0.12	CS
NGC 2276	.SXT5..	5.0	11.8	-21.1	2417	1.45	0.12	0.02	CS
NGC 2336	.SXR4..	4.0	10.6	-21.6	2200	1.85	0.05	0.26	C
NGC 2460	.SAS1..	1.0	12.3	-19.6	1451	1.39	0.14	0.12	CS
NGC 2639	RSAR1*\$	1.0	12.2	-21.1	3336	1.26	0.18	0.22	GD
NGC 2903	.SXT4..	4.0	9.1	-20.2	556	2.10	0.03	0.32	C
NGC 2985	PSAT2..	2.0	11.0	-20.8	1322	1.66	0.07	0.10	TW
NGC 3032	.LXR0..	-2.0	12.8	-18.9	1533	1.30	0.17	0.05	LW
NGC 3079	.SBS5./	7.0	10.4	-20.8	1114	1.90	0.04	0.74	HI
NGC 3081	RSXR0..	0.0	12.6	-20.0	2367	1.32	0.16	0.11	GD
NGC 3145	.SBT4..	4.0	11.8	-21.5	3652	1.49	0.11	0.29	CS
NGC 3227	.SXS1P.	1.0	11.2	-20.4	1152	1.73	0.06	0.17	C
NGC 3300	.LXRO*\$	-2.0	13.0	-20.2	3075	1.28	0.17	0.28	N
NGC 3351	.SBR3..	3.0	10.3	-19.3	778	1.87	0.04	0.17	C
NGC 3362	.SX.5..	5.0	13.2	-22.0	8318	1.15	0.24	0.11	N
NGC 3368	.SXT2..	2.0	9.8	-20.3	897	1.88	0.04	0.16	CS

Table 3—Continued

Name	RC3	T	$B_T$	$M_B$	$v$	$D_{25}$	$20''\text{frac}$	$R_{25}$	Nuc Class
NGC 3393	PSBT1*	1.0	12.6	-21.8	5750	1.34	0.15	0.04	CS
NGC 3458	.LX.*	-2.0	13.2	-19.2	1818	1.14	0.24	0.20	N
NGC 3486	.SXR5..	5.0	10.8	-19.7	682	1.85	0.05	0.13	LW
NGC 3516	RLBS0*	-2.0	12.1	-20.8	2540	1.24	0.19	0.11	LW
NGC 3627	.SXS3..	3.0	9.1	-20.6	727	1.96	0.04	0.34	C
NGC 3718	.SBS1P.	1.0	11.2	-20.0	994	1.91	0.04	0.31	C
NGC 3786	.SXT1P.	1.0	13.0	-19.8	2737	1.34	0.15	0.23	LW
NGC 3865	.SXT3P*	3.0	12.6	-21.8	5702	1.31	0.16	0.14	CS
NGC 3982	.SXR3*	3.0	11.7	-19.5	1188	1.37	0.14	0.06	GD
NGC 4030	.SAS4..	4.0	11.2	-20.9	1460	1.62	0.08	0.14	TW
NGC 4117	.L.0*	-2.3	14.0	-16.9	943	1.25	0.19	0.31	LW
NGC 4143	.LXS0..	-2.0	11.9	-19.1	985	1.36	0.15	0.20	LW
NGC 4151	PSXT2*	2.0	10.7	-20.8	970	1.80	0.05	0.15	LW
NGC 4253	PSBS1*	1.0	13.8	-19.7	3836	0.98	0.35	0.06	GD
NGC 4254	.SAS5..	5.0	10.1	-21.0	2407	1.73	0.06	0.06	CS
NGC 4258	.SXS4..	4.0	8.5	-20.8	449	2.27	0.02	0.41	HI
NGC 4260	.SBS1..	1.0	12.3	-20.4	1958	1.43	0.12	0.30	C
NGC 4303	.SXT4..	4.0	10.1	-20.8	1585	1.81	0.05	0.05	GD
NGC 4314	.SBT1..	1.0	11.2	-18.8	963	1.62	0.08	0.05	LW
NGC 4380	.SAT3*\$	3.0	12.1	-19.2	970	1.54	0.10	0.26	CS
NGC 4388	.SAS3*/	3.0	10.8	-20.3	2535	1.75	0.06	0.64	HI/C
NGC 4395	.SAS9*	9.0	10.6	-17.2	318	2.12	0.03	0.08	C
NGC 4569	.SXT2..	2.0	9.8	-21.3	-245	1.98	0.03	0.34	C
NGC 4593	RSBT3..	3.0	11.4	-21.6	2492	1.59	0.09	0.13	TW
NGC 4725	.SXR2P.	2.0	9.8	-20.8	1206	2.03	0.03	0.15	C
NGC 4939	.SAS4..	4.0	11.2	-22.0	3111	1.74	0.06	0.29	C
NGC 4941	RSXR2*	2.0	11.7	-18.3	1111	1.56	0.09	0.27	LW
NGC 4968	PLX.0..	-2.0	13.4	-19.8	2957	1.27	0.18	0.34	C
NGC 5005	.SXT4..	4.0	10.2	-21.5	1022	1.76	0.06	0.32	C
NGC 5033	.SAS5..	5.0	10.2	-21.1	892	2.03	0.03	0.33	C
NGC 5054	.SAS4..	4.0	11.1	-21.1	1741	1.71	0.06	0.24	LW
NGC 5064	PSA.2*	2.5	11.7	-21.3	3002	1.39	0.14	0.34	TW
NGC 5135	.SBS2..	2.0	12.4	-21.3	4112	1.41	0.13	0.15	GD
NGC 5252	.L.....	-2.0	13.9	-20.9	6926	1.14	0.24	0.21	CS
NGC 5256	.P.....	99.0	0.0	-35.2	8239	1.08	0.28	0.05	C
NGC 5273	.LAS0..	-2.0	12.4	-18.7	1089	1.44	0.12	0.04	CS
NGC 5283	.L...?.	-2.0	14.1	-18.8	2697	1.03	0.31	0.04	CS
NGC 5347	PSBT2..	2.0	13.1	-19.7	2335	1.23	0.20	0.10	GD
NGC 5383	PSBT3*P	3.0	11.9	-20.9	2250	1.50	0.11	0.07	GD
NGC 5427	.SAS5P.	5.0	11.7	-21.2	2618	1.45	0.12	0.07	LW
NGC 5506	.S..1P/	1.0	12.3	-20.0	1815	1.45	0.12	0.52	HI/LW
NGC 5548	PSAS0..	0.0	12.8	-21.3	4981	1.16	0.23	0.05	TW
NGC 5614	.SAR2P.	2.0	12.4	-21.2	3892	1.39	0.14	0.08	TW
NGC 5643	.SXT5..	5.0	10.2	-20.9	1199	1.66	0.07	0.06	GD
NGC 5674	.SX.5..	5.0	13.6	-21.4	7442	1.04	0.30	0.02	CS
NGC 5691	.SXS1*P	1.0	12.5	-19.9	1870	1.27	0.18	0.12	C
NGC 5695	.S?....	3.0	13.4	-20.4	4209	1.19	0.22	0.15	LW
NGC 5929	.S..2*P	2.0	14.1	-18.8	2504	0.98	0.35	0.03	CS

Table 3—Continued

Name	RC3	T	$B_T$	$M_B$	$v$	$D_{25}$	$20''\text{frac}$	$R_{25}$	Nuc Class
NGC 5953	.SA.1*P	1.0	13.3	-19.3	1965	1.21	0.21	0.08	TW
NGC 5970	.SBR5..	5.0	11.8	-20.7	1963	1.46	0.12	0.17	C
NGC 6221	.SBS5..	5.0	9.8	-21.7	1482	1.55	0.09	0.16	CS
NGC 6300	.SBT3..	3.0	10.2	-20.6	1110	1.65	0.07	0.18	C
NGC 6384	.SXR4..	4.0	10.6	-20.9	1663	1.79	0.18	0.05	C
NGC 6412	.SAS5..	5.0	12.1	-19.8	1324	1.40	0.13	0.06	C
NGC 6744	.SXR4..	4.0	8.8	-21.2	841	2.30	0.02	0.19	C
NGC 6814	.SXT4..	4.0	11.3	-20.5	1563	1.48	0.11	0.03	GD
NGC 6890	.SAT3..	3.0	12.8	-19.7	2419	1.19	0.22	0.10	GD
NGC 6946	.SXT6..	6.0	7.8	-20.9	52	2.06	0.03	0.07	C
NGC 6951	.SXT4..	4.0	10.7	-21.2	1426	1.59	0.09	0.08	LW
NGC 7096	.SAS1..	1.0	12.6	-20.2	3100	1.27	0.18	0.06	N
NGC 7126	.SAT5..	5.0	12.4	-20.5	3054	1.45	0.12	0.34	TW
NGC 7130	.S..1P.	1.0	12.9	-21.2	4842	1.18	0.22	0.04	GD
NGC 7177	.SXR3..	3.0	11.5	-19.8	1150	1.49	0.11	0.19	CS
NGC 7392	.SAS4..	4.0	12.2	-20.8	3128	1.33	0.16	0.23	LW
NGC 7469	PSXT1..	1.0	12.6	-21.5	4790	1.17	0.23	0.14	TW
NGC 7496	.SBS3..	3.0	11.8	-19.7	1649	1.52	0.10	0.04	C
NGC 7582	PSBS2..	2.0	10.8	-20.4	1575	1.70	0.07	0.38	HI/C
NGC 7674	.SAR4P.	4.0	13.6	-21.8	8662	1.05	0.30	0.04	GD
NGC 7682	.SBR2..	2.0	13.7	-20.6	5107	1.09	0.27	0.05	LW
NGC 7716	.SXR3*.	3.0	12.5	-20.1	2571	1.33	0.16	0.08	CS
NGC 7743	RLBS+..	-1.0	12.2	-19.4	1658	1.48	0.11	0.07	LW
NGC 7814	.SAS2*/	2.0	11.0	-19.6	1054	1.74	0.06	0.38	HI
UGC 12138	.SB.1..	1.0	13.8	-21.3	7487	0.92	0.40	0.08	GD
UGC 6100	.S..1?.	1.0	14.0	-21.3	8778	0.92	0.40	0.18	LW
UM 146	.SAT3..	3.0	13.9	-20.4	5208	1.10	0.26	0.10	LW

Note. — Morphological data, including our nuclear classifications (col. 10), for all 123 galaxies in the sample. Most of these data were obtained from the RC3 catalog, including the morphological classification (col. 2),  $T$  type (col. 3), total  $B$  magnitude (col. 4), diameter  $D_{25}$  (col. 7), and axis ratio  $R_{25}$  (col. 9). The absolute  $B$  magnitude (col. 5) was derived based on the distance given in Table 2, the heliocentric velocity  $v$  (col. 6) is from either the RC3 or NED, and  $20''\text{frac}$  (col. 8) is the fraction of the galaxy diameter  $D_{25}$  contained within the  $20''$  field of view shown in Figures 1 and 32. The classification codes in column 10 are: GD: grand design nuclear spiral; TW: tightly wound spiral; LW: loosely wound spiral; CS: chaotic spiral; C: chaotic circumnuclear dust; N: no circumnuclear dust structure. These classes are defined in §3.1. Galaxies with axis ratios  $R_{25} > 0.35$  are classified as HI (high inclination), along with a nuclear classification if possible. Galaxies with  $R_{25} \geq 0.30$  are still too highly inclined for accurate classifications and are not included in the upper left panels of Figures 34 and 35.

Table 4. Ring Properties

Name	RC3	$R$ ["]	$R$ [pc]	$D(\text{ring})/D_{25}$	Note
ESO 138-G1	.E?...	6.2	1100	0.20	smooth in $V$ and $H$
Mrk 477	.S...*P	2.8	2100	0.22	smooth in $V$ and $H$
NGC 864	.SXT5..	0.6	60	0.004	very small, starburst
NGC 1300	.SBT4..	6.8	500	0.037	smooth in $V$ and $H$ , dusty
NGC 1667	.SXR5..	7.3	2100	0.14	stars, incl. young clusters
NGC 1672	.SBS3..	5.1	360	0.026	stars, incl. young clusters
NGC 2273	.SBR1*.	2.3	310	0.012	stars, incl. young clusters
NGC 3081	RSXR0..	4.5	700	0.072	smooth in $V$ and $H$ , dusty
NGC 3351	.SBR3..	5.6	220	0.025	stars, incl. young clusters
NGC 4314	.SBT1..	5.6	260	0.045	stars, incl. young clusters
NGC 5427	.SAS5P.	5.6	1000	0.066	stars, incl. young clusters
NGC 6890	.SAT3..	7.9	1200	0.17	stars, incl. young clusters
NGC 6951	.SXT4..	3.9	460	0.033	stars, incl. young clusters
NGC 7469	PSXT1..	1.4	450	0.032	very bright SB ring

Note. — Properties of the rings shown in Figure 1. Columns 1 and 2 list the name and morphology for each galaxy from Table 2. The angular (col. 3) and physical (col. 4) radius is listed next, followed by the ratio of the ring size to the galaxy diameter (col. 5). A note on the appearance of each ring is listed in the last column.